CHARACTERIZATION AND COMPOSITION OF CORROSION SCALES IN DRINKING WATER DISTRIBUTION SYSTEMS

by

Adam Schmidt

A Thesis Submitted in

Partial Fulfillment of the

Requirements for the Degree of

Master of Science

in Engineering

at

The University of Wisconsin-Milwaukee

December 2022

ABSTRACT

CHARACTERIZATION AND COMPOSITION OF CORROSION SCALES IN DRINKING WATER DISTRIBUTION SYSTEMS

by

Adam Schmidt

The University of Wisconsin-Milwaukee, 2022
Under the Supervision of Professor Dr. Yin Wang

Internal corrosion of drinking water pipes has received considerable attention recently in the media and in academic studies due to compliance and monitoring regulations with the Lead and Copper Rule (LCR) established by the EPA in 1991. Notable health crises involving municipalities exceeding the LCR in Washington D.C. and Flint, Michigan occurred when corrosion scale conditions changed from stable to soluble lead compounds due to changing water chemistry, leaching high amounts of lead into consumers drinking water. Understanding the role of the corrosion scale in the process of leaching lead and other toxic trace metals such as arsenic is vital to ensure clean drinking water. Field-studies examining real-world corrosion scales in municipalities provide a glimpse into the effects of variable water chemistry conditions that can prove complimentary to bench-scale theory. In this study, three municipalities were chosen with different water quality, corrosion inhibitor, and disinfectant residual. The effect of water chemistry on corrosion scale formation within copper, iron, and lead pipes were important in the formation of corrosion scale minerals. Elemental analysis of the corrosion scales and their binding fractions were studied to derive the mechanisms of release so that water resource engineers can prevent this in the future.

TABLE OF CONTENTS

LIST OF FIGURES

LIST OF TABLES

LIST OF ABBREVIATIONS

AAS	Atomic Absorption Spectroscopy
DWDS	Drinking Water Distribution System
EDS	Energy-Dispersive Spectroscopy
EPA	Environmental Protection Agency
HCl	Hydrochloric Acid
HNO_3	Nitric Acid
ICP-MS	Inductively Coupled Plasma Mass Spectrometry
LCR	Lead and Copper Rule
LOD	Limit of Detection
LOQ	Limit of Quantification
mg	Milligram
mL	Milliliter
ORP	Oxidation-Reduction Potential
ppb	Parts Per Billion
SEM	Scanning Electron Microscope
STD	Standard Deviation
XPS	X-Ray Photo-Electron Spectroscopy
XRD	X-Ray Diffraction

ACKNOWLEDGEMENTS

Funding for this research was supported by the National Science Foundation (2027233). Any opinions, findings, and conclusions or recommendations expressed in this work are those of the author and do not necessarily reflect the views of the National Science Foundation.

Chapter 1: Introduction

1.1 Adverse Health Effects from Drinking Water Pipes

Drinking water infrastructure in the United States and in many other countries around the world have received a lot of attention and scrutiny from governments following crisis-level events in Washington D.C. in 2001, and in Flint, Michigan in 2014. Residents of Washington D.C. noticed elevated levels of lead in their drinking water after the drinking water treatment plant switched from free chlorine disinfection to chloramines (Renner, 2004). This switch in disinfectants produced a lower oxidation-reduction potential (ORP) in the drinking water distribution system (DWDS) which reduced the insoluble lead dioxide pipe deposits to soluble lead minerals (Edwards & Abhijeet, 2004).

Citizens of Flint, Michigan experienced extremely high lead levels in their drinking water following a switch in source water from the Detroit Water and Sewer Department to treated Flint River water. A combination of higher chloride levels from addition of ferric chloride ($FeCl_3$) as a coagulant, high chloride-to-sulfate mass ratio (which can be indicative of corrosivity), and a lack of corrosion inhibitors contributed to destabilization of soluble lead scales on the inside of drinking water pipes (Pieper et al. 2017). Lead dioxide or other lead (IV) corrosion scales on the inside of the drinking water pipes were reduced and subsequently released into the drinking water to be consumed by the citizens of Flint, Michigan.

Consumption of lead can lead to many health problems, particularly in young children. Lead can easily enter the bloodstream and cause long-lasting damage targeting the brain and nervous system (CDC, 2022). Children with exposure to lead over longer periods of time have

exhibited decreased performance in school, supported not just by test score metrics but through behavioral and learning developmental problems that persist throughout their lifetimes. The Center for Disease Control and Prevention (CDC) recommends blood lead level screening for infants and uses a threshold of 5 micrograms per deciliter of blood as the cutoff for normal blood lead levels (CDC, 2022). One study of blood lead levels in children from Flint, Michigan revealed that the percentage of children with elevated blood lead levels prior to the water source switch was 2.4% (compared to 0.7% in a region outside of Flint) which rose to 4.8% after the switch to Flint River water (Hanna-Attisha et al. 2016). One school even reported lead levels of 101 ppb in their drinking water.

The Lead and Copper Rule (LCR) was established in 1991 by the EPA to further decrease the allowable level of lead and copper in consumer drinking water. It established an action level of lead at 15 ppb, and copper at 1.3 ppm and made monitoring for these metals mandatory (EPA[1], 2021). Lead is the primary focus for news coverage and legislation due to its known health effects, but copper in water can also have adverse health effects. Copper is well known as an essential nutrient for all mammals and has been quantified as the sixth most prevalent trace metal in human tissue such as the heart, kidneys, liver, and spleen (Schroeder et al. 1966). Related health effects of prolonged elevated levels of copper include stomach and intestinal discomfort, and potential damage to the liver or kidneys, which can accumulate large amounts of copper.

Iron is not monitored by the EPA under the Primary Drinking Water Regulations, but it is included in the Secondary Drinking Water Regulations. Although this designation means the EPA regulation is not enforceable, it still provides a baseline for water treatment facilities to

aim to avoid detrimental health effects (EPA[2], 2022). The official secondary limit for iron in drinking water is set at 1.3 ppm, the same as copper. Iron is also an essential nutrient for humans (utilized to transport oxygen in the bloodstream) and is the most abundant trace metal in human tissues (Schroeder et al. 1966). Iron levels in drinking water are generally considered safe but non-aesthetically pleasing, leading to red and orange coloration and staining on contacted surfaces.

Among the many sources of these metals, the most common sources for drinking water are the pipes that carry the finished water to the consumers tap. For this reason, it is essential to understand internal corrosion mechanisms through theory and field observations. Lab studies provide the foundation of uncovering the formation mechanisms of the corrosion scales, and field observations compliment them by offering a glimpse of changing real-world conditions that are difficult to replicate in the lab. The combination of these studies infer how water resource engineers can engineer corrosion to their benefit. By preferentially creating a stable passive film over the base metal, the pipe wall can be protected to avoid pitting and crevice corrosion which cause leaks and pipe failure. Over time the stable films may accumulate trace metals which are low in concentration in the water but can reach toxic levels from long periods of contact time leading to adsorption and complexation. Controlling the release of the trace metals goes hand in hand with understanding the characteristics of the corrosion scales and creating a stable passive layer that prevents drinking water toxicity.

1.2 Field vs Lab Studies

Two types of research are conducted which attempt to uncover the hidden mechanisms of internal corrosion in drinking water pipes. Lab studies, which are done in controlled conditions chosen by the researchers, and field studies, which survey drinking water pipes from active distribution systems. Lab studies derive the theoretical mechanisms by which corrosion attacks the inside of a drinking water pipe. Metal coupons with minimal surface roughness placed in a solution prepared to mimic a water quality parameter such as high alkalinity are analyzed for corrosion rate and corrosion solid formation. Model pipe loops for flowing water effects are used to create microcosms of distribution systems, offering a glimpse into how pipes are conditioned over time by scale deposition.

Field studies take harvested pipe sections from distribution systems to assess the corrosion solids which have already formed. The age of the pipe and the water chemistry are used to contrast the hypotheses formed in laboratory experiments. Field studies may obtain pipes from many distribution systems that have similar or differing water quality (pH, disinfectant residual, alkalinity etc.) and propose a reason for the variances or similarities in minerals identified.

Lab studies paired with field studies have become essential in proving theory from the lab. Dynamic water quality conditions are difficult to maintain and model in the laboratory but creating a system that tests a particular water chemistry effect, such as pH increases on the solubility of copper corrosion minerals, helps aid field studies in explaining what is observed.

1.3 Identifying a Research Need

While it is apparent that laboratory studies are essential to deriving the mechanisms of pipe corrosion, full-scale experimentation of corrosion scales is very difficult to achieve. For water engineers to fully develop a corrosion prevention plan, their unique water chemistry must be analyzed on a case-by-case basis. Large-scale surveys of multiple distribution systems and pipe materials must also be conducted. Most field studies focus on a single pipe material and consider the corrosion response of water quality. There is a clear need for a multi-distribution system survey with diverse pipe materials, water quality, and pipe type (mains and laterals).

1.4 Research Objectives

In this project the main objectives were to determine the corrosion scale mineralogy and morphology as well as the elemental abundance within each scale. De-commissioned pipes from three municipalities in South-Eastern Wisconsin were harvested and the corrosion scales were analyzed to determine the effect of:

(1) Corrosion scale composition on various pipe materials (Copper, Lead, Iron)

(2) Pipe service type (Main vs Lateral)

(3) Trace metal accumulation and binding

This study presents the first findings from three different pipe materials within the same distribution system (Milwaukee), and examination of mains and laterals from three different distribution systems.

1.5 Thesis Overview

Chapter 2 provides an extensive literature review on the history of drinking water pipe infrastructure material selection, and then corrosive mechanisms and products occurring for each material type. A comprehensive examination of corrosion products found in field studies of lead pipes is provided. Factors affecting corrosion are discussed such as pH, water chemistry, and disinfectant residuals. Corrosion inhibition measures are mentioned prior to a brief introduction to corrosion scale accumulation of trace metals.

Chapter 3 covers the methods and standard procedures used in the field study, as well as the performance objectives of the respective instruments. Included are the steps or adaptations of previously defined experiments as well as a description of reagents involved. Chapter 4 details the results from each experimental method with appropriate statistical analysis and figures. A discussion precedes each subsection to commentate on the findings. Chapter 5 follows the results as a final word of conclusion and recommendations for future work.

Chapter 2: Literature Review

2.1 Drinking Water Pipe Materials and History

When considering which piping material to use to transport drinking water to citizens, a municipality must focus on factors such as durability and cost. Water mains are responsible for carrying the treated water from the plant to the edge of the service line, which can be many miles. Materials chosen for water mains are usually concrete or iron. The laterals that transport the water from the street to the faucet must possess the ability to withstand high amounts of pressure (to transport water vertically if required) and be able to bend to transport water throughout different parts of the buildings.

Prior to 1986 lead had been a popular material choice for drinking water laterals due to its cost-effectiveness and malleability. In 1986 the United States Government amended the Safe Drinking Water Act to reduce the implementation of lead-containing pipes, joints, and solders in drinking water distribution systems (EPA[3], 2020). This ruling set the allowable lead content in drinking water materials at a maximum of 8% by weight. Further, in 2011 the United States Government passed the Reduction of Lead in Drinking Water Act which lowered the maximum allowable lead content in contacting drinking water materials from 8% to 0.25% by weight (US Congress, 2022). Although this was a large step in the right direction, the continued use of already-in-place lead pipes is slow to be phased out.

In 1992 the Madison Water Utility exceeded the LCR due to its use of lead service laterals. The water utility became the first in the country to fully replace their lead piping with over 10,000 lead service laterals removed in an effort spanning from 2001-2010 (Denig-Chakroff, 2001; Schock et al, 2014). The cost for the water utility to conduct the full lead pipe replacement was $15.5 million, but the total cost was significantly higher as property owners were required to pay for the removal of their own pipes (Madison Water Utility, 2022). Due to the high cost to the property owners, partial service line replacement may include a copper pipe (from the municipality installation) connected to a lead pipe (Swertfeger et al. 2006). If contact persists between the two dissimilar metals (if a plastic coupling is not installed), the galvanic connection could increase lead corrosion and lead to higher subsequent release (Triantafyllidou & Edwards, 2011; Nguyen et al. 2011; Wang et al. 2012).

According to the Milwaukee Water Works Annual 2021 report, the municipality is responsible for ownership of 70,970 lead service lines (Milwaukee Water Works, 2022). An additional 70,945 lead pipes are privately owned. Approximately $3.5 million was spent on lead service line replacement in 2021 in which 3,124 pipes were removed representing approximately a 4% decrease year over year. During the same time frame 3,173 private lead service lines were also replaced, as shown in Table 2-1 (Milwaukee Water Works, 2022). This represents a decrease of approximately 4% year-over-year. A map from 2016 showing the geospatial distribution of the lead pipes in Milwaukee is shown in figure 2-1. The city of Milwaukee estimates it will require a $750 million investment in infrastructure to remove all of the remaining lead service lines, at a cost of $10,200 per pipe (Milwaukee Water Works, 2022).

The EPA estimates there are still 6 – 10 million lead service lines in use in the country as of 2016, and with an average estimate of replacement costs totaling $4,700 per lead pipe, it can be conservatively calculated that the total cost to replace the nations lead pipes falls in the range of $28.2 billion and $47 billion (EPA[4], 2022). In June of 2022 the Biden-Harris Lead Pipe and Paint Action plan provided funding in the form of $2.9 billion for lead service removal throughout the country (Whitehouse, 2021).

In addition to lead, copper, and iron, PVC pipes are also chosen for service lines within homes and buildings due to their low cost and corrosion resistance. Despite the economic benefits to a homeowner, scaling can still occur on the inner walls of the PVC as evidenced in field studies where arsenic and zinc concentrations were higher in the non-metal tubes' corrosion scales (Lytle et al. 2004). Proliferation of biofilm growth has been observed in cross-linked polyethylene and ethylene propylene diene monomer drinking water pipes at higher rates under similar drinking water conditions as copper and stainless-steel tubes (Waines et al. 2011). For this reason, these plastic materials may be seen as unfit for drinking water applications as biofilms may contain pathogenic fungi such as *Aspergillus spp.* despite cast iron having similar biofilm growth (Liu et al. 2014).

Table 2-1. Pipe material in Milwaukee as of the end of 2021 (Milwaukee Water Works, 2022).

Pipe Material	Pipe Quantity Start of 2021	Pipe Quantity End of 2021	Change
Copper (Utility)	82,540	85,814	3,274
Copper (Private)	82,900	85,750	2,850
Cast Iron (Utility)	3,713	4,896	1,183
Cast Iron (Private)	3,711	5,870	2,159
Ductile Iron (Utility)	4,227	3,028	-1,199
Ductile Iron (Private)	4,230	1,380	-2,850
Lead (Utility)	74,094	70,970	-3,124
Lead (Private)	74,118	70,945	-3,173

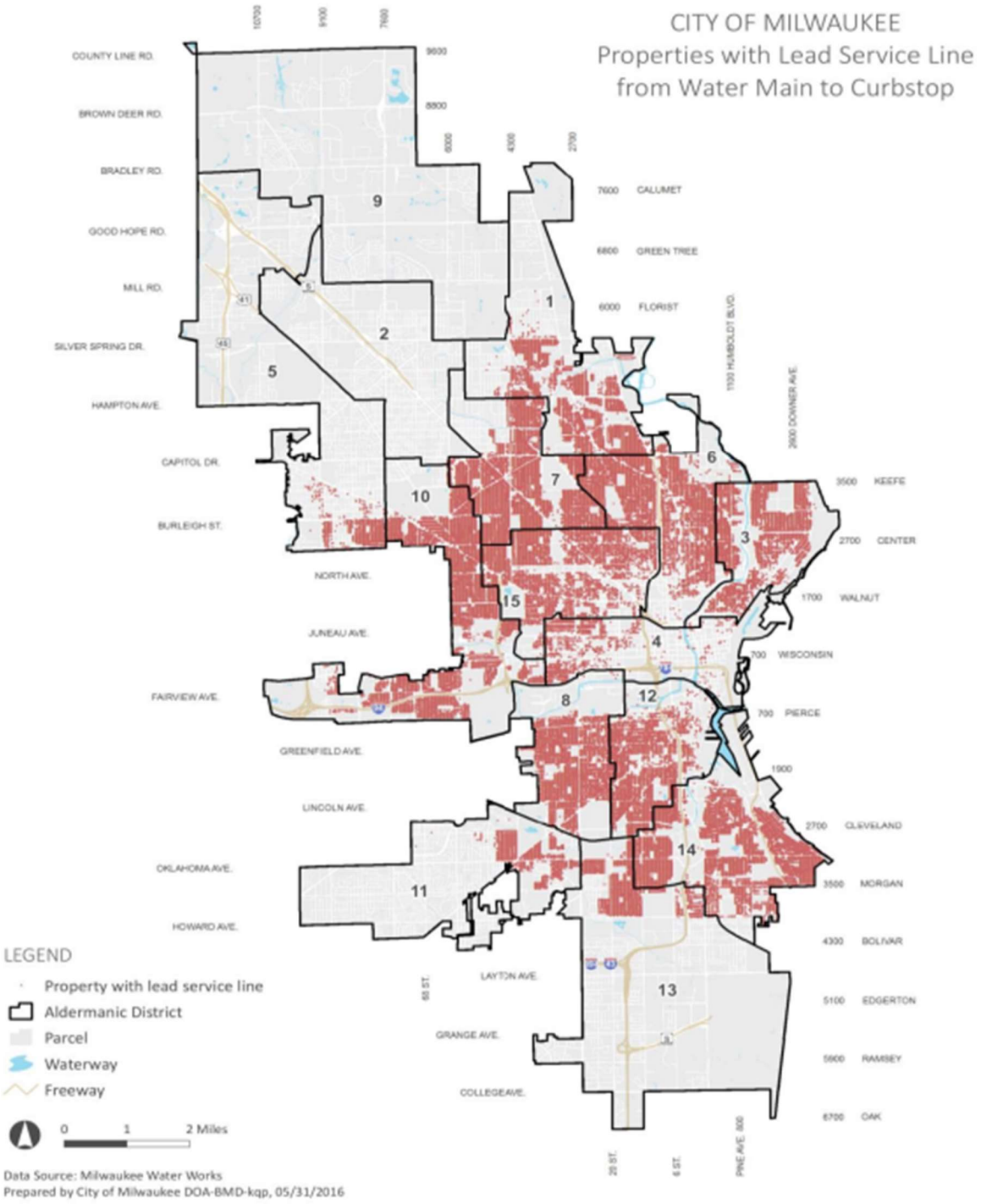

Figure 2-1. 2016 Municipal map of Milwaukee, with red coloration indicating lead service line use (Milwaukee Water Works, 2022).

2.2 Lead Corrosion Minerals

Many types of external corrosion are possible in the environments that drinking water pipes are present in as the pipes may be underground in saturated soils exposed to moisture. Stress-induced cracking, galvanic corrosion, and pitting are among the possibilities that engineers must consider. Despite this, the main focus of corrosion control is focused on the internal corrosion of the pipe wall. Many factors give way to the formation of these corrosion scales, such as pH, water chemistry, oxidation-reduction potential, and corrosion inhibitors. For corrosion to occur a corrosion cell consisting of an anode, an electron path, a cathode, and an ion path are required. Corrosion is initiated by the transfer of electrons from an anode to the cathode, as seen in equations 1-3 with lead acting as the electron donor to oxygen (Vasquez, F.A. et al. 2006). Equation 3 is the summation of the reactions. Another such reaction occurs with the galvanic coupling of lead with a more noble metal such as copper. Lead is more active (has a lower standard potential) compared to copper, and when in contact the lead sample will undergo corrosion (Figure 2-3, Jones, 1996).

$$2Pb_{(s)} \rightarrow 2Pb^{2+} + 4e^{-} \quad (1)$$

$$O_{2\,(aq)} + 4H^{+} + 4e^{-} \rightarrow 2H_2O \quad (2)$$

$$2Pb_{(s)} + O_{2\,(aq)} + 4H^{+} \rightarrow 2Pb^{2+} + 2H_2O \quad (3)$$

Table 2-2. Standard half-cell reactions of metals and their associated potential. In a galvanic series, the metal with the lower standard potential will be more active and preferentially corrode (Jones, 1996).

Reaction	Standard Potential e^o (volts vs SHE)
$O_2 + 4H^+ + 4e^- = 2H_2O$ (pH 0)	+1.229
$O_2 + 2H_2O + 4e^- = 4OH^-$ (pH 7)	+0.82
$Fe^{3+} + e^- = Fe^{2+}$	+0.771
$O_2 + 2H_2O + 4e^- = 4OH^-$ (pH 14)	+0.401
$Cu^{2+} + 2e^- = Cu$	+0.337
$2H^+ + 2e^- = H_2$	0.000
$Pb^{2+} + 2e^- = Pb$	-0.126
$Fe^{2+} + 2e^- = Fe$	-0.440

Pourbaix diagrams are often used to predict corrosion behavior of metals in environments exposed to water. Figure 2-2 is the standard Pourbaix diagram for lead with dissolved inorganic carbon (DIC) at 25°C. Above the two dotted lines represents the region where oxygen evolution will occur in the system, and this occurs at higher potentials which are oxidizing conditions. Across a wide range of pH values the high potential system creates the lead dioxide mineral with the lead chemical state at +4. Between the dotted lines is the region where water is stable. Within this area lead is found mostly in the +2-oxidation state forming complexes with a singular oxygen molecule, or higher oxides with hydrogens. Other relevant minerals such as lead carbonates and phosphates may form in this region. In most drinking water distribution systems, the conditions fall in the pH range of 7 – 8.5 and have a potential between 0.25 and 1.0 V (Lyon, 2010). This puts the lead oxidation in the +2 state with the ability to form many minerals. Below the bottom dashed line is the hydrogen evolution region where reducing conditions are present and lead is mainly in the elemental (base metallic) form.

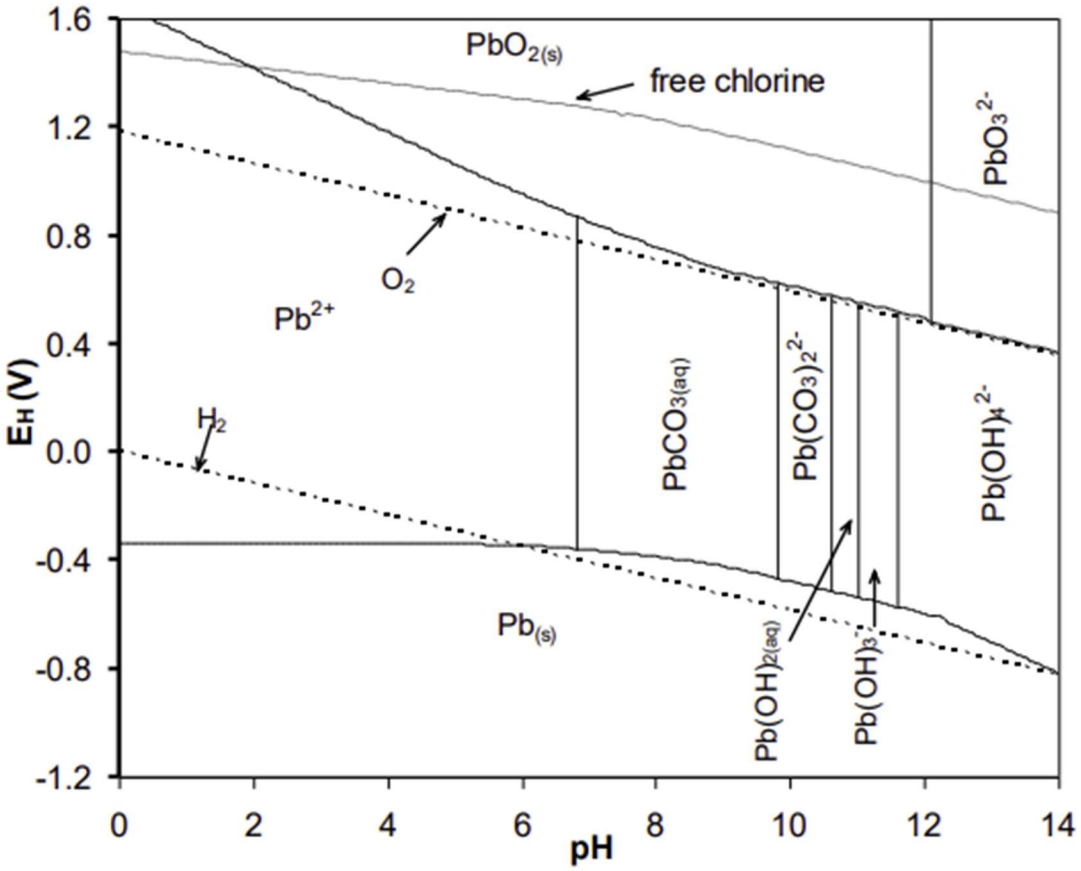

Figure 2-2. Pourbaix diagram of lead at 25° C. In between the dotted lines represents the conditions where water is stable. Common drinking water conditions would be in the range of 7 – 8.5 pH and a voltage of 0.25 – 1.0 V (Wang, 2012).

Observing the Pourbaix diagram it is easy to see that potential has a significant role in the culmination of lead chemical state. Figure 2-3 is a potential vs pH diagram that indicates the stability of common disinfectants used in water treatment such as free chlorine and chloramines (Vasquez et al. 2006). The top of the diagram shows the stable free chlorine species (HOCl and OCl^-). The high potential indicated in this region gives the ability to fully oxidize the lead species in water from Pb -> Pb(II) -> Pb(IV) which would occur in the PbO_2 portion of figure 2-2. On the contrast, chloramines (e.g., NH_2Cl) are associated with a lower

potential across the range of pH found in distribution systems and would not be expected to fully oxidize to PbO_2.

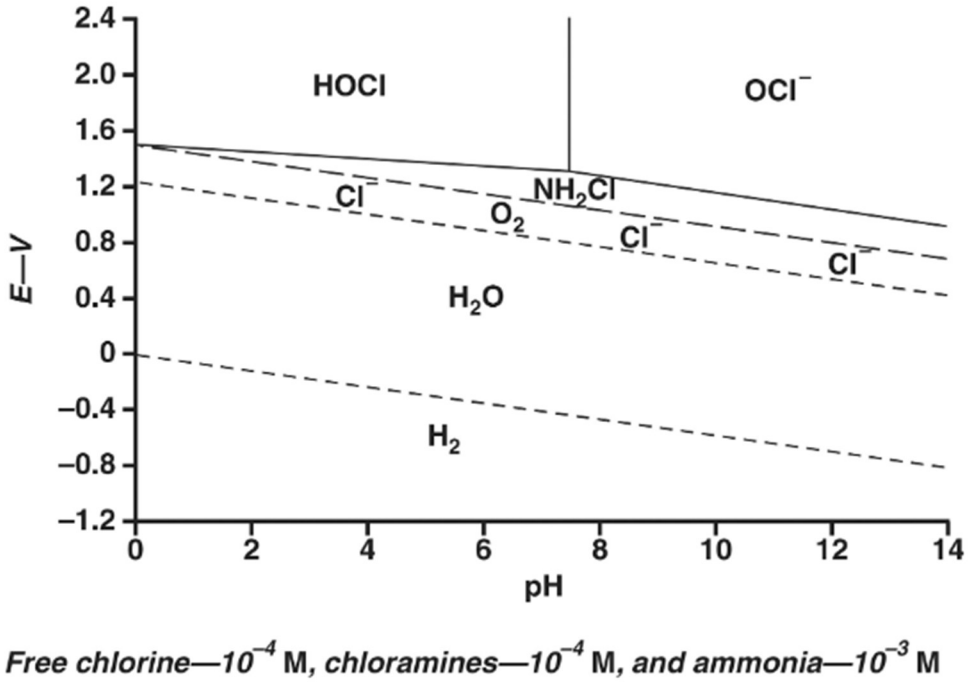

Figure 2-3. Stability potential of disinfectants free chlorine (HOCl, OCl^-) chloramine (NH_2Cl) and ammonia (NH_3) at similar concentrations (Vasquez et al. 2006).

This hypothesis is confirmed by many laboratory and field studies of corrosion scale minerals. One of the most notable cases was in the nation's capital of Washington D.C. where the disinfectant was switched from free chlorine to chloramines. The switch occurred in 2000, and until 2004 the residents of Washington D.C. were exposed to lead levels greatly exceeding the LCR (Edwards & Dudi, 2004). The change from high to lower potential reduced lead from the +4 to the +2-oxidation state, where solubility is higher and thus dissolved and particulate lead are higher (Schock et al. 2005; Wang et al. 2010; Xie et al. 2010). Use of a phosphate corrosion inhibitor is recommended when a switch from free chlorine to monochloramine is made (Bae et al. 2019).

The lead corrosion minerals can be characterized into groups based on the major ion groups associated with them. Lead carbonates typically require a dissolved inorganic carbon level in the water which may come from carbonates associated with hard water (Shock & Giani, 2004). Common lead carbonate minerals include cerussite ($PbCO_3$), hydrocerussite ($Pb_3(CO_3)_2(OH)_2$), and plumbonacrite ($Pb_5O(OH)_2(CO_3)$). A typical formation pathway for the lead ion precipitation with carbonate and phosphate groups is shown in equations 4-6 (Schock & Giani, 2004). These minerals exist in the Pb(II) oxidation state but solubility is controlled by maintaining alkaline pH levels, unless dissolved inorganic carbon exceeds 60 mg/L (Maynard, 2008; Noel et al. 2014). These minerals are often found associated with lead dioxides, indicating that they serve as a precursor to more soluble minerals (Lyle & Schock, 2004; Liu et al. 2008).

$$3Pb^{2+} + 2H_2O + 2CO_3^{2-} \rightarrow Pb_3(CO_3)_2(OH)_{2(s)} \quad (4)$$

$$5Pb^{2+} + 3PO_4^{3-} + H_2O \rightarrow Pb_5(PO_4)_3OH_{(s)} \quad (5)$$

$$3Pb^{2+} + 2PO_4^{3-} \rightarrow Pb_3(PO_4)_{2\,(s)} \quad (6)$$

In many distribution systems with lead pipes the water engineers will opt for orthophosphate as a corrosion inhibitor. The dosing of this corrosion inhibitor is intended to form lead phosphate compounds such as hydroxylpyromorphite ($Pb_5(PO_4)_3(OH)$), chloropyromorphite ($Pb_5(PO_4)_3Cl$), or lead-substituted apatite minerals (calcium-phosphate complexes) (Maynard, 2008). In many cases, insoluble lead dioxide complexes are formed, achieving the same desired effect (Schock et al. 1996). Corrosion inhibitors will be examined further in section 2.5.

Common lead oxides include litharge (PbO) and massicot (PbO), and the lead dioxide minerals plattnerite (β-PbO_2) and scrutinyite (α-PbO_2). The lead oxide minerals such as litharge are hypothesized to form first and are found often on the inner pipe walls in field studies (Kim & Herrera, 2010). Litharge and massicot have lower solubility than scrutinyite and plattnerite, and water engineers aim to create insoluble lead dioxide films which cover the more soluble minerals, preventing mass lead release. Increases in dissolved inorganic carbon concentrations tend to favor formation of lead carbonate minerals, even if insoluble lead dioxide minerals are present (Schock, 1980). The transition to carbonate mineral deposition over the lead oxide scale subsequently increases lead release.

Natural organic matter (NOM) can also behave as a reductant to lead dioxide minerals. This finding complicates solubility equilibrium modeling of lead, adding a layer of complexity that requires more research. One study using various NOM sources to reduce plattnerite found that within 10 days lead concentrations within all reactors were greater than 1000 ppb (Dryer & Korshin, 2007). Lead release continued to increase at a similar rate for the duration of the 50+ day experiment. The mechanism has been confirmed as reduction from Pb(IV) to Pb(II), and not particulate lead release (Lin & Valentine, 2007). Monochloramine and free chlorine can be expected to reduce these effects by providing a strong redox influence to preserve the PbO_2 scale (Lin & Valentine, 2009).

2.2.1 Field Studies

Field studies have analyzed the lead corrosion products on the inside of drinking water pipes using XRD to identify specific mineral constituents. Of the found studies that published

distinct minerals found in the corrosion scales, lead carbonates hydrocerussite and cerussite were the most common. Next in frequency was the lead oxide litharge, followed by plattnerite. Plattnerite or scrutinyite may form preferentially based on pH and oxidant conditions, as well as pipe age. Older pipes with high oxidation potential waters are more likely to exhibit thermodynamically stable lead dioxides, representing the final oxidation stage of lead (Lytle & Schock, 2005). Plattnerite may be more thermodynamically stable compared to scrutinyite. For this reason, scrutinyite was found at a much lower frequency than plattnerite. Table 2-2 shows the frequency of each mineral found in literature. Studies that focused on a sole mineral as the findings were not included (such as vanadinite).

Table 2-3. Frequency of lead corrosion minerals reported in field study literature (Davidson et al. 2004; Schock & Giani, 2004; Gerke et al. 2009; Kim & Herrera, 2010; Wang et al. 2012; Schock et al. 2014; Triantafyllidou et al. 2015; Hayes et al. 2016; Hopwood et al. 2016; Wasserstrom et al. 2017; Winning et al. 2017; DeSantis et al. 2018; Trueman et al. 2018; Tully et al. 2019; DeSantis et al. 2020; Lytle et al. 2020; Guo & Herrera, 2021).

Lead Mineral	Number of Reported Samples
Hydrocerussite	54
Cerussite	44
Litharge	43
Plattnerite	25
Plumbonacrite	12
Hydroxylpyromorphite	5
Scrutinyite	4
Massicot	2
Chloropyromorphite	1

As distribution systems differ on disinfectant residual, pH, and corrosion inhibitor (as well as other factors not examined here such as water chemistry), these must also be examined. High residual free chorine levels typically above 4.0 mg/L are favorable for complete oxidation of Pb(II) to Pb(IV) but are rarely observed in actual drinking water distribution systems (Wang et al. 2010). From field samples collected under free chlorine residual conditions, 28 of the 42 individual corrosion specimens contained lead dioxide minerals. Further subdividing the data into reports that included free chlorine concentration levels above 1.0 mg/L, 2 of the 6 samples contained lead dioxides. Comparatively, for conditions below 1.0 mg/L the frequency of lead dioxide was found in 11 of the 19 samples. Meanwhile, systems that used chloramines only found lead dioxide in 2 of 5 samples. Despite this small sample size, it is further proof that free chlorine has the capacity to oxidize lead to stable Pb(IV) compounds, and pipe age may be just as important as free chlorine concentration.

To examine the effects of corrosion inhibitor, the systems that used phosphate treatment saw lead dioxide minerals in 6 of 28 samples, while lead phosphate minerals were found in 9 of 28 samples. The difference in blended phosphates, polyphosphates, and orthophosphate will be further discussed in section 2.5. Briefly, the systems that were dosed with orthophosphate observed lead phosphate minerals in 7 of the 8 samples, agreeing with lab studies that found the phosphate interaction with lead should create lead phosphate compounds (Ng et al. 2012). Systems that were not exposed to a corrosion inhibitor all used free chlorine to create an insoluble PbO_2 layer on the pipe walls. This was found to work successfully as 19 of the 21 samples had some form of lead dioxide minerals.

The effect of pH may also play an important role in the formation of lead dioxide corrosion scales within lead pipes, although this was not found to be profound in the field pipe samples. For pH levels greater than 8, lead dioxide was detected in 5 of 10 samples. On the contrary, 26 of the 50 samples with a pH less than 8 contained lead dioxides. The role of pH is influenced by disinfectant residual type and corrosion inhibitor, but pH greater than 8.5 can increase stability of lead dioxides.

2.3 Iron Corrosion Minerals

Corrosion of iron drinking water pipes is a well-defined field that was given attention prior to lead drinking water pipe issues in the United States. Cast and ductile iron are very popular pipe materials chosen by drinking water distribution systems. The corrosion process for iron is similar to that of lead, with the main difference being the final elemental constituency. In general, a cast iron pipe is a special alloy of iron where the carbon content is larger than 2%. Silicon may also be present at variable weight percentages. As the name suggests, ductile iron pipes have more ductile properties thanks to their nodular graphite inclusions (Liu et al. 2002). The variability in formation processes to create cast iron will also play a significant role in the corrosion (Rajani & Makar, 2000).

In the process of forming cast iron pipes, a natural iron oxide layer develops on the surface of the inner pipe wall which provides a natural corrosive-resistant barrier (Larson & Skold, 1957). Cast iron corrosion had been reported extensively and can be defined by accumulation of nodules on the pipe wall called tubercles. The composition of the tubercles may or may not have similar characteristics and composition of the surrounding corrosion

scales. Growth proliferation of the tubercles creates the same effect of head loss and trace metal accumulation (McNeill & Edwards, 2001). The tubercles can create small crevices where localized pitting and crevice corrosion can occur of the base metal which can cause water loss through leaks (Mohebbi & Li, 2011).

Cast iron pipes are slowly being phased out for alternative materials such as steels, but it comes at a steep economic cost. In 1999 the American Water Works Association (AWWA) predicted the total cost to the United States Government for cast iron pipe replacement would be approximately $325 billion over 20 years (McNeill & Edwards, 2001). This study comes greater than 20 years after the AWWA's prediction and cast iron pipes are still greatly in use today in many distribution systems. From published field studies it is known that many of these pipes exceed 100 years of service life without replacement. In areas where partial lead service line replacements have been conducted, new iron pipes can create a galvanized connection that continues lead release (McFadden et al. 2011).

Ductile iron pipes have been a popular replacement choice for cast iron pipes since the 1960's (Szeliga & Simpson, 2003). The slower adoption of ductile iron pipes due to their later discovery and creation means that most of the pipes are much younger in service age and have not received as extensive of an internal corrosion overview. Ductile iron pipes are still susceptible to external corrosion via localized pitting and graphitization (Szeliga & Simpson, 2003). Few, if any, field studies have reported corrosion scaling mechanisms and products within ductile iron pipes.

Corrosion mechanisms and scale composition of cast iron pipes are well documented in past literature. Water quality parameters such as pH, alkalinity, disinfectant, and corrosion

inhibitor affect the final corrosion scale minerals (McNeill & Edwards, 2001; Zhu et al. 2014). General trends from bench-scale experiments find higher pH (above 9) leads to lower iron loss, and the inverse (pH below 9) produces more tubercles, and more iron is corroded (Larson & Skold, 1958; McNeill & Edwards, 2001). The effect of high alkalinity (and high concentrations of calcium) has been found to decrease the corrosive nature of cast iron pipes (Larson & Skold, 1957; Larson & Skold, 1958; McNeill & Edwards, 2001). The deposition of carbonate minerals that create a passivating layer of the pipe wall surface can prevent cast iron corrosion.

A standard pourbaix diagram for cast iron is not beneficial due to the additive variances of carbon in production. As a reference of pure iron speciation within water, figure 2-4 is included. From this figure we can garner that pure iron is stable across the entire pH spectrum under reducing conditions. When system potential increases, iron species are oxidized to Fe^{2+}, which increase in solubility. At even higher potentials Fe^{3+} species dominate, which have lower solubilities than Fe^{2+}. An empirical relationship to describe this phenomenon of solubility and oxidation state is described by the ratio below.

$$\frac{Z^2}{r}$$

Here, Z is the charge on the atom and r is the radius. The ratio of charge and radius gives an empirical approximation of the acidity. Ionic radii increase with increasing positive charge, and as the ratio increases the cation acidity increases. The calculated ratio for Fe^{3+} is higher than for Fe^{2+} and is categorized as a weakly acidic cation (Wulfsberg, 1987). Weakly acidic cations tend to form hydroxide minerals which are moderately insoluble. Thus, the solubility limit for Fe^{3+} compounds in drinking water conditions is higher than for Fe^{2+}, and the same is

true for the previously discussed lead speciation where higher oxidation states have lower solubility (Wulfsberg, 1987). In figure 2-4 it can be noted that increasing potential gives way to +3 chemical states of iron which could form insoluble corrosion scale films.

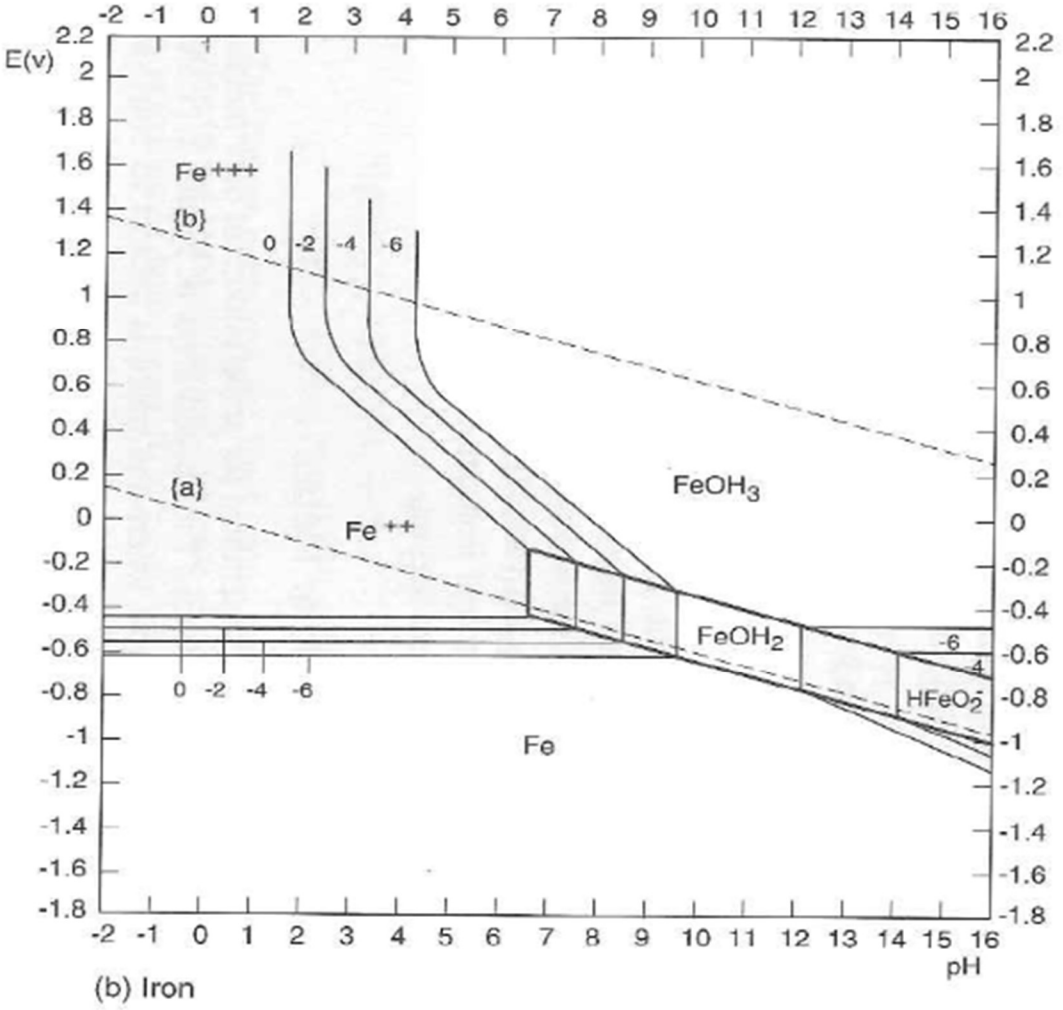

Figure 2-4. Pourbaix diagram of pure iron in water at 25° C (Jones, 1996).

Increasing levels of dissolved oxygen in distribution systems has the ability to oxidize elemental iron to ferrous (Fe(II)), and then ferric (Fe(III)) iron. A typical reaction may proceed in the following equations which are reversible (McNeill & Edwards, 2001).

$$Fe_{(s)} + \frac{1}{2}O_2 + H_2O \rightarrow Fe^{+2} + 2OH^- \quad (7)$$

$$Fe^{+2} + \frac{1}{4}O_2 + \frac{1}{2}H_2O + 2OH^- \rightarrow Fe(OH)_3 \quad (8)$$

In the equation 8 the base metal iron is oxidized to ferrous iron where it may form oxides or simple hydroxide/ionic complexes. If excess dissolved oxygen exists (or in the presence of a strong disinfectant residual which can promote high system potential) the ferrous iron complexes are oxidized to ferric compounds which form the more insoluble corrosion scales on the pipe walls.

An example of the many types of iron compounds found in corrosion scales can be found in table 2-4 (McNeill & Edwards, 2001). Iron in the +2-oxidation state may be present in the form of ferrous hydroxide, wustite, siderite, or vivianite. Some of these oxides and hydroxides may serve as stable precursors to +3-oxidation state complexes such as goethite, lepidocrocite, ferric hydroxide, akageneite, maghemite, ferric oxyhydroxide, iron hydroxycarbonate, and strengite. Minerals that feature a mixture of both chemical states are termed green rusts (Simon et al. 1997). These minerals often include other ions capable of substitution such as carbonates, sulfates, or hydroxides.

Table 2-4. Iron corrosion scale compounds found within drinking water pipes (McNeill & Edwards, 2001).

Name	Chemical Formula	Iron Oxidation State
Ferrous Hydroxide	$Fe(OH)_2$	II
Ferric Hydroxide	$Fe(OH)_3$	III
Wustite	FeO	II
Goethite	α-FeOOH	III
Akageneite	β-FeOOH	III
Lepidocrocite	γ-FeOOH	III
Hematite	α-Fe_2O_3	III
Maghemite	γ-Fe_2O_3	III
Magnetite	Fe_3O_4	II and III
Ferric Oxyhydroxide	$FeO_x(OH)_{3-2x}$	III
Siderite	$FeCO_3$	II
Iron Hydroxycarbonate	$Fe_x(OH)_y(CO_3)_z$	III
Green Rust	$Fe(III)_x(Fe(II)_x(OH)_y(CO_3,SO_4)_z$	II and III
Vivianite	$Fe_3(PO_4)_2{\cdot}8H_2O$	II
Strengite	$FePO_4$	III
Schrebersite	Fe_4P	Not Known

With abundance of alkalinity or dissolved inorganic carbon, carbonate-containing iron minerals such as siderite may form stable passivating layers preventing further corrosion (Sontheimer et al. 1981). Most iron minerals found within literature are oxides or hydroxides. The most frequently reported corrosion scale minerals in municipality surveys are goethite (α-FeOOH), lepidocrocite (ϒ-FeOOH), magnetite (Fe_3O_4), maghemite (α-Fe_2O_3), and siderite ($FeCO_3$) (Sarin et al. 2001; Lin et al. 2001; Sarin et al. 2004; Lytle et al. 2004; Copeland et al. 2007; Tammie et al. 2008; Teng et al. 2008; Peng et al. 2010; Yang et al. 2012; Li et al. 2016).

There are scarcely $Fe(OH)_3$ minerals identified, and a reason for this could be dehydration of the minerals leading to formation of FeOOH minerals such as goethite or lepidocrocite which are more stable (Lin et al. 2001).

Associated minerals found in real-world distribution systems vary based on water chemistry parameters such as corrosion inhibitor and water hardness. Some of the most frequently found minerals include quartz, calcite, and dolomite (Tuovinen, et al. 1980; Sarin et al. 2001; Lytle et al. 2004; Copeland et al. 2007; Tammie et al. 2008; Teng et al. 2008; Peng et al. 2010; Yang et al. 2012; Li et al. 2016). These are often analytically confirmed with EDS and ICP methods. In these studies, silicon in the treated water is commonly measured on the order of 2 – 10 mg/L but incorporated into the scales can be as high as 9% of the total weight (Sarin et al. 2001; Lin et al. 2001). The source of silicon may be from water contacting sand filtration media in the water treatment process, with silicon sorbing onto iron mineral surfaces of goethite, magnetite, and siderite (Philippini et al. 2006). This sorption behavior is profound in acidic conditions but decreases above pH 9.

Speciation of iron minerals can vary greatly based on water chemistry and pipe age. Increases in concentration of dissolved oxygen led to higher degree oxidation states of iron minerals by increasing the transfer of electrons from iron (LeChevallier et al. 1993). Natural organic matter in water has shown the ability to decrease corrosion rates, while total organic carbon levels may encourage the release of trace metals incorporated into the scales (McNeill & Edwards, 2001). Organic matter can compete for binding with metals such as iron to form stable complexes which reduce iron corrosion similarly to carbonate scales (LeChevallier et al. 1993). Corrosion rates generally decrease as pipes continue to age when stable scale layers are

formed, but accumulation persists when iron levels reach supersaturation and precipitate out of solution.

Biological factors within the municipality can alter the corrosion of iron. Biofilms may decrease the available surface for which iron corrosion scales may form, but they can also scavenge for oxygen which is required for scale formation (Lee et al. 1980). The type of bacteria present in the biofilm can also affect the iron corrosion scale by reducing or oxidizing present minerals (LeChevallier et al. 1993; Teng et al. 2008; Wang et al. 2012). Targeted disinfection practices aimed at killing bacterial populations can subsequently alter the corrosion minerals by changing the system potential. As previously mentioned (section 2.2), the choice of disinfectant and residual concentration has significant influence over the oxidation/reduction potential.

Changing water chemistry conditions or mechanical disturbances can dislodge or release iron and any accumulated trace metals back into the water. Excessive iron release from drinking water pipes is not an immediate health concern but can pose problematic odor and water color that can stain sinks and faucets. Iron is listed under the secondary contaminants with a maximum contaminant level of 0.3 mg/L (EPA[5], 2022). This is a non-enforceable standard established by the EPA as a guideline to avoid the aforementioned problems.

Accumulation of arsenic by adsorption onto iron minerals is a major problem for water resource engineers. Arsenic levels leaving drinking water plants must fall below the EPA standard of 10 ppb (EPA[2], 2022). The concentration of arsenic measured within iron corrosion scales may often be an order of magnitude greater, meaning that control of its release is essential to protect consumers (Lytle et al. 2004). Adsorption onto iron oxide/hydroxide minerals such as lepidocrocite have been key discoveries that translate to treatment

technologies for arsenic removal from water (Wang & Giammar, 2015). One study even found an arsenic-iron mineral, bukovskyite ($Fe_2(AsO_4)(SO_4)(OH)\cdot 7H_2O$), which would add more complexity to the accumulation of arsenic in iron corrosion scales (Lytle et al. 2004). Desorption and release into the water can be caused by pH shifts or orthophosphate addition as orthophosphate will compete with arsenic for binding sites on iron surfaces (Copeland et al. 2007).

2.4 Copper Corrosion Minerals

Copper drinking water pipes have been a popular choice due to their high corrosion resistance in many drinking water conditions. Copper itself is an essential nutrient required by humans at low levels, and it is speculated that the majority of the copper in most humans' diets could come from direct copper release or water/copper interactions in distribution systems (Zacarias et al. 2001). Copper is especially suitable for municipalities replacing lead service lines. In situations with partial replacement, contact between lead and copper can result in galvanic corrosion of lead which is documented extensively (Ng et al. 2020). In the galvanic coupling of lead and copper, lead will be more active and corrode preferentially while copper is protected. Not documented as extensively are the copper compounds and associated minerals found in real distribution system corrosion scales.

When elemental copper is exposed to moist air it develops an iconic green layer of corrosive film, as seen most famously on the Statue of Liberty. In atmospheric conditions this is likely a corrosive film of copper carbonate and hydroxide minerals. This film is passive corrosion and works to protect the underlying base material from severe damage. The same is true within

drinking water, where corrosive effects are magnified by elemental contamination and corrosive water. Initially exposed to water, the inner copper wall will form a cuprous oxide (Cu(I)) layer (Lane, 1993). When Cu(I) is oxidized to Cu(II) it can form a wide variety of minerals (Turek, 2006). Cupric oxide is an example of this, as are copper hydroxide and carbonate minerals such as malachite ($Cu_2CO_3(OH)_2$). Malachite is very stable and has low solubility in drinking water (Scaife, 1957).

The formation of cuprous oxide as a protective barrier on the pipe surface is itself a form of corrosion control. A few field studies uncovered a decreasing trend of copper corrosion with relative pipe service age. In these studies, younger pipes exceeded the EPA water standard for copper at a higher rate than older pipes (Knobeloch et al. 1998; Cantor et al. 2000). This finding assumes that the passive film is stable under consistent environmental conditions and inhibits release of copper.

Like with iron and lead pipes, there are trends that lead to corrosive behavior of drinking water pipes. General trends such as low alkalinity, calcium, and dissolved oxygen, as well as high concentrations of disinfectant residual (free chlorine) can increase the level of corrosion scaling on the copper base material. With low alkalinity and calcium concentrations (soft water) it becomes difficult for carbonate minerals to precipitate in metal minerals or as associate minerals such as calcite and dolomite. Increased dissolved oxygen levels and highly oxidizing disinfectant use of free chlorine can promote corrosion by accepting electrons (oxygen as the electron acceptor) and raising the system potential (figure 2-5).

Copper in the elemental state can be found at a wide range of pH values at mostly negative potentials. Within the water-stable dotted lines copper can be found in as Cu(0), Cu(I),

and Cu(II) dependent on the pH and potential. The Cu(I) state appears in a very small sliver at neutral potential values and at a pH spectrum that covers drinking water conditions and beyond. Increasing potential creates Cu(II) species such as oxides, hydroxides, and other complexes with ions. Variability in water chemistry such as switching the disinfectant residual from chloramines to free chlorine would increase the potential to oxidizing conditions, changing the scale composition from insoluble cuprous oxide to soluble cupric oxides. If the reverse is true, chloramine or dissolved oxygen may act as electron acceptors and cuprous minerals will precipitate onto the pipe walls (Palit & Pehkonen, 2000).

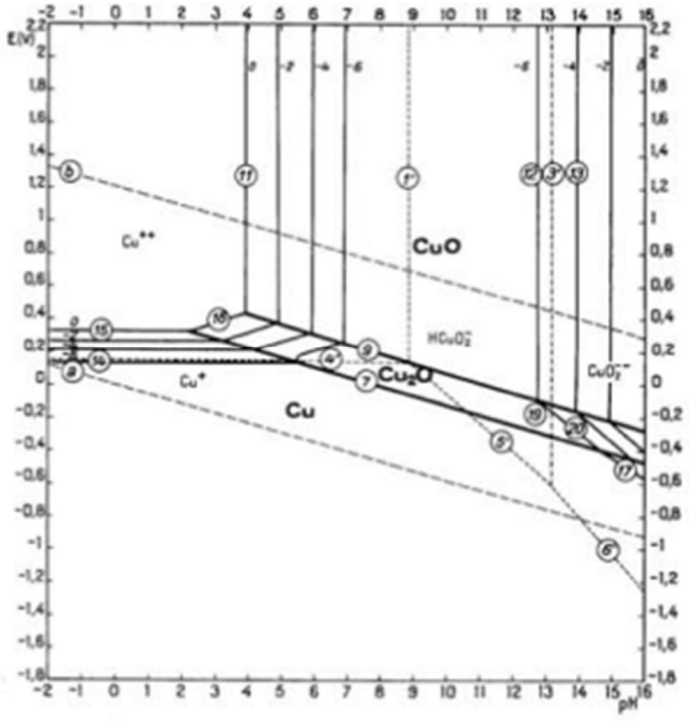

Figure 2-5. Pourbaix diagram of copper in H_2O system at 25° C. Potential in volts on the y-axis with pH on the x-axis (King, 2010).

A theoretical foundation for the corrosion of copper is shown through electrochemical potential of half-cell reactions for copper below. Contrasted against dissolved oxygen reduction

in water, both half reactions involving copper oxidation and reduction have lower potentials (Jones, D. A. 1996). Thus, copper will serve as the anode in either state and transfer electrons to oxygen. This reaction will proceed until the dissolved oxygen is fully consumed, such as in stagnant water.

$$Cu^{+1} + e^{-} \rightarrow Cu \qquad E^{o} = -0.52\ V \tag{9}$$

$$Cu^{2+} + 2e^{-} \rightarrow Cu^{+1} \qquad E^{0} = 0.342\ V \tag{10}$$

$$O_{2\,(g)} + 4H^{+} + 4e^{-} \rightarrow 2H_2O \qquad E^{o} = 1.23\ V \tag{11}$$

Recent studies of these minerals and their formation mechanisms have sprouted around the LCR as municipalities aim to be compliant with dissolved copper concentrations. The EPA has established a maximum contaminant limit of 1.3 ppm in treated water effluent (EPA[2], 2022). Understanding the pathways to formation affected by water quality is important in controlling the release of copper and associated contaminants to the water. For instance, Cu_2O films which usually form first in drinking water systems can be destabilized by pH at or above 8.5 and high dissolved organic carbon concentrations (Palit & Pehkonen, 2000). The film is converted to copper-carbonate minerals such as malachite, or if the concentrations are sufficient, calcite or dolomite which are stable. Cu_2O can be quickly converted to $Cu(OH)_2$ or copper-carbonate minerals, which dehydrates over time to form CuO (Patterson et al. 1991).

Oxides and hydroxides are the main forms of copper corrosion minerals found in pipe scales, but there are many ions that can complex with copper. Copper in the +1-chemical state is mainly found as cuprite (Cu_2O) but can be found with other ions with a single negative charge such as CuCl (Turek, 2006). The more insoluble cupric minerals include tenorite (CuO), and

malachite ($Cu_2(CO_3)(OH)_2$) (Lagos et al. 2001). Other minerals featuring more complex ions include langite ($Cu_4(OH)_6(SO_4)\cdot H_2O$), atacamite ($Cu_2(OH)_3Cl$), brochanite ($Cu_4(SO_4)(OH)_6$), and azurite ($2CuCO_3\cdot Cu(OH)_2$) (Lagos et al. 2001; Turek, 2006). Bench and field studies have agreed that at pH levels above 7 the initial cuprite mineral is oxidized to malachite or tenorite, while pH below 6 could see scale transformation to langite or brochantite (Lagos et al. 2001). Malachite is often found in aged pipes and controls the release of copper ions and trace metals into solution due to its low solubility (Scaife, 1957; Lagos et al. 2001; Turek, 2006). This supports the hypothesis that copper release decreases as service life increases.

2.5 Corrosion Inhibition

To control internal corrosion of the pipe wall, many drinking water plants add a chemical that creates a stable passive film. While some municipalities opt for a direct corrosion inhibitor, some plants leverage pH control or disinfectant residual levels to preferentially select for a passive layer. Drinking water engineers have discovered that many naturally occurring minerals can accomplish this feat, such as calcite precipitation in cast iron pipes (Heyer, 1888; Larson & Skold, 1957). Calcite in the presence of high alkalinity and pH precipitates from solution below the theoretical solubility limit and can be engineered to protect less stable iron minerals to stop iron or trace metal release. Another carbonate mineral, siderite ($FeCO_3$) can perform the same task of corrosion inhibition in iron pipes and may even perform better than +3-oxidation state iron minerals (Sontheimer et al. 1981; McNeill & Edwards, 2001).

Bench experiments and field-scale surveying of internal corrosion are important in identifying the mechanisms of corrosion scale accumulation. The at-large goal is to engineer

scales on the pipe walls that display high stability under day-to-day drinking water chemistry changes with low solubility. Typically, this can be accomplished by oxidizing from moderately soluble metal minerals such as litharge (PbO) to plattnerite or scrutinyite (PbO_2 species). Disinfectant residuals and dissolved oxygen are environmentally important oxidizers present in distribution system water. Free chlorine as a disinfectant residual is often chosen when lead pipes are in service to ensure PbO_2 scale formation. Chloraminated waters have lower redox potential and may not be able to fully oxidize to more insoluble corrosion minerals (Edwards & Dudi, 2004). Switching from chloramines to free chlorine may be beneficial in lead corrosion control but can lead to consumer complaints about smell, as well as the ability to form more disinfection byproducts. Switching from free chlorine to chloramines should be done with great caution to not revert the corrosion scales to higher solubility phases (Lin & Valentine, 2008). This can be accomplished by coupling the change in disinfectant residual with pH changes.

The pH equilibria in formation processes for corrosion minerals are very complex systems that rely on water chemistry parameters such as dissolved inorganic carbon content and dissolved oxygen. Following the formation of insoluble lead minerals plattnerite (β-PbO_2) and scrutinyite (α-PbO_2), raising pH levels above 8.5 will increase the stability of the minerals, but may also encourage calcite deposition (Maynard, 2008). A drop in redox potential can transform plattnerite to either cerussite or hydrocerussite, depending on the pH as depicted in figure 2-6. Thus, it can be observed that increasing pH levels in the absence of corrosion inhibitor can preferentially induce formation of relatively insoluble lead minerals.

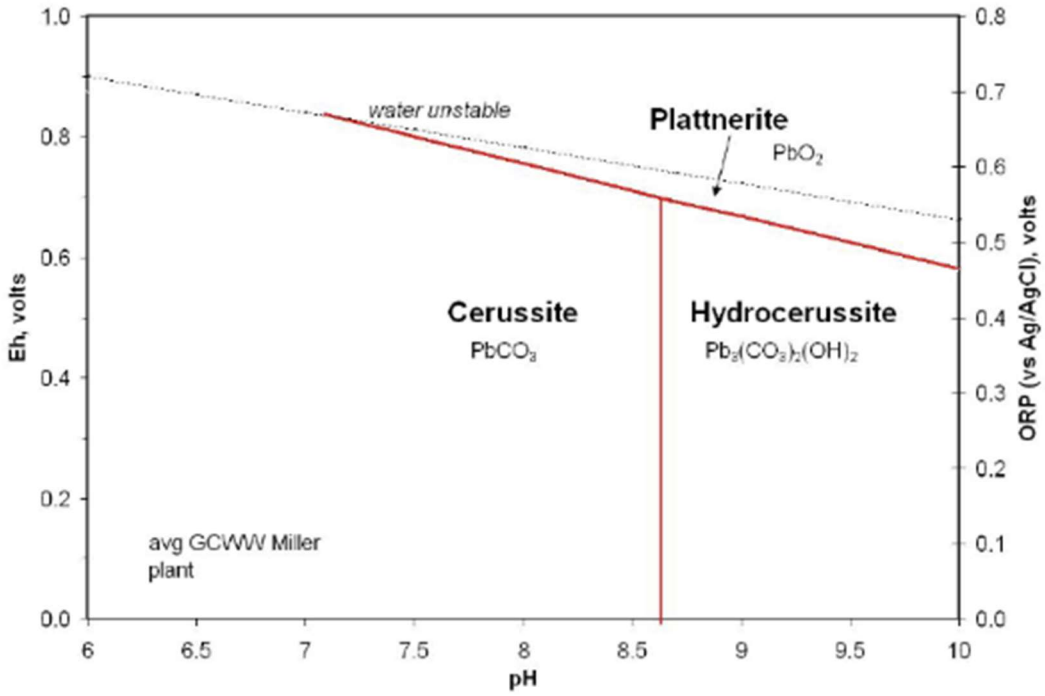

Figure 2-6. pH relationship between cerussite, hydrocerussite and plattnerite transformation in high redox conditions (Maynard, 2008).

Understanding the effect of pipe age is very important, as water with lower redox potentials may still form stable layers that passivate and protect against corrosion, such as calcite. While initially the accumulation of a carbonate layer is a beneficial protection, significant accumulation will decrease flow. Adding corrosion inhibitors can limit the quantity of calcium precipitation. Copper release from laterals has been shown to decrease as service life increases, a positive trend that can be attributed to a constant source of dissolved oxygen or disinfectant residuals. This theory is nullified if conditions are not conducive to oxidize directly to malachite or tenorite, and intermediate copper phases are formed such as phosphates (Edwards et al. 2001). In lab studies it has been found that low pH and soft waters combined to increase copper release (Boulay & Edwards, 2001). In the absence of sufficient alkalinity,

increasing pH above 9 under free chlorine conditions has prevented copper release (Edwards & Fergusion, 1993). It should be noted that many of these lab studies could not reproduce the diverse drinking water conditions, and had short experimental lifecycles compared to real-world applications.

Many distribution systems opt for an additive corrosion inhibitor to induce passive films. Among the chosen chemicals for corrosion inhibition are silicates and phosphates. Polyphosphate and orthophosphate have well-understood mechanisms of corrosion control for lead, copper, and iron. Polyphosphates in the presence of high pH tend to revert to orthophosphate which has demonstrated high performance in reducing lead release as evidenced by lower concentrations at the tap (Schock & Clement, 1996). Orthophosphate addition controls the release of lead by having the ability to complex with lead creating compounds such as hydroxypyromorphite ($Pb_5(PO_4)(OH)$) or chloropyromorphite ($Pb_5(PO_4)_3Cl$) which is very stable (Ng et al. 2012). By creating lead phosphate minerals, orthophosphate inhibits the development of PbO_2 minerals even in the presence of free chlorine, allowing the lead phosphate minerals to control lead speciation and release (Lytle et al. 2009). Although orthophosphate controls the release of dissolved lead concentrations, it may still increase particulate lead release (Xie & Giammar, 2011).

Optimum pH values for orthophosphate dosing for lead control are between 7.2 – 7.8 but are also dependent on dissolved inorganic carbon concentration (Shock & Clement, 1996). Many distribution systems must manage pipes of varying material and can't choose the optimum pH value based on corrosion control mechanisms for a single material, such as lead. If orthophosphate is chosen as the corrosion inhibitor in a distribution system that has lead and

copper pipes, a pH below 8 is essential (Shock & Clement, 1996). Without an added corrosion inhibitor, increasing pH above 9 in systems with low dissolved inorganic carbon can achieve the same effect (Xie & Giammar, 2011). If PbO_2 scales are not already present, lead-carbonate minerals such as hydrocerussite could also be controlled by increasing pH without addition of orthophosphate (Noel et al. 2014). Temperature effects should not be neglected either. Seasonal temperature variance (increasing temperature from 5° C to 20° C) can have a larger effect on the solubility of hydrocerussite than increasing pH from 7 – 9.5 (Mohammadzadeh et al. 2015). Temperature has been studied to a lesser extent and warrants further consideration in future projects.

Polyphosphate and blended phosphates in high concentrations have proven to be detrimental to lead release. Polyphosphate exhibits a strong ability to remove iron from water and prevent excessive calcium carbonate scale formation (Klueh & Robinson, 1988; Cantor et al. 2000). Natural transformation to orthophosphate mitigates the aforementioned feature of sequestration. A pH increase also decreases sequestration ability and corrosion inhibition of polyphosphate.

Lead and iron corrosion control are often linked due to sorption mechanisms between the two. One study examining the effects of lowering pH from 10.3 to 9.7 found that iron was controlled more effectively at the higher pH, whereas lead release peaked at higher pH (Masters & Edwards, 2015). From the many publications of iron corrosion studies, the role of water chemistry on corrosion inhibition has been extensively investigated. Higher pH levels (generally above 8) and increased alkalinity decreases iron release and subsequent by-product release (McNeill & Edwards, 2001).

Silicates are less commonly used but have a long history as a corrosion inhibitor. Silica is present in most source water naturally and helps to assume this preventative action, but some distribution systems opt for additional sodium silicate. Originally proposed for lead control, it showed strong performance in prevention of iron and copper corrosion as well (Stericker, 1938). The mechanism by which corrosion inhibition occurs is through silica incorporation into existing scale minerals, such as iron hydroxides and lead carbonates (Lintereur et al. 2010; Woszczynski et al. 2015). Incorporation into the scale matrix may take a few months. Iron and manganese have strong affinity for sodium silicate and can adsorb onto silicate particles, effectively reducing concentrations in the bulk water (Robinson et al. 1992).

In head-to-head comparisons of orthophosphate and sodium silicate applications on identical water, orthophosphate reduced lead concentrations by an order of magnitude (Li et al. 2021). Higher dosing concentrations of sodium silicate increased the release of both iron and lead. Hydrocerussite was found to be the primary lead corrosion mineral responsible for controlling lead release.

Cost must also be considered when choosing a corrosion inhibitor. When alkalinity and dissolved inorganic carbon are low, pH adjustment alone will not suffice to precisely control lead release. Addition of orthophosphate could become costly, as in 2007 - 2008 the price of phosphorus skyrocketed 800% (McGill, 2012). Doubled as a finite commodity that sees extensive uses in fertilizers, sodium silicate is a cheaper alternative. It can clearly be stated that corrosion control mechanisms are complex and require full understanding of the entire water chemistry, including comprehensive forensic analysis of the current corrosion scales in place in a distribution system. That is why field studies like this are so important.

2.6 Accumulation of Trace Metals

Corrosion scale composition has many effects on the accumulation and release of trace metals. Corrosion control measures are put in place not just to control release of the base metal, but to also limit release of the trace metals incorporated into the scale. The mechanism of trace metal accumulation may be multi-fold: supersaturation from the bulk water, adsorption from contact, oxidation/reduction reactions, and complexation with the scale material. The abundance and degree of trace metals in corrosion scales is often unique to each individual distribution system and highly dependent on the source water and water treatment processes.

Aluminum levels may be raised by direct addition of alum (aluminum sulfate or polyaluminum chloride) as a coagulant. High concentrations of aluminum can lead to supersaturation and precipitation of compounds such as aluminum hydroxides, which could sorb lead and induce mass release of lead back into the water (Kvech & Edwards, 2001). Even if aluminum-containing minerals are not observed, amorphous aluminum phases could be persistent sources of aluminum. Other factors such as a high chloride to sulfate mass ratio (CSMR) and alkalinity increase the adsorption of lead onto aluminum (Knowles et al. 2015). Correlations of high concentrations of aluminum in corrosion scales and lead are thus expected.

Manganese is often a very prevalent metal in corrosion scales. It has many natural sources and can be found in carbonate minerals and forms oxides that precipitate on scales or adsorbs into iron scales with relative ease (Gerke et al. 2016). These deposits have a strong affinity for sorbing other metals such as iron and lead. Sequential extraction analyses of trace

metal binding to manganese deposits help uncover the potential release mechanisms. If pipe deposits are recognized as sinks for trace metals, their stability is pivotal for limiting release to drinking water. In cases of very high levels of manganese, scale formation may compete with metals such as lead and force particulate concentrations to be higher by limiting binding sites.

Galvanic connections of pipes can cause corrosion of the anodic metal with mass release of that metal which can adsorb onto the cathodic material. Direct iron and lead connections can cause lead to corrode and become adsorbed to the surface of iron corrosion minerals. Even after lead pipes have been partially or fully replaced, the residual lead can incorporate into the iron scale which then controls the release of lead (McFadden et al. 2011). The same can be said for copper pipes which are cathodic to lead when galvanically connected.

Trace metals must be examined on the basis of their potential sources with respect to each source water which is unique to a distribution system. Treated water conditions meeting the EPA's water quality standards will not have sufficient trace metal concentrations which will precipitate from solution; adsorption from long contact in stagnant water will play a large role on the incorporation of these elements into corrosion scales. In most studies the total weight of a trace metal (exempting aluminum, manganese, magnesium, calcium, iron, copper, and lead) is not likely to exceed 1%. As pipes continue to age the concentrations might appreciate significantly to the point where their release could cause detrimental health effects on consumers.

2.7 Knowledge Gaps in Literature

Many studies have covered the presence of drinking water pipe corrosion products in real distribution systems, but they only cover a single pipe material, or a single distribution system. For the studies that encompass many distribution systems, the examination of a single pipe material is not representative of the plumbing of the entire system. The need for different materials to produce mains and laterals requires dissimilar metals to be used as service lines, and thus should also be studied. There is a need to understand the effect of water chemistry in a single distribution system on different pipes materials, such as lead, iron, and copper.

In addition, examining multiple pipe materials from different distribution systems with dissimilar water chemistry (source water, disinfectant residuals, corrosion inhibitor, etc.) has not been studied. Cast iron internal corrosion has been well-documented by field studies, but a comparison of ductile iron, which is also widely used, has never been done before. The extent of mineral speciation and trace metal accumulation in ductile iron pipes is poorly understood compared to cast iron.

Finally, sequential extraction experiments derived from soil analysis have been adapted recently for pipe deposits of iron pipes. There has yet to be an extension of this experiment to copper and lead pipes, despite the high frequency of use in distribution systems. This experiment is essential in uncovering the binding fractions for which trace metals are found within pipe deposits and may be indicative of their release mechanisms. The aforementioned knowledge gaps are what will make this study novel, by building off of the extensive work of past researchers in this field.

Chapter 3: Methods

3.1 Study Area

This research examined three drinking water distribution systems in the Milwaukee-Metropolitan area: Milwaukee, Oak Creek, and Waukesha. A geographic representation of the study area is shown in figure 3-1. Milwaukee residents are supplied drinking water by the Milwaukee Water Works. Two drinking water treatment plants in Milwaukee, Howard Avenue and Linnwood, provide water to roughly 867,000 residents (Milwaukee Water Works, 2022). First, water pumped from Lake Michigan undergoes ozone disinfection for primary treatment to kill potentially pathogenic microorganisms. Removal of solids, fats, and greases is accomplished through coagulation (through addition of chemicals such as alum) and flocculation, followed by settling. Biologically active filtration precedes secondary disinfection by dosing chlorine. A residual level of chloramines (0.8 - 1.4 mg/L) is maintained in the distribution system to ensure bacterial levels aren't proliferating in the drinking water pipes. Orthophosphates are utilized as a corrosion inhibitor. Table 3-1 lists the finished water quality for each municipality.

The Oak Creek Water and Sewer Utility draws water from Lake Michigan to provide drinking water to the 70,000 residents of Oak Creek, the neighboring city of Franklin, and the village of Caledonia (Oak Creek Water and Sewer Utility, 2022). Oak Creek has won national awards for water quality, their water treatment facility, and the maintenance of the distribution system network of pipes. Oak Creek has not had lead pipes in operation since 1993 and opts not to add a corrosion inhibitor for additional protection. The general water treatment process

is similar to that of Milwaukee, and free chlorine is chosen as the disinfectant residual at a concentration of 0.8 – 1.2 mg/L.

The Waukesha Water Utility pumps water from deep sandstone wells located in the St. Peter Sandstone aquifer at depths of 1,600 – 2,300 feet, and shallower sand and gravel wells located at depths of 105 – 149 feet (Waukesha Water Utility, 2022). This sandstone layer contributes to significantly harder water compared to Oak Creek and Milwaukee. Stuck between a shale layer, groundwater recharge has become too slow to meet the demands of the growing population of Waukesha and has been significantly drawn down. Arsenic and radium are naturally occurring in this geologic layer and in the past have exceeded EPA limits of drinking water regulations. Hydrous manganese oxide treatment processes are in place to remove radium. As of 2016 Waukesha was awarded the right to become the first non-bordering entity to obtain access to Lake Michigan water, an undergoing project that is set to complete around 2023. Waukesha water is served to over 72,000 residents.

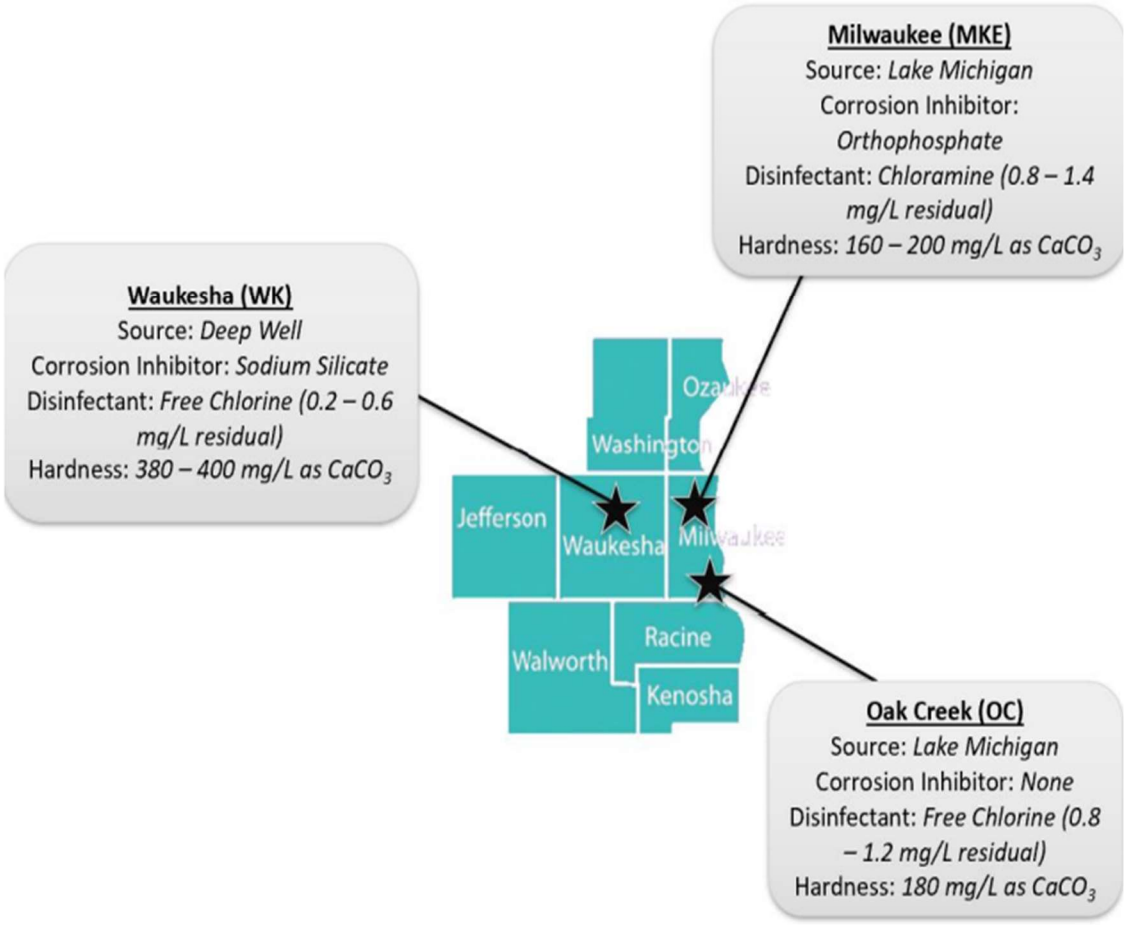

Figure 3-1. Geographic depiction of Waukesha, Oak Creek, and Milwaukee DWDS service area.

De-commissioned lead, iron, and copper drinking water pipes were obtained from each drinking water distribution system from 2017 – 2021. Service life of the pipes ranged from 15 – 105 years old. Due to the large size of some mains, corrosion scales were scraped, and the solids were collected directly in the field. Pipe samples were wrapped in plastic and sealed to preserve moisture content and avoid further oxidation during transport and storage prior to solids analysis. The full list of samples is listed in table 3-1.

Table 3-1. Pipe sample material and age from respective DWDS.

Sample ID	DWDS	Material	Service Type	Age (Years)
MKE-1	Milwaukee	Copper	Lateral	69
MKE-2	Milwaukee	Lead	Lateral	74
MKE-3	Milwaukee	Lead	Lateral	89
MKE-4	Milwaukee	Cast Iron	Main	66
MKE-5	Milwaukee	Cast Iron	Main	69
MKE-6	Milwaukee	Lead	Lateral	79
MKE-7	Milwaukee	Cast Iron	Main	63
MKE-9-Cu	Milwaukee	Copper	Lateral	100
MKE-9-Pb	Milwaukee	Lead	Lateral	100
MKE-10	Milwaukee	Lead	Lateral	93
MKE-11	Milwaukee	Cast Iron	Main	66
MKE-12	Milwaukee	Cast Iron	Main	64
MKE-13	Milwaukee	Copper	Lateral	-
MKE-14	Milwaukee	Ductile Iron	Lateral	15
MKE-15	Milwaukee	Cast Iron	Main	66
MKE-17	Milwaukee	Cast Iron	Main	-
MKE-17-1	Milwaukee	Cast Iron	Main	-
OC-1	Oak Creek	Copper	Lateral	54
OC-2	Oak Creek	Ductile Iron	Main	38
OC-4	Oak Creek	Ductile Iron	Main	33
OC-5	Oak Creek	Ductile Iron	Main	38
OC-6	Oak Creek	Ductile Iron	Main	38
OC-7	Oak Creek	Ductile Iron	Lateral	-
WK2-Pb	Waukesha	Lead	Lateral	105
WK2-Fe	Waukesha	Cast Iron	Lateral	105
WK3-Fe	Waukesha	Cast Iron	Lateral	72
WK-Cu	Waukesha	Copper	Lateral	-

3.2 Characterization Methods

The harvested pipes were cut longitudinally using a table saw so that the insides of the pipe could be examined. The corrosion scales were scraped from the pipe walls and collected. The samples were then ground to a homogenous fine powder using a mortar and pestle. Morphological analysis was conducted on the solid samples using X-ray diffraction (XRD) to determine the mineralogical composition and crystalline structure. XRD was performed using a Bruker D8 Discover A25 diffractometer utilizing copper-Kα radiation. The X-rays were generated in a copper tube at 40 kV and 40 mA. 2Θ stepwise scanning was conducted over the range of 10 - 80° at a 0.03° step size. Diffraction patterns were analyzed using the Bruker software featuring a reference pattern database provided by the International Center for Diffraction Data (ICDD, 2022).

X-ray photo-electron spectroscopy (XPS) is a quantitative technique for examining elemental speciation within the top few nanometers (normally 1 – 10 nm) of a sample. X-rays penetrate the sample and emit photoelectrons which have a binding energy that can be quantified by the instrument. The binding energy is determined by the bonding of the atoms, so the chemical state of the atom can be determined by plotting the binding energy against the intensity and comparing it to reference spectra. This is a useful supporting technique for XRD for distinguishing compounds that may have multiple reference patterns that exhibit overlapping peaks. XPS was conducted using a PerkinElmer PHI 5400 ESCA instrument utilizing a magnesium anode to generate X-rays.

Energy-dispersive spectroscopy (EDS) provides a semi-quantitative analysis of elements using a spectrometer in a scanning electron microscope (SEM). Analysis was performed on a JEOL 6460LV SEM utilizing an EDS Oxford detector at accelerating voltages of 5 – 15kV. This analysis was included as a check to determine the presence of constituents such as oxygen, carbon, phosphorus, and silicon. SEM images were obtained from a Hitachi S-4800 Ultra High-Resolution Cold Cathode Field Emission Sanning Electron Microscope.

3.3 Elemental Quantification Methods

Elemental quantification for trace metal constituents in the corrosion scales was conducted via inductively coupled plasma mass spectrometry (ICP-MS). This required acid digestion using concentrated nitric acid (HNO_3) and hydrochloric acid (HCl) to release the inorganic elements into solution. The chemical digestion was conducted by adding 2 mL of ICP-MS analytical grade HCl and 8 mL ICP-MS analytical grade HNO_3 to approximately 20 mg of corrosion scale sample. Corrosion scale samples were ground down to a fine, homogenized powder using a mortar and pestle.

The acidified solutions were carefully inverted in sealed test tubes to ensure complete mixing. The test tubes were heated for 4 hours at 100° C using a Thermo Scientific Orion COD165 Thermoreactor. The test tube caps were loosened during heating to prevent pressure buildup due to boiling and subsequent gas release during the reaction. The test tubes were allowed to cool to room temperature prior to dilution with water. Many sample dilutions were required based on elemental concentrations outside of the calibration curve or limit of

detection/quantification (LOD/LOQ) of the ICP-MS instrument and ranged from 100 – 10,000x. HNO_3 and HCl concentrations in the final samples were kept at 2% and 1% by volume respectively, and an internal standard for instrument accuracy was added at 1% by volume. Any remaining suspended particles were filtered using 0.22 µm polyethersulfone membrane filters attached to a plastic syringe.

ICP-MS analysis was performed using a Thermo Scientific Element 2. The quantified inorganic elements of interest were Al, As, Ba, Cr, Cu, Fe, Mn, Ni, Pb, V, U, and Zn. The LOD and LOQ for each element analyzed by the ICP-MS instrument is shown in table 3-2. Samples and method blanks were run in triplicate for quality assurance and data reproducibility. Hypothesis testing for statistical significance was conducted using a p-value of 0.05 assuming unequal variances between the samples.

Table 3-2. LOD and LOQ for ICP-MS elemental analysis.

Element	STD (ppb)	LOD (ppb)	LOQ (ppb)
As	0.018	0.058	0.176
Al	0.356	1.174	3.557
Ba	0.015	0.049	0.148
Co	0.013	0.043	0.131
Cr	0.024	0.079	0.241
Cu	0.021	0.07	0.211
Fe	0.231	0.761	2.305
Mn	0.048	0.158	0.478
Ni	0.024	0.079	0.239
Pb	0.022	0.072	0.217
Se77	0.043	0.142	0.431
Se78	0.037	0.123	0.373
Th	0.088	0.289	0.876
Tl	0.029	0.095	0.288
V	0.015	0.051	0.154
U	0.02	0.065	0.197
Zn	0.145	0.479	1.451

Atomic absorption spectroscopy (AAS) enabled the quantification of calcium and magnesium, which did not have very precise calibration curves on the ICP-MS instrument. AAS was performed using an iCE-3000 series instrument featuring Visimax II Hollow cathode lamps for calcium and magnesium. An internal standard of 5% lanthanum oxide (La_2O_3) was added to the samples at 2% by volume.

3.4 Sequential Extraction Method

Sequential extraction experiments were performed on the corrosion scale solids to determine the speciation of inorganic contaminants within five fractions as described by Tessier (Tessier et al. 1979). This method was adapted from the soil sciences as a means to identify the accumulation of trace metals within different types of sediments. The fractions represent the method of accumulation for the trace metals and can also be indicative of release mechanisms. The five fractions are ordered by likelihood of release back into the distribution system under drinking water conditions. In order by most likely to be released under drinking water conditions:

Fraction 1) Exchangeable

Fraction 2) Bound to Carbonates

Fraction 3) Bound to Iron/Manganese Oxides

Fraction 4) Bound to Organic Matter

Fraction 5) Residual

For each corrosion scale analyzed, the samples were reproduced in triplicates with method blanks. The effects of solid loading on each metal's majority fraction were also analyzed and are described further in the results. The Exchangeable fraction is the most susceptible fraction to release trace metals back into the water system from corrosion scales.

To release this fraction from the solids, the Tessier method was applied (Tessier et al. 1979). A 1 M solution of magnesium chloride (8 mL) was added to each sample and the pH was kept constant at 7.0. The samples were inserted into a shaker table for constant agitation at 275 revolutions per minute for 1 hour.

For the Carbonates fraction, a 1 M solution of sodium acetate (8 mL) was added to the remaining solid from the exchangeable fraction and the pH was constant at 5.0 by addition of acetic acid (Tessier et al. 1979). The samples were placed onto a shaker table for constant agitation at 275 revolutions per minute for 5 hours. The remaining solids were carried over to analyze the Iron/Manganese Oxides fraction. A solution of 0.04 M hydroxylamine hydrochloride (20 mL) was prepared in 25% (by volume) acetic acid and added to the solids (Tessier et al. 1979). The samples were heated to 96° C inside of an oven for 6 hours. The samples were inverted for mixing every 30 minutes.

For the Organic Matter fraction a solution of 0.02 M HNO_3 (3 mL) and 30% hydrogen peroxide (5 mL) were added to the remaining solids (Gupta & Chen, 1975; Tessier et al. 1979). Additional HNO_3 was added to keep the solution pH at 2.0. This solution was heated to 85° C for 3 hours and the samples were inverted every 30 minutes for mixing. An additional 3 mL of 30% hydrogen peroxide was added to each sample and heated again to the same temperature for 3 hours with mixing every 30 minutes. The samples were then allowed to cool prior to addition of 3.2 M ammonium acetate (5 mL) in 20% (by volume) HNO_3. Ultrapure water was added to reach a final solution volume of 20 mL, and the samples were placed on a shaker table at 275 revolutions per minute for 30 minutes.

The final Residual fraction represents the portion of trace metals that are not likely to be released under drinking water conditions (Tessier et al. 1979). Acid digestion was conducted using the same method listed previously (Section 3.4). Briefly, 8 mL HNO_3 and 2 mL HCl were added to the remaining solids from the previous fraction. The samples were heated to 100° C for 4 hours and all solids were extracted. All samples were analyzed using the ICP-MS (section 3.4).

Following each reaction period for the respective fractions, ultrapure water was added to dilute the total sample volume to 20 mL (unless the samples were already at this volume) and centrifuged at 6000 revolutions per minute for 20 minutes (Tessier et al. 1979). Following the resulting separation of solid and liquid, the supernatant was collected via pipette and filtered through a 0.22 µm polyethersulfone membrane filters fixed at the end of plastic syringes. This was repeated twice to collect and filter the supernatant and the final volume was fixed to 50 mL using ultra-pure water. The remaining solid in the centrifuge tubes were carried over to the next fraction. The residual liquid was analyzed using ICP-MS for elemental constituents similar to the total digestion analysis. The liquified samples were acidified using HNO_3, HCl, and an internal standard was added for ICP-MS analysis as stated previously (Section 3.4).

Chapter 4: Results and Discussion

4.1 XRD Results and Discussion

4.1.1 XRD Analysis of Iron Pipes

XRD analysis was performed on all available samples regardless of sample size. Samples were homogenized into a fine powder using a mortar and pestle and spread evenly into a sample holder so that a consistent sample height was maintained. Smaller samples were placed onto a quartz puck which was inserted into the center of the sample holder. This ensured the sample height was consistent with the sample holder for accurate measurements. Chemical filters and reference patterns from the International Center for Diffraction Data (ICDD, 2022) were provided in the packaged software through Bruker.

All three municipalities had iron pipes, predominantly used as mains to transport water from the water treatment plants to the edge of the service property. 9 samples were collected from Milwaukee (8 cast iron mains, 1 ductile iron lateral), 4 from iron mains (all ductile iron) in Oak Creek, including 1 ductile iron lateral in Oak Creek, and two cast iron lateral pipes from Waukesha. Some duplicates were run, representing different sampling areas within the same pipe. OC-5 and OC-6 are duplicate samples from different sections along the same pipe, as are MKE-17 and MKE-17-1. The pipe ages ranged from 14 – 105 years of service, with Oak Creek

having younger service lives (Table 3-1). The full XRD results for iron are shown in table 4-1 below.

Table 4-1. XRD results for Iron pipe samples.

Sample ID	XRD Match
MKE-4	Goethite, Lepidocrocite
MKE-5	Goethite, Lepidocrocite
MKE-7	Goethite, Lepidocrocite
MKE-11	Goethite, Lepidocrocite, Dolomite
MKE-12	Goethite, Lepidocrocite
MKE-14	Amorphous Iron Phase, Calcite, Dolomite, Quartz
MKE-15	Goethite, Lepidocrocite, Dolomite
MKE-17	Amorphous Iron Phase, Calcite, Dolomite, Quartz
MKE-17-1	Goethite, Lepidocrocite
OC-2	Amorphous Iron Phase, Calcite, Dolomite, Quartz
OC-4	Amorphous Iron Phase, Calcite
OC-5	Amorphous Iron Phase, Quartz, Dolomite
OC-6	Amorphous Iron Phase, Calcite, Dolomite
OC-7	Goethite, Calcite
WK2-Fe	Goethite, Calcite
WK3-Fe	Goethite, Quartz

In general, the dominant iron corrosion products were goethite (α-FeOOH) and lepidocrocite (γ-FeOOH). Goethite was detected in 10 of the 16 samples, while lepidocrocite was found in 7 of the 16 samples. Figure 4-1 shows an example of a corrosion scale from Milwaukee with the coexistence of goethite and lepidocrocite as the dominant corrosion crystalline solids.

Interestingly, no iron crystalline phases were observed for several corrosion scales, particularly the mains samples from Oak Creek made of ductile iron, suggesting the possible presence of amorphous iron phases in those scales. Other authors have identified a similar non-crystalline phenomenon despite iron being the most abundant element in solids analysis (Copeland et al. 2007). The lack of identified iron corrosion products may be related to the relatively short service life of those pipes, along with the less corrosive nature of ductile iron pipes in comparison to cast iron pipes. The ductile iron lateral from Oak Creek did have a discernible iron phase (goethite) where iron may have precipitated onto pipe walls during long stagnation periods.

The corrosion scale formation on cast iron and ductile iron pipes found an interesting trend. All but one cast iron pipe (MKE-17) had identifiable crystalline iron phases, while ductile iron pipes were mostly amorphous except for a lateral from Oak Creek (OC-7). For this ductile iron lateral, it is plausible that stagnant conditions when the water is not in use caused deposition of iron onto the pipe walls that accumulated at a more rapid rate. This finding indicates that ductile iron pipes have less corrosive tendencies compared to cast iron, but age is also an important factor. The ductile iron pipe samples were considerably younger (14 – 38 years of service) than the cast iron samples (63 – 105 years of service). Pipe maturation contributes greatly to the stable scale formation of Fe(III) minerals such as goethite and lepidocrocite. Pipe ageing effects will be explored further in section 4.5.

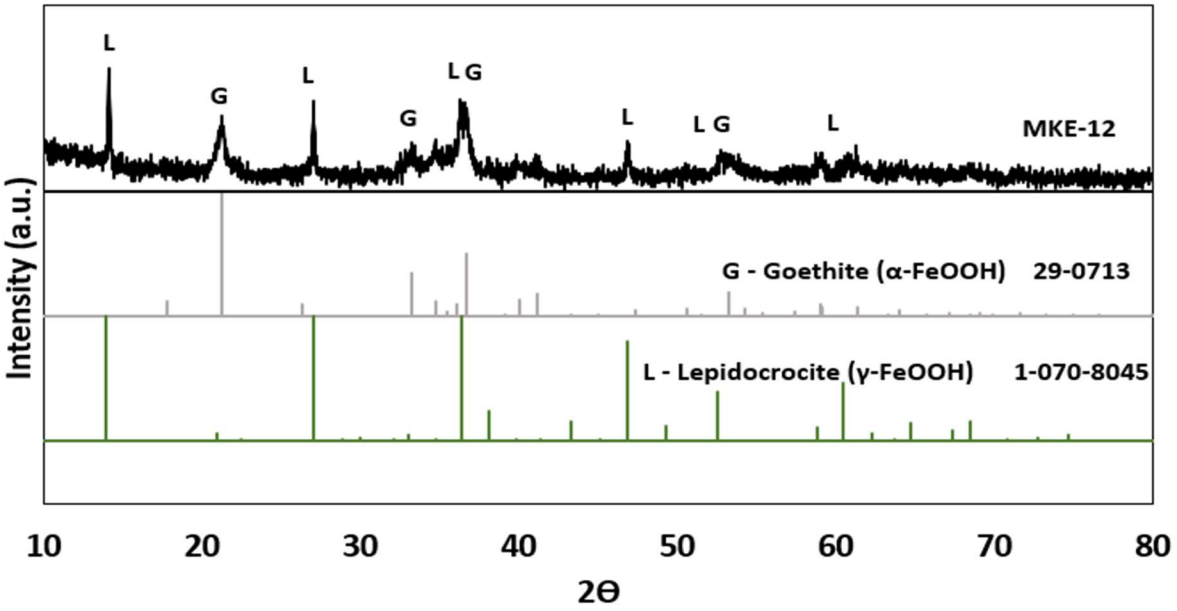

Figure 4-1. XRD pattern of a cast iron drinking water main harvested from Milwaukee. The reference XRD patterns for Goethite (JCPDS 00-029-0713) and Lepidocrocite (JCPDS 01-070-8045) were shown for comparison.

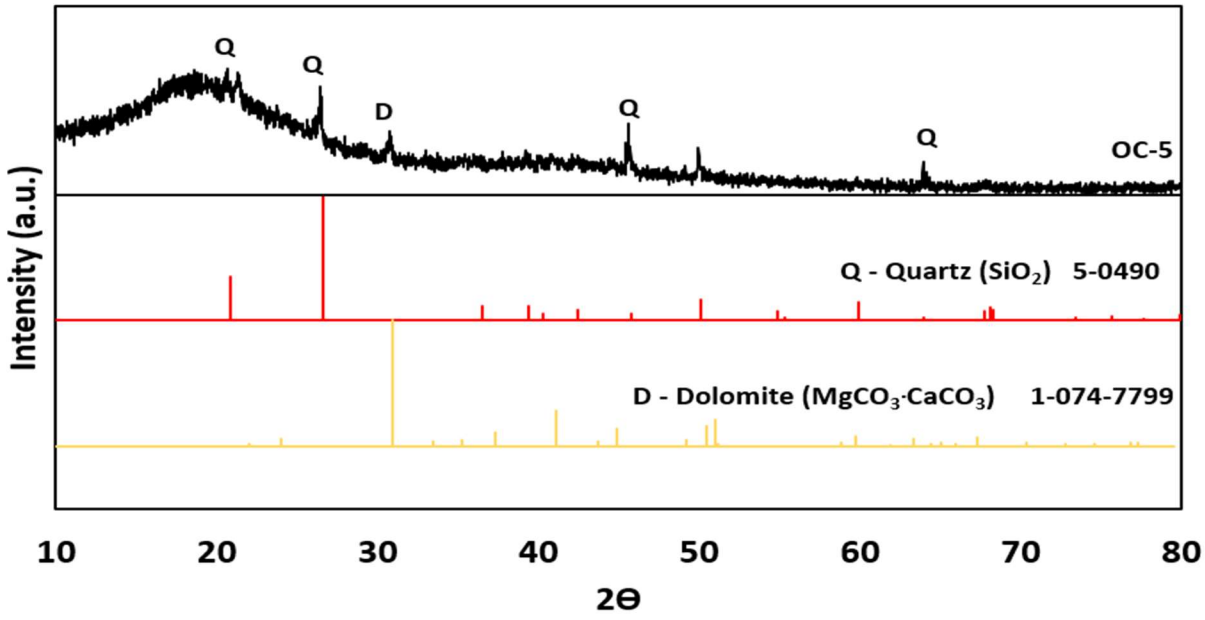

Figure 4-2. XRD pattern of a ductile iron drinking water main harvested from Oak Creek. The reference XRD patterns for Goethite (JCPDS 00-029-0713), Dolomite (JCPDS 01-074-7799), and Quartz (JCPDS 00-005-0490) were shown for comparison. The broad peak centered at 17° may indicate the presence of a possible amorphous phase.

In addition to iron corrosion products, several minerals were also observed in the corrosion scales, including dolomite ($MgCO_3 \cdot CaCO_3$), calcite ($CaCO_3$), and quartz (SiO_2). Dolomite and calcite are common constituents in corrosion scales associated with hard water sources (Nancollas et al. 1981; Tavanpour et al. 2016; Wasserstrom et al. 2017). Waukesha source water is obtained from deep wells with high water hardness (finished water hardness is approximately 380 – 400 mg/L as $CaCO_3$, see figure 3-1), and calcite was detected in 1 of the 2 iron samples from Waukesha. Quartz was detected in 1 sample (more analysis in section 4.4). Waukesha's dosing of sodium silicate as a corrosion inhibitor (Na_2SiO_3) likely precipitates a thin film of silica on the inner pipe wall, allowing quartz nucleation (Lehrman & Shuldener, 1952; Lehrman & Shuldener, 1959).

Milwaukee and Oak Creek source their drinking water from Lake Michigan with moderate water hardness (see figure 3-1). Dolomite was detected in 4 of the 9 Milwaukee pipes, followed next in frequency by quartz and calcite at 2 each. The presence of quartz as a scale constituent in Milwaukee and Oak Creek samples could be due to contact with quartz grains in the sand filtration treatment step that are transported and deposited later (Lytle et al. 2004). Silica is also naturally found in most drinking water sources and could readily pair with oxygen to form scale minerals.

4.1.2 XRD Analysis of Lead Pipes

A total of 6 lead pipes were harvested, five from Milwaukee and one from Waukesha. Oak Creek does not have lead pipes in their distribution system. These pipes represent laterals

only, and their service lives ranged from 74 – 105 years old. The XRD analysis for each pipe sample is shown in table 4-2 below.

Table 4-2. XRD results for Lead pipe samples.

Sample ID	XRD Match
MKE-2	Hydrocerussite, Plumbonacrite
MKE-3	Hydrocerussite, Plumbonacrite
MKE-6	Hydrocerussite, Plumbonancrite, Cerussite
MKE-9-Pb	Hydrocerussite, Litharge, Dolomite, Quartz
MKE-10	Hydrocerussite
WK2-Pb	Cerussite, Plattnerite

Lead (II) corrosion products were prominent in all Milwaukee samples. This is not surprising given the lower oxidizing potential of the residual disinfectant monochloramine that is used by the Milwaukee Water Works (Milwaukee Water Works, 2022). These corrosion products were hydrocerussite (found in every Milwaukee lead sample), cerussite, litharge, and plumbonacrite. Cerussite and hydrocerussite are often found together in distribution systems as they share a similar formula, with hydrocerussite being the hydrated form of cerussite (Kim & Herrera, 2010; Schock et al. 2014; Triantafyllidou et al. 2015; Hopwood et al. 2016; Wasserstrom et al. 2017; Tully et al. 2019; Lytle et al. 2020). Litharge (also Pb^{+2}) was only detected in MKE-9. Litharge is hypothesized to be the first corrosion product to form on exposed lead in drinking water distribution systems from examination of corrosion scale layer Kim & Herrera, 2010).

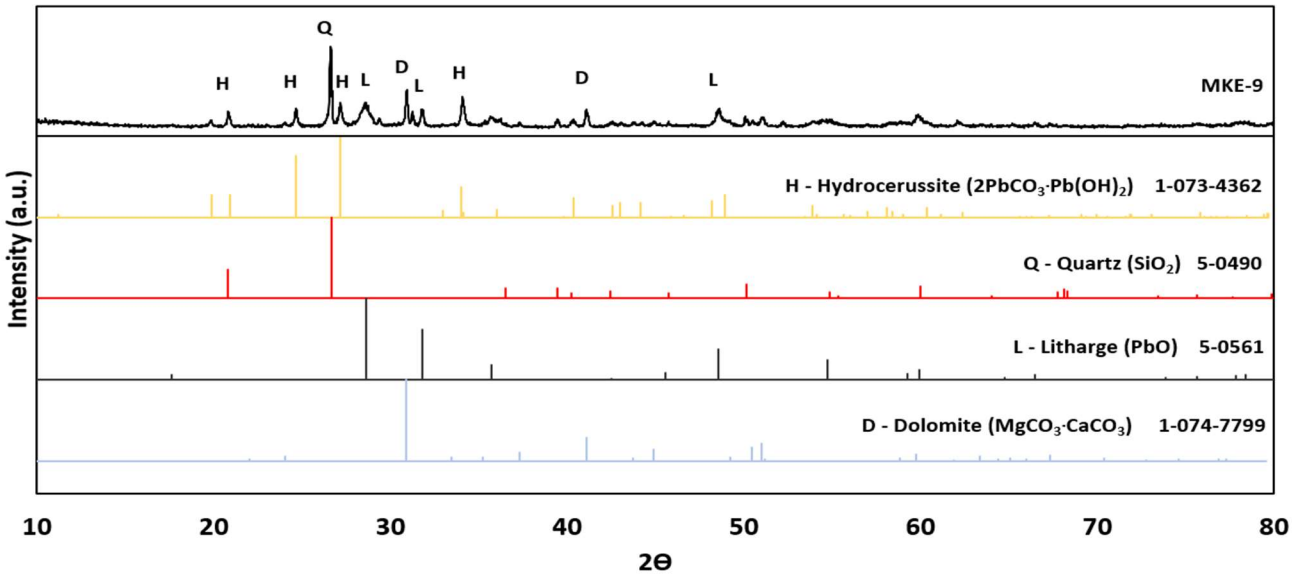

Figure 4-3. XRD spectra of a lead drinking water pipe harvested from Milwaukee. Reference patterns for hydrocerussite (JCPDS 01-073-4362), quartz (00-005-0490), litharge (00-005-0561), and dolomite (JCPDS 01-074-7799) are shown for comparison. Hydrocerussite has multiple overlapping peaks with scrutinyite (not shown) which require further investigation.

Formation of Pb(IV) oxides plattnerite and scrutinyite from Pb(II) corrosion products requires a high oxidation potential provided by a strong oxidant such as free chlorine (Lytle & Schock, 2005; Wang et al. 2010). In contrast, dissolved oxygen or a mild disinfectant residual like chloramines may not be sufficiently strong enough to fully oxidize Pb(0) or Pb(II) to Pb(IV) products (Liu et al. 2008). Plattnerite (β-PbO_2) and scrutinyite (α-PbO_2) are very insoluble in water and usually represent the final corrosion scale layer on pipe walls. Because hydrocerussite shares a notable peak with plattnerite at ~48° and multiple peaks with scrutinyite, XPS can be used as a complimentary technique to distinguish between the chemical oxidation states (figures 4-3, 4-4). As Milwaukee utilizes monochloramine for a disinfectant

residual, the oxidation potential in the system may not be high enough to fully oxidize Pb(0) and Pb(II) products to Pb(IV) (Wang et al. 2010).

Notably, plattnerite coexisted with cerussite in the lone Waukesha sample, which may serve as a stable precursor to plattnerite (figure 4-4) (Lytle & Schock, 2005; Liu et al. 2008, Wang et al. 2010). The conditions required for such scale formation feature the presence of a strong oxidizer, and Waukesha uses free chlorine as a disinfectant residual. As plattnerite is more insoluble than cerussite, it likely produced a protective layer over the more soluble lead carbonate, preventing it from being released into the drinking water (Kim & Herrera, 2010; Schock et al. 2014). Plattnerite is also more thermodynamically stable than cerussite, so its presence indicates that the complete oxidation from cerussite occurred in some parts of the scale more rapidly than others enabling the protective film over cerussite (Kim & Herrera, 2010; Schock et al. 2014).

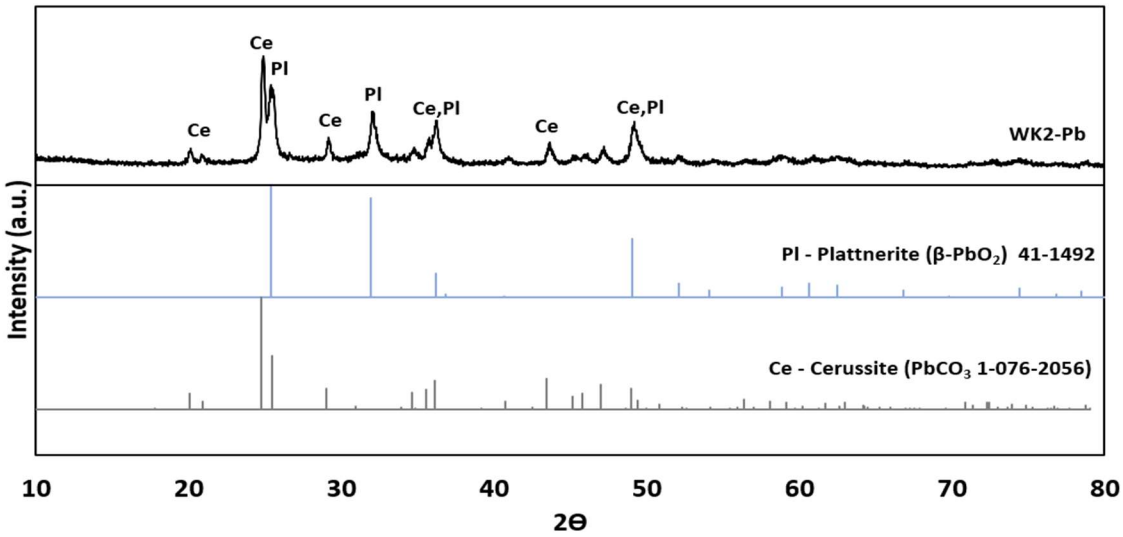

Figure 4-4. XRD spectra of a lead drinking water pipe obtained from Waukesha. Reference patterns for plattnerite (JCPDS 00-041-1492) and cerussite (JCPDS 01-076-2056) are shown for comparison. Note the peak overlap at ~50° which requires further investigation.

Associated minerals in the lead pipes were quartz and dolomite. Lead carbonates were detected in every lead sample, so dolomite being found as an associated mineral was expected due to the availability of carbonate ions. Milwaukee applies orthophosphate as a corrosion inhibitor but lead phosphate corrosion minerals were not found. In the absence of lead phosphate compounds, some field studies report calcium complexation with phosphate. These were not identified in this study either. Although Waukesha uses sodium silicate as a corrosion inhibitor, quartz was found in a Milwaukee sample (MKE-9) but not in the Waukesha pipe. These ideas will be discussed further in section 4.4.

4.1.3 XRD Analysis of Copper Pipes

A total of 5 copper pipes were analyzed by XRD, three from Milwaukee, one from Oak Creek, and one from Waukesha. All samples were used as laterals and service ages ranged from 54 – 100 years old. Copper pipes are chosen for their excellent corrosion resistance and the evidence was visibly clear with minimal corrosion scaling compared to iron and lead pipes, as shown in figure 4-5.

Figure 4-5. Longitudinal cross sections displaying corrosion scales from copper (A), lead (B), and iron (C) pipes.

Elemental copper was found in 3 of the 5 samples and was likely a product of scraping the soft and worn metal from the inside of the pipe when sampling. Cuprous oxide (Cu_2O) and malachite ($Cu_2CO_3(OH)_2$) were the second most common corrosion products, and each were found in 2 of the 5 samples (table 4-3). The presence of malachite may be related to the high amounts of dissolved inorganic carbon in the source water (Turek, 2006). Malachite is a very insoluble mineral in drinking water conditions (Edwards et al. 2001). Additionally, dolomite and quartz were observed in a Milwaukee sample, which were the only non-copper associated minerals in the samples.

Table 4-3. XRD results for copper pipe samples.

Sample ID	XRD Match
MKE-1	Copper
MKE-9-Cu	Copper, Dolomite, Quartz
MKE-13	Cuprous Oxide
OC-1	Malachite
WK-Cu	Cupric Oxide, Malachite

Malachite is a very stable corrosion product and can regulate the release of copper and other trace metals from the scale into the water. It usually forms as a later-stage corrosion product if the pipes have aged sufficiently and helps contribute to the trend of copper release decreasing with pipe age. Malachite may be formed as an oxidation transformation product of cuprous oxide, given an abundant source of dissolved inorganic carbon in the water for carbonate formation (Palit & Pehkonen, 2000). When the pipes are harvested and exposed to air, malachite may dehydrate and form cupric oxide, which was also present in the WK-Cu sample (Patterson et al. 1991). Due to the time delay between sample harvesting and XRD analysis, it is difficult to say whether dehydrating played a role in the speciation of both cupric oxide and malachite. Cupric oxide is also stable under drinking water conditions, as referenced in the pourbaix diagram (figure 2-5).

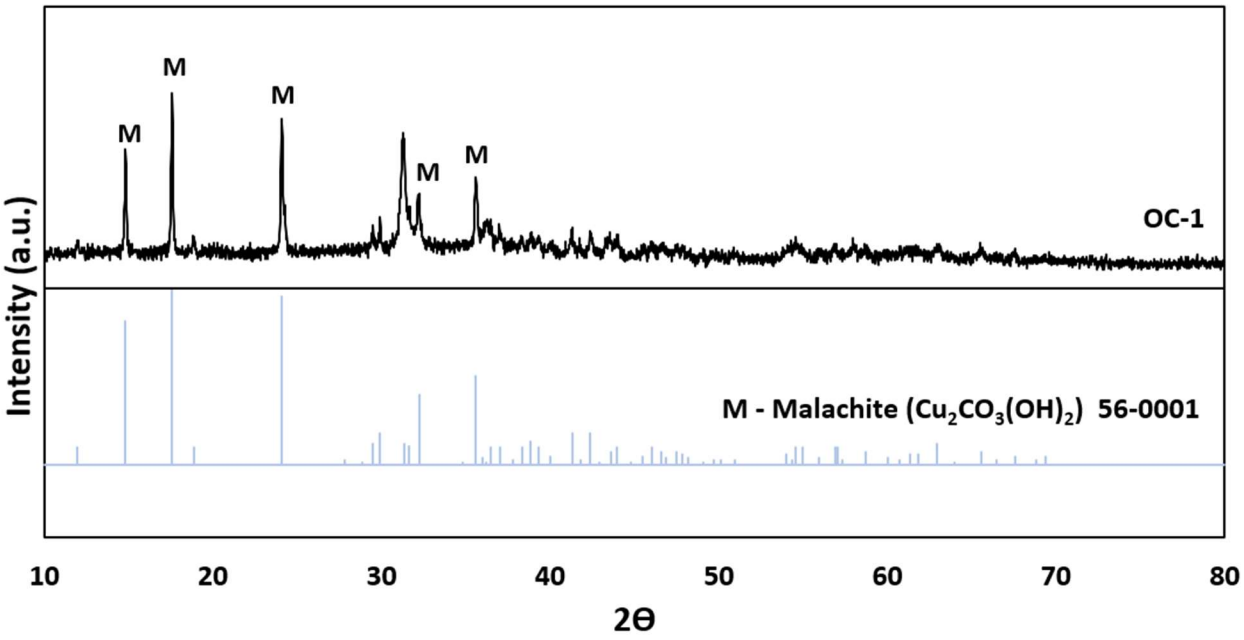

Figure 4-6. XRD spectra for Oak Creek copper lateral OC-1. Malachite is the primary mineral in this corrosion scale and its reference pattern is shown (JCPDS 00-056-0001).

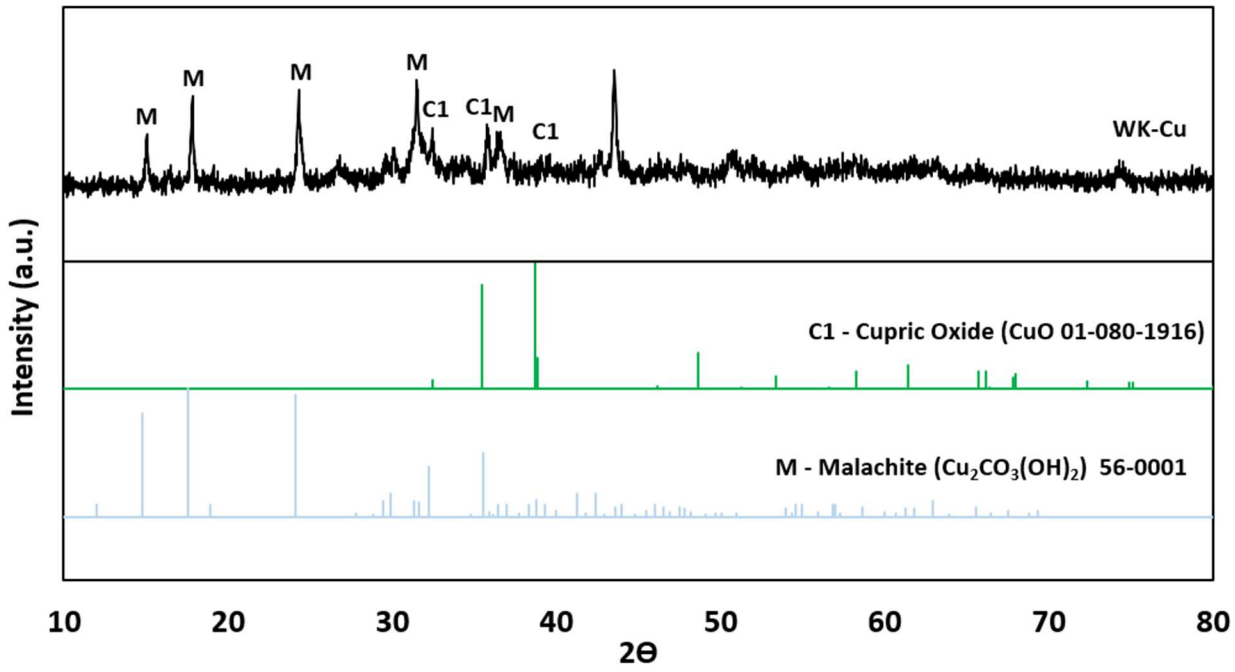

Figure 4-7. XRD spectra for Waukesha Copper pipe WK-Cu. Malachite was likely the primary mineral while in service, and upon sampling partially dehydrated to form cupric oxide.

4.2 XPS Results and Discussion

XPS analysis of selected iron, lead, and copper samples was performed to determine the oxidation states of major elements (Fe, Pb, Cu, respectively). Solids standards of cuprous oxide (Cu(I)), cupric oxide (Cu(II)), magnetite (Fe(II,III)), goethite (Fe(III)), lead phosphate (Pb(II)), and plattnerite (Pb(IV)) were used as references. A database of XPS peaks curated and maintained by the National Institute of Standards and Technology (NIST) was the source for information to properly classify peaks. The NIST X-ray Photoelectron Spectroscopy Database lists the binding energy of orbital peaks for each element, but there may be a range of binding energy values associated with each orbital (NIST Standard Reference Database 20, Version 4.1). Discretion was used to select the proper peak after consideration from XRD data, drinking water conditions (such as disinfectant applied) and other references. The XPS data were fitted by analyzing the binding energy to each peak by adjusting the full-width half max (FWHM) built in function in the XPSPeak41 software, a free program offered by Washington State University.

Lead samples that may have contained a mixture of oxidation states between +2 and +4 based on the XRD pattern matching were analyzed using XPS to determine the correct oxidation states. Three samples from Milwaukee had peaks that overlapped and matched with hydrocerussite, cerussite, and plattnerite, requiring further analysis. Figure 4-8 shows the samples MKE-2, MKE-6, and MKE-9 which match clearly the Pb(II) oxidation state.

Sample MKE-2 (designated A in figure 4-8) and MKE-6 (designated B) have similar $4f_{5/2}$ and $4f_{7/2}$ orbital binding energies, while MKE-9 peaks are shifted at higher energy levels. Peak values from the NIST database suggest that $4f_{7/2}$ binding energy for Pb(II) is typically reported between 137.7 and 138.1 eV, and $4f_{5/2}$ binding energy is around 142.7 eV (NIST Standard

Reference Database 20, Version 4.1). These values are shifted higher in the XPS data shown but offset from the instrument calibration when analyzing the carbon 1s orbital (adjusted to a binding energy centerline of 284.6 eV) must be calculated to appropriately shift the peaks. Another explanation for the higher values is the non-homogenous mix Pb(II) minerals present in the scale. Several authors have reported different Pb(II) complexes with $4f_{7/2}$ binding energy varying between 137 and 138 eV which may suggest the inconsistency between samples A and B with C (Pederson, 1982; Rondon & Sherwood, 1998).

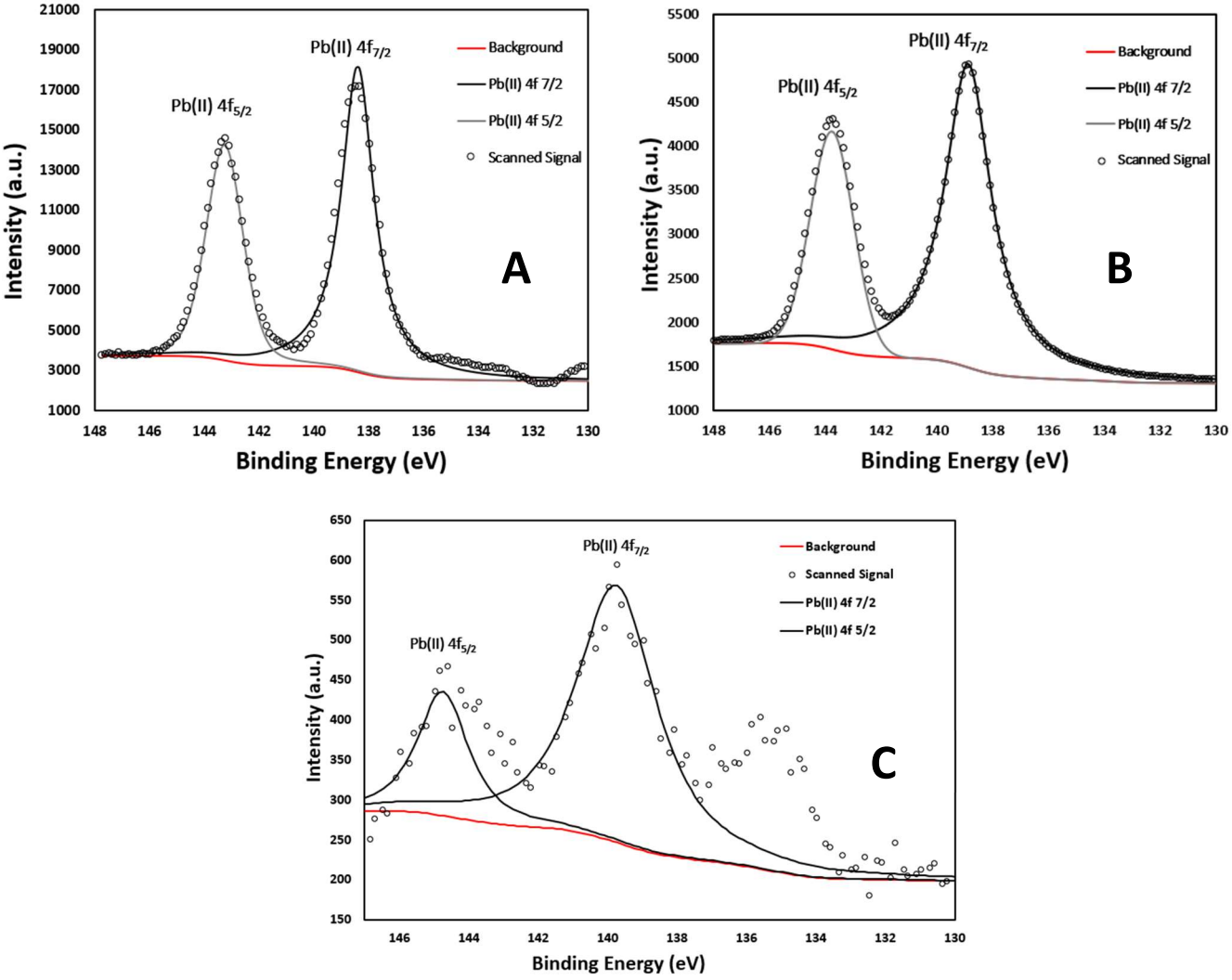

Figure 4-8. XPS peak matching for MKE-2 (A), MKE-6 (B) and MKE-9 (C) lead pipes. Scanned signals are represented by the open circles indicate the presence of Pb(II) oxidation states.

Sample C in figure 4-8 (MKE-9) has a satellite peak centered around 135 eV not seen in sample A or B. This is known as a shake-up satellite peak, wherein a 4f electron is reduced to a lower energy through interaction with a valence electron during photoionization (Chusuei et al. 1999). This interaction leaves the core electrons in the d^9 configuration, producing an unidentifiable peak at lower binding energy than chemical state peaks (Wu et al. 2006).

It can be determined that only Pb(II) minerals exist in the Milwaukee pipe scales as Pb(IV) chemical states were not observed in the XPS spectra. One Waukesha lead sample was chosen for XPS analysis as the XRD data indicated the presence of cerussite and plattnerite (WK2-Pb). Figure 4-9 displays the XPS measurements for the sample including the peak fits. The presence of a non-uniform gradient on the downslope of the right shoulder for each peak means multiple chemical states are possibly present. The distinction between Pb(II) and Pb(IV) peaks required standard reference materials since the 4f orbital peaks have similar binding energy. The reference materials included commercially available PbO_2 and lab-synthesized hydroxylpyromorphite ($Pb_5(PO_4)_3(OH)$) and are shown in figure 4-10.

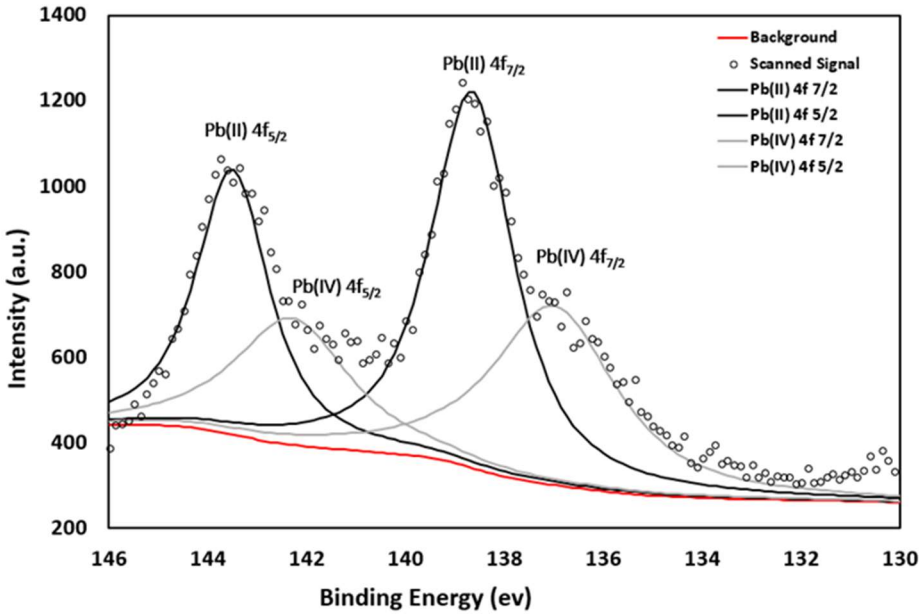

Figure 4-9. XPS spectra for WK-2 Pb sample from Waukesha. The extended shoulder at the offset from the center, rather than a smooth gradient, means the inclusion of both chemical states are present.

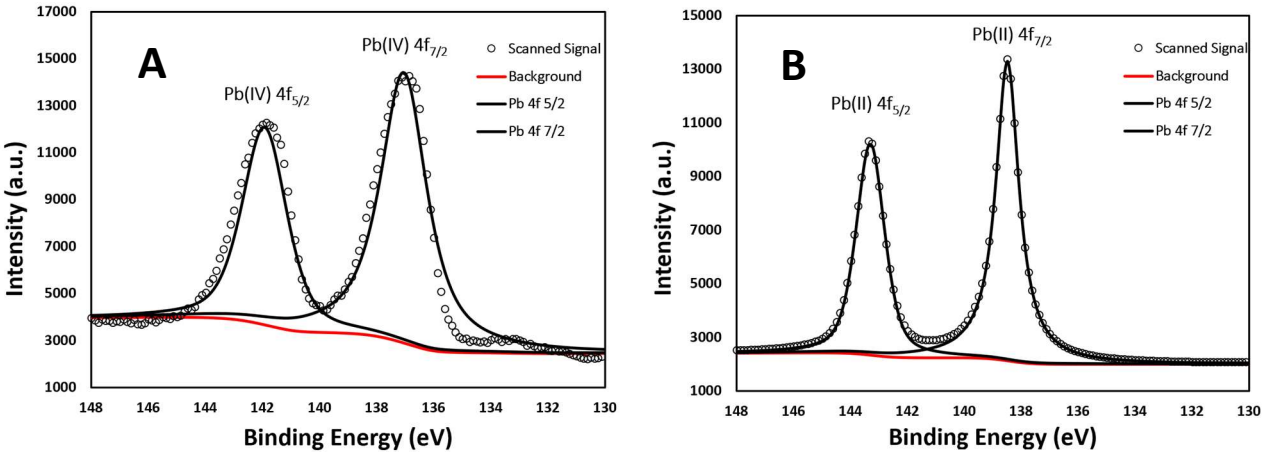

Figure 4-10. Reference XPS patterns of commercial PbO_2 (A) and synthesized hydroxylpyromorphite ($Pb_5(PO_4)_3(OH)$) (B). The center peak location is at higher binding energy for Pb(II) chemical states.

Despite the plethora of binding energies available in the NIST database, the reference materials provide excellent peak-centering locations for the two chemical states. From the

hydroxylpyromorphite reference XPS data it can be estimated that the apex of the 4f orbital peaks fit well with Pb(II). The shoulder peaks to the right of the main peaks (at lower binding energies) are in good agreement with the centering from the PbO_2 reference material. This complimentary technique suggests that there is enough evidence to support the XRD data and it can be concluded that both Pb(II) and Pb(IV) coexist within the Waukesha lead sample (WK2-Pb).

The same procedure was followed for iron and copper samples to determine chemical state speciation within samples. The only iron crystalline minerals (excluding the amorphous regions) identified were iron oxide hydroxides goethite and lepidocrocite. For these compounds iron is in the +3-chemical state, and XPS was leveraged to confirm this. Figure 4-11 shows the Milwaukee and Waukesha iron samples MKE-17-1 and WK3 which had XRD matches of goethite and lepidocrocite (WK3-Fe only matched with goethite). This was done using an XPS peak match of the $2p_{3/2}$ orbital at ~711 eV (NIST Standard Reference Database 20, Version 4.1). From this we can observe that the only chemical state for iron in the samples is +3. Oak Creek ductile iron pipes are not shown as the small mass percentage of amorphous iron phases could not produce any discernible spectra to analyze iron chemical state.

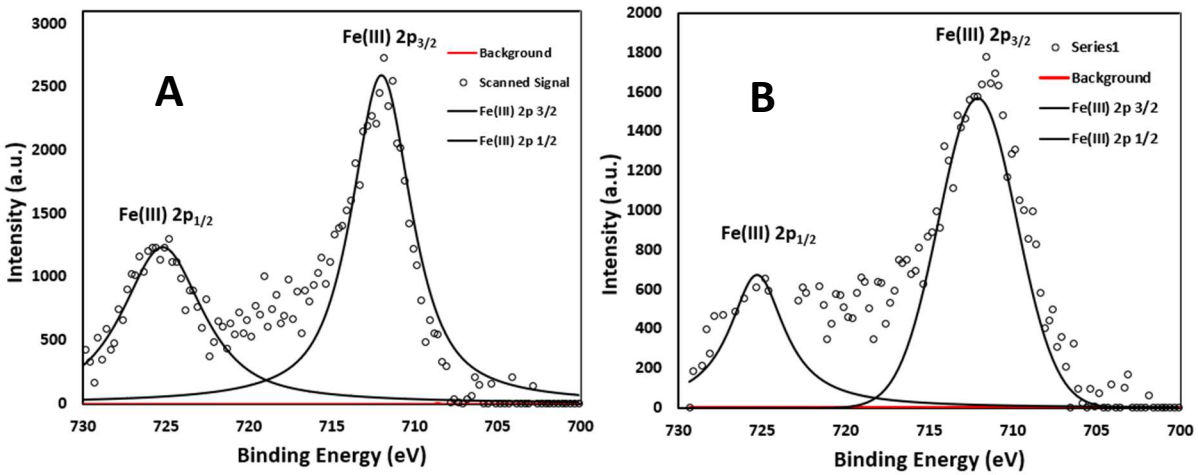

Figure 4-11. XPS spectra for iron samples MKE-17-1 (a) and WK3 (b) fit by XPSPeak41 software. Experimental data matched well with Fe(III) peaks to confirm the presence of goethite and lepidocrocite.

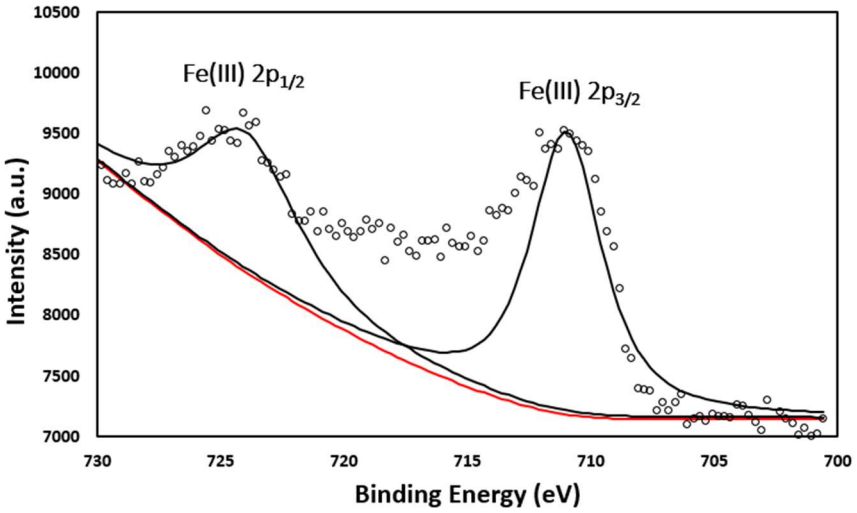

Figure 4-12. Reference XPS spectra for synthetically produced goethite featuring Fe(III) peaks.

Copper sample MKE-13 (A in figure 4-13) was chosen to verify the presence of Cu(I) which was the only XRD mineral match, while WK-Cu (B in figure 4-13) was chosen for XPS analysis as initially (during reference pattern matching) multiple XRD matches corresponded to Cu(0), Cu(I), and Cu(II). The reference peaks in the commercially purchased cupric and cuprous

oxide were tricky to analyze. Cu(II) is known to have prominent satellite peaks while Cu(I) should not. This was not the case for cuprous oxide standard, which featured small remnants of satellite peaks and wide shoulders implying the presence of Cu(II) (figure 4-14A). This could be due to excitation of the electrons in the sample during exposure to x-rays so looking at published reference peaks will be useful in determination of oxidation state (Wu et al. 2006).

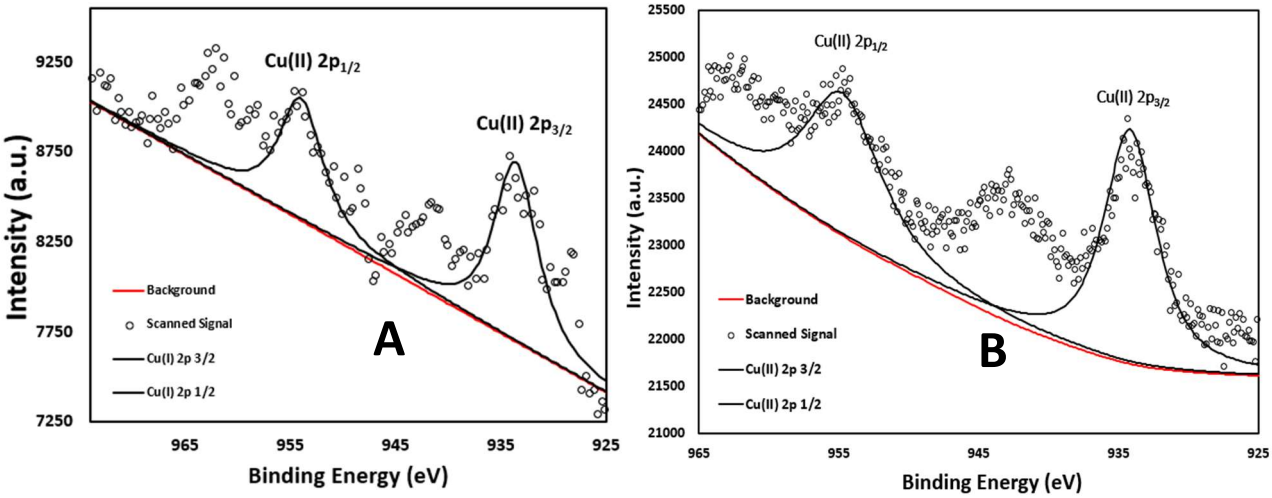

Figure 4-13. XPS spectra of copper samples MKE-13 (A) and WK-Cu (B) which correspond with Cu(II) chemical states.

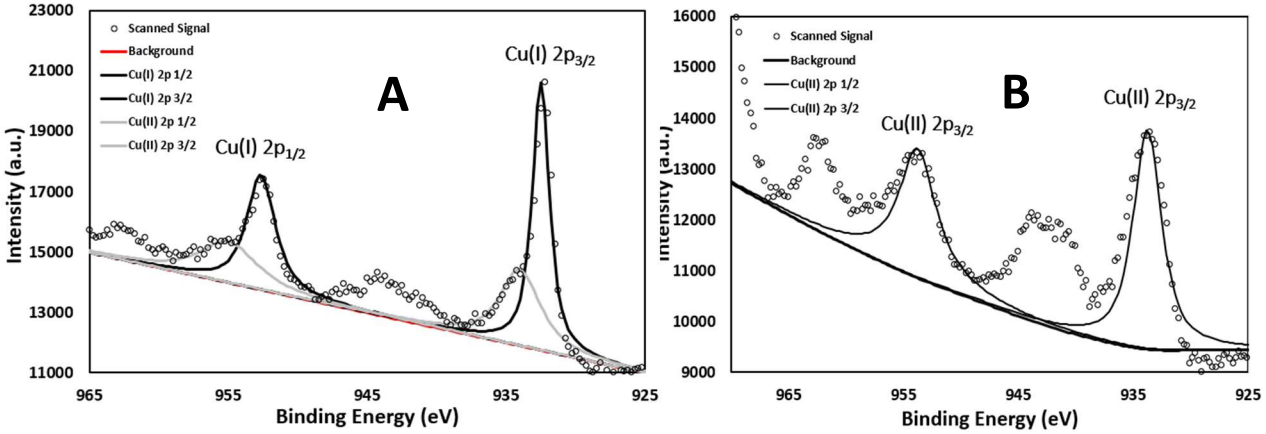

Figure 4-14. Reference peaks for commercially purchased cupric and cuprous oxides to display Cu(I) (image A)and Cu(II) (image B) peaks.

In addition to the change in oxidation state by excitation of x-ray, the commercially purchased cuprous oxide may have partially oxidized upon opening the sample and exposure to the atmosphere. This explains the wide shoulder of the binding energy peak, and the small satellite peaks to the left of them which are characteristic of Cu(II) oxides (Brown & Weser, 1979; Wu et al. 2006; Ghodselahi et al. 2008). Real-world sample analysis of copper corrosion is rarely reported on in literature, and the reference peaks in textbooks and databases are from laboratory-based research. Cu(I) oxide solids have reported $2p_{3/2}$ binding energies ranging from 933.20 – 934.60 eV, and Cu(II) oxides are reported between 932.0 and 932.70 eV (NIST Standard Reference Database 20, Version 4.1).

Sample MKE-13 displayed the characteristic satellite peaks found in CuO samples, despite only observing Cu_2O in XRD. There are a few possible reasons for this. First, the corrosion scale may have oxidized over time since the initial analysis by XRD. XPS is a sensitive technique which only measures binding energy within the top few nanometers of a material. The corrosion minerals were ground up, potentially creating more surface area which could be oxidized and detected by XPS as Cu(II). Another explanation could be that excitation of the electrons at the surface gave the false impression of CuO existence. Sample WK-Cu had very similar 2p orbital peak locations and satellites, so it was determined that Cu(II) was the primary chemical state within the scale.

4.3 SEM Images

4.3.1 SEM of Iron Samples

SEM imaging provided another complimentary technique to solid phase identification by morphological analysis of the grain structure. A working distance of ~9 mm was maintained for imaging at 5 kV. Morphologies of synthetic goethite and lepidocrocite were used as visual standards for identification of corrosion minerals. Goethite has been reported as long needle-like rods with sharp edges, while lepidocrocite particles have rounder edges (Kosmulski et al. 2004; Legodi & de Waal, 2007; Das et al. 2013). Quartz grains have many possible morphologies but are much larger than the iron oxide particles (Itamiya et al. 2019). Dolomite particles are identified as blocky with sharp edges (Feng et al. 2000). Size was noted but not used as a defining characteristic due to possible discrepancy of synthetic and real-world minerals formation mechanisms.

In figure 4-15 below, the sample in image A found quartz and goethite minerals detected in XRD. WK3-Fe did not feature any noticeable goethite, but large quartz grains were everywhere. The smaller particles nucleating on the surface of the quartz and in the background were potentially iron particles, perhaps goethite that could not grow fully. This will be discussed further in section 4.4. The sample from Oak Creek in image B had amorphous iron, quartz, and dolomite. The large grain in the center of the image is the quartz grain, of which many particles are deposited on. It is difficult to distinguish the dolomite particles from the amorphous iron, so EDS will be required to determine the extent of iron complexation. Finally, image C from sample MKE-17-1 features the rods that are characteristic of goethite and

lepidocrocite. Although the rods are rounded at the edges, it is difficult to determine if this is lepidocrocite or goethite that did not form properly.

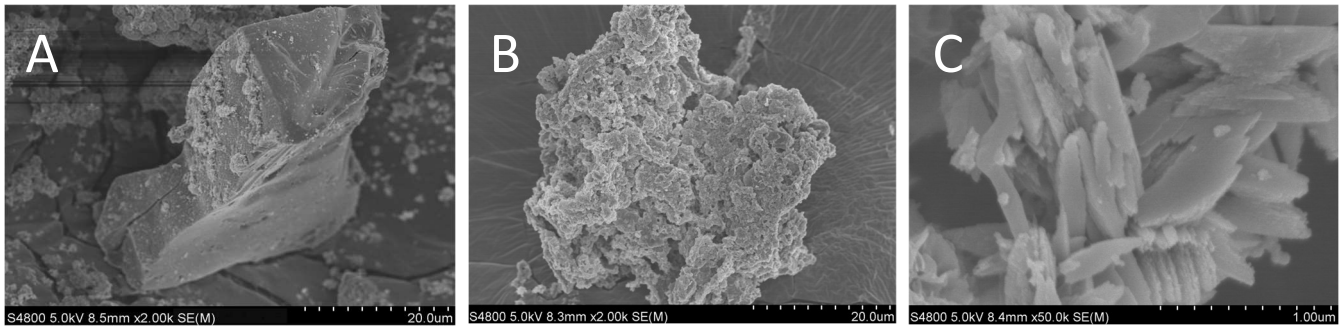

Figure 4-15. SEM images of A) iron material deposited on a large quartz grain in WK3-Fe, B) amorphous iron conglomerate from OC-5 and C) needle-like rods characteristic of goethite and lepidocrocite in MKE17-1.

4.3.2 SEM of Lead Samples

The known or suspected morphologies of lead compounds were used to confirm the identity of lead corrosion minerals. Pipe sample MKE-10 was chosen for its sole constituent of hydrocerussite. Samples MKE-6 consisted of hydrocerussite, cerussite, and plumbonacrite. WK2-Pb featured cerussite and plattnerite. Synthesis imaging of lead corrosion minerals from other studies were used as a reference of morphology. The size and shape of the particles from these studies were used to distinguish the compounds. Figure 4-16 below displays the SEM images from the lead samples.

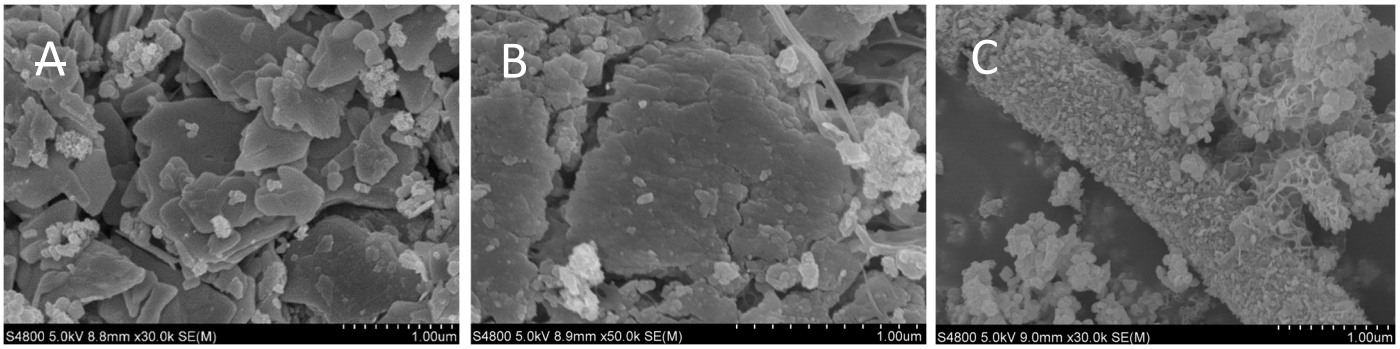

Figure 4-16. SEM images from lead samples A) MKE-6 featuring hydrocerussite, cerussite, plumbonacrite, B) MKE-10 featuring platy mineral hydrocerussite, and C) WK-2Pb with elongated cerussite particle covered by plattnerite.

Hydrocerussite is characterized by platy hexagonal particles that are seen in A and B in figure 4-16 above (Liu et al. 2008; Mendoza-Flores et al. 2017). Although these particles are imperfect in comparison to the synthetically produced hydrocerussite, the platy appearance is distinguishable in these figures in larger particles that appear to have aggregated. Similarly, for cerussite particles, which are known to form elongated prisms, the real-world imperfections from the references were noticeable but fine enough to identify their presence. Cerussite was confirmed in A and C above. The smaller aggregates of particles were assumed to be plumbonacrite or amorphous lead compounds, as these images have scarcely been reported on, if at all.

In image C above, the elongated cerussite particle is covered with smaller plattnerite particles. This confirms the hypothesis that cerussite forms as a precursor to plattnerite and becomes protected by it. This would likely halt the production of cerussite as there are fewer ion exchange sites for carbonates, and plattnerite would then control the release of lead while protecting cerussite. In image B, there are a few web-like shapes that were not identified as lead and could represent organic material such as a biofilm.

4.3.3 SEM of Copper Samples

Copper particles were difficult to distinguish as the morphology of Cu_2O and CuO are both spherical and similar in size (Prakash et al. 2007; Dhineshbabu et a. 2016). In figure 4-17 below, the presence of these spherical particles was used in conjunction with XRD to confirm that species of copper. Image A from sample MKE-13 had the distinct spherical conglomeration of cuprous oxide. This was the only mineral detected in the sample, and the spherical particles took up the entire image. In image B, malachite was identified by its long fibrous particles (Zhang et al. 2004). Dispersed among these long fibers are smaller spherical particles which are likely cupric oxide particles.

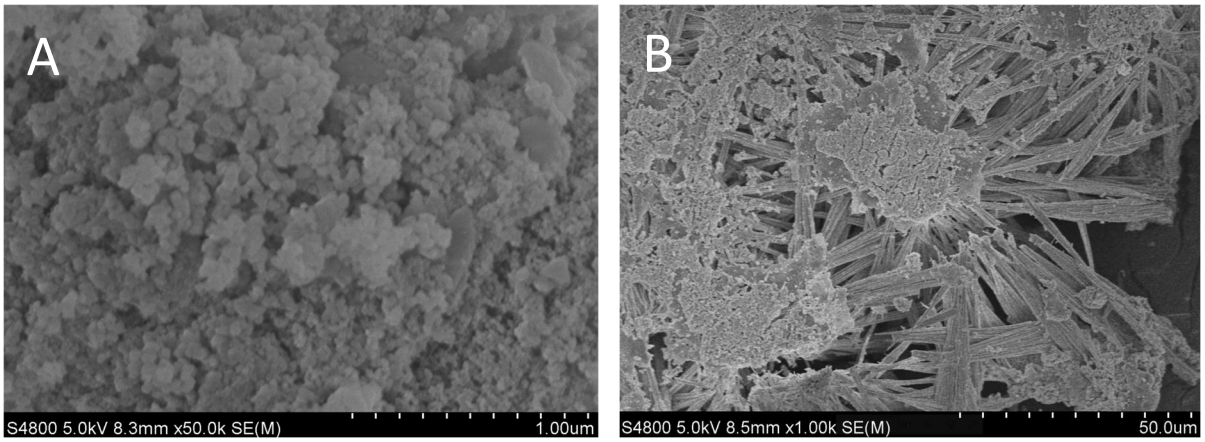

Figure 4-17. SEM images of copper samples A) MKE-13 featuring rounded aggregates of cuprous oxide and B) fibrous particles of malachite from WK-Cu.

4.4 EDS Results and Discussion

To further substantiate the inorganic non-metal contaminants within the corrosion scales, energy dispersive spectroscopy was used. Several elements were semi-quantitatively

identified within samples that can't be measured by ICP-MS. These elements include silicon, carbon, phosphorus, oxygen, and chlorine. This method is semi-quantitative as the measured chemicals and their weight percentage may depend on the sample grain observed. Different grains may feature vastly different morphologies on a microscopic scale and thus have different chemical properties. For this reason, the elements found were purely qualitatively used to prove their existence within the samples. Several grains were observed per sample and the weight percentages were averaged. Table 4-4 shows selected samples and inorganic elements. Many of the cast iron samples from Milwaukee had similar trends of elemental weight percentage and are not shown to avoid repetitiveness.

Table 4-4. Weight % determined from EDS several major inorganic constituents in selected corrosion scales.

Sample ID	Weight %				
	C	O	Si	P	Cl
MKE-1	6.87	38.63	1.65	5.82	-
MKE-3	6.79	34.97	3.33	3.56	-
MKE-4	32.36	30.86	0.14	0.23	0.32
MKE-9-Pb	18.03	28.91	6.93	-	-
MKE-12	38.44	24.57	-	0.34	-
MKE-13	19.41	28.10	1.38	5.49	1.10
MKE-14	55.19	27.62	1.97	-	-
MKE-17-1	42.57	27.71	0.47	1.51	0.48
WK3-Fe	17.39	26.23	4.47	-	-
OC-1	22.61	25.76	0.88	0.38	-

The inclusion of silicon and phosphorus within the copper sample MKE-1 did not show up in any discernible crystalline phases when examined by XRD. There was a possible amorphous phase prior to 40° that may have included these elements (Appendix). Overall, phosphorus within Milwaukee pipes is explainable by virtue of the municipalities dosing of orthophosphate. Since there were no phosphate minerals within the XRD patterns it is likely that these inclusions formed amorphous phases that were not detected by XRD.

Silicon was observed in all samples except for MKE-12 which was an iron sample. There were no matches for quartz within this iron sample. Waukesha doses sodium silicate as a corrosion inhibitor, and the inclusion of silicon within the corrosion scale was predicted and observed as quartz within sample WK3-Fe. Silicon in the Milwaukee and Oak Creek samples could be due to contact through filtration, or from naturally occurring silicon in the water. Chlorine was not detected in any solid sample complexes but could have formed amorphous solids.

To elucidate the findings from the SEM images, elemental mapping from EDS was used to show the spatial presence of elements where morphology was not certain. For instance, in sample OC-5 the amorphous iron could not be distinguished from any other particles in the image. Figure 4-18 below shows the elemental mapping for this sample that also includes quartz and dolomite. The amorphous iron could not be distinguished through SEM, but the extent of iron can be seen by the red inclusions in the elemental mapping. Although harder to observe, it appears that the quartz and dolomite may have formed around the amorphous iron

as the iron region appears deeper into the large grain.

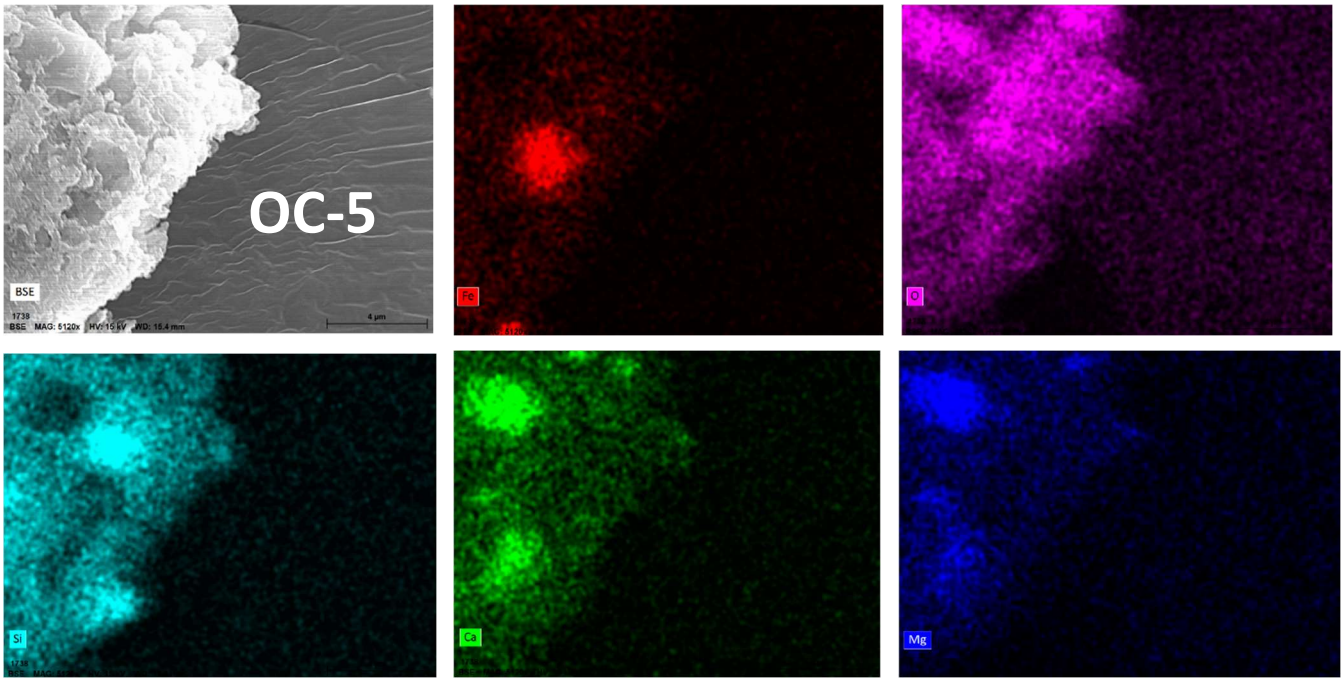

Figure 4-18. EDS elemental mapping of sample OC-5. Calcium and magnesium are present to show the possible location of dolomite, silicon for quartz, and amorphous iron.

The same elemental mapping procedure was carried out for copper samples MKE-13 and WK-Cu in figure 4-19 below. Sample MKE-13 found only cuprous oxide from XRD, and copper and oxygen were the only major elements observed in EDS. Sample WK-Cu had malachite which was observable through the plain-view version of the elemental mapping, and similarly to MKE-13 found only major elements to be copper and oxygen. Carbon could not be justified as a major element because of the carbon-based tape that the samples were loaded onto.

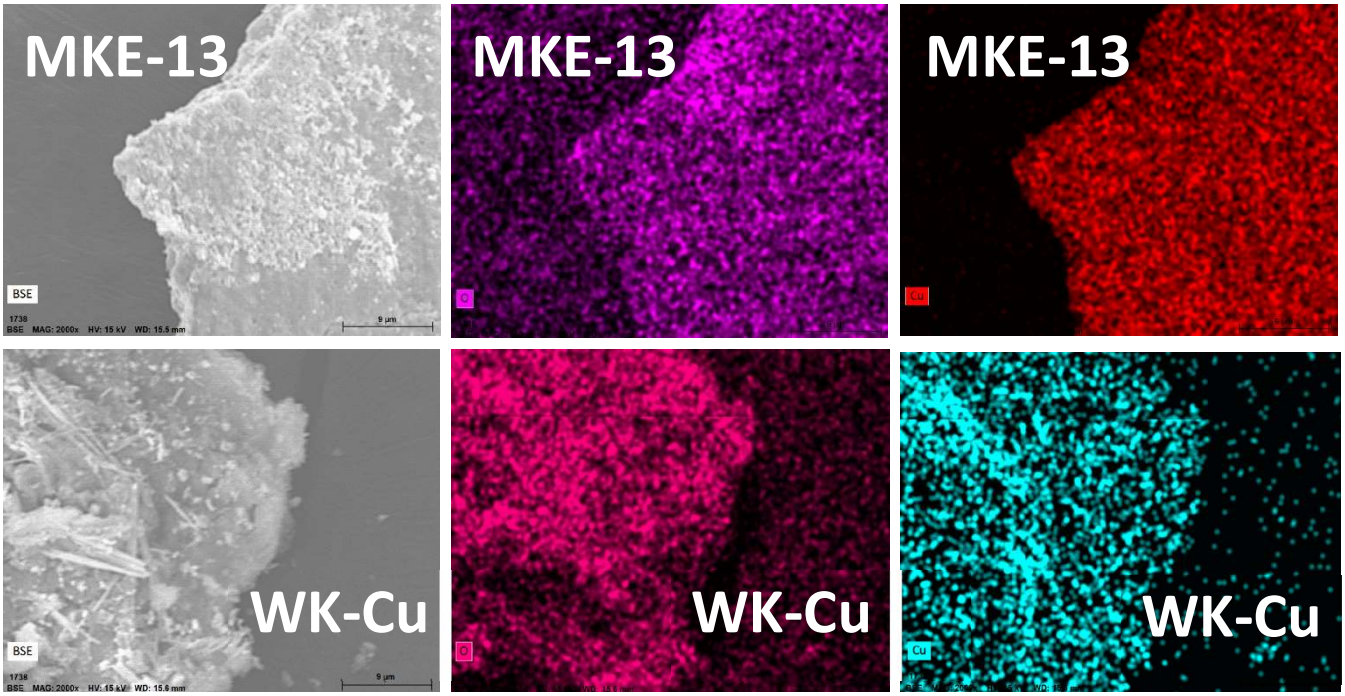

Figure 4-19. Elemental mapping of copper samples MKE-13 and WK-Cu, showing the presence of only copper and oxygen.

4.5 ICP-MS Results and Discussion

To fully quantify the extent of major and trace metal contamination within the corrosion scales, ICP-MS was performed. Small quantities of each sample were fully digested, and the results were standardized to a concentration of µg/g. Each sample was run in triplicate for statistical significance testing against the blank samples which was ultrapure water. All glassware was washed prior in a 15% HNO_3 bath to ensure a clean surface with zero metal contamination.

First, all samples of each pipe material were averaged according to their five most abundant metals (Figure 4-20). All samples regardless of base-material had relatively high levels of aluminum, manganese, iron, magnesium, and calcium. The base material was the highest in

each sample by weight percentage. Following next in weight was iron for both lead and copper pipes. This could be due to upstream release of iron from mains. The remaining elements in each top five were either calcium, aluminum, magnesium, or manganese. Magnesium and calcium were expected at high concentrations as they formed distinct crystalline phases within many corrosion scales seen as calcite and dolomite. Manganese was not specifically seen in any minerals but may have formed complexes as an associated mineral in carbonate complexes as it can easily substitute for calcium and magnesium.

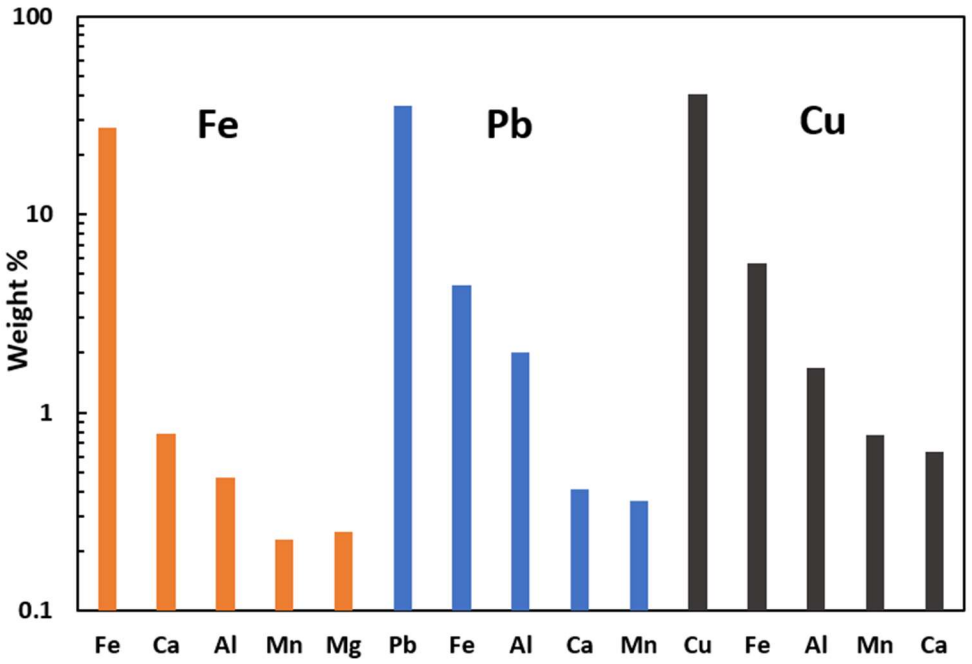

Figure 4-20. Major element analysis of each pipe material. All pipes of each material were averaged and calculated into a weight percentage of the total sample.

Aluminum was found to be a major element in all of the pipe materials as a likely by-product of reactions from aluminum sulfate addition as a coagulant for water treatment. Milwaukee adds aluminum sulfate (Al_2SO_4) and has a total average aluminum concentration of

11,836.60 µg/g. Comparatively, Oak Creek adds poly aluminum chloride (PACl) and has similarly high levels of aluminum accumulation at 13,336.31 µg/g. Waukesha draws from groundwater and does not require advanced coagulation and flocculation, thus their average aluminum concentration was lower at 538.23 µg/g. The total ICP-MS measurements are found in table 4-5.

Material	Sample	Element mass (µg/g)													
		Ba	Pb	U	Al	V	Cr	Mn	Fe	Ni	Cu	Zn	As	Mg	Ca
Fe	MKE-4	93.51	45.40*	2.33	3,864.23	77.82	110.82	736.39	304,984.98	1,457.01*	363.00	6.77	74.81	1,182.68	1,346.19
	MKE-5	170.70	-	8.10	5,778.23	20.91	-	305.58	283,471.63	0.81	27.52	12.36	17.65	1,503.95	1,662.34
	MKE-7	661.67	2.91*	5.87	3,617.12	71.93	61.33	1,636.68	270,146.27	61.03	306.56	58.95	54.11	943.29	3,390.32
	MKE-11	93.05	1.64*	1.91	2,288.58	2.05*	11.66*	315.93	261,261.85	-	53.18	5.05*	13.88	1,860.14	4,091.24
	MKE-12	29.44*	-	1.54*	5,922.21	-	-	160.96*	404,153.26	-	-	-	6.29*	344.54	666.80
	MKE-14	47.47	6.50	0.28	2,114.07	78.57	518.79	1,364.68	263,935.93	262.37	824.81	29.15	12.18	14,842.21	19,980.85
	MKE-15	485.30	-	6.69	3,737.47	9.30*	11.02	309.12	277,512.79	-	38.03	9.26	17.24	2,060.98	3,353.17
	MKE-17	1,275.20	3.28	8.62	9,035.46	45.92	36.18	415.44	474,960.94	-	78.58	40.50	28.31	2,679.50	6,954.02
	MKE-17-1	715.86	2.78*	9.14	7,763.67	52.62	54.06	311.10	242,495.45	78.89*	262.81*	13.64	53.10	5,098.45	7,148.37
Pb	MKE-2	87.54	401,793.30	10.89	25,592.28	90.45	13.65	24.09	19,659.91	4.27	261.41	55.50*	29.63	726.33	2,281.21
	MKE-3	315.51	400,675.90	32.34	37,824.49	172.90	20.25	18.82	35,028.53	29.35	305.03	3,368.30*	91.39	1,166.21	4,953.87
	MKE-6	372.96	284,524.00	33.80	36,353.90	339.53	78.19	55.02	76,671.94	1.74	893.82*	97.91*	121.02	3,094.80	6,057.99
	MKE-9	42.89	307,101.60	16.26	6,652.82	20.74	-	286.63	7,154.29	94.36	1,897.60	402.92	5.08	4,588.71*	5,511.30
	MKE-10	1,740.34*	262,288.90	2,605.33	13,024.21	1,478.17	234.62	125.96	11,980.80	232.86	2,872.90	543.94	194.61	108.93*	2,815.84
Cu	MKE-1	6,425.94	2,373.91	191.10	19,177.16	1,710.43	715.48	2,075.96	90,594.02	207.25	78,605.19	1,738.03	1,141.43	1,730.49*	8,497.82
	MKE-13	2,065.76	1,497.77	21.23	6,639.77	47.19	44.41	3,069.88	7,801.11	229.07	566,188.55	575.52	731.76	2,428.62	5,665.71
Fe	WK2-Fe	337.58	2,161.83	0.74	260.08	9.84	6.20	9,618.45	481,502.90	19.57	1,009.47*	9,898.66	49.44	1,141.21	28,932.52
	WK3-Fe	289.17	1,562.84	0.28	615.94	86.41	55.09	11,887.04	624,598.90	69.09	2,070.48	-	159.51	1,191.65	3,498.92
Pb	WK2-Pb	74.62	453,258.03	2.61	738.67	35.84	-	21,097.81	114,865.90	-	236.99	61.69*	74.29	913.58	2,861.96
Cu	OC-1 Cu	324.54	1,222.24	5.20	35,338.37	193.96	2.80*	22,728.44	121,297.50	64.49	395,393.10	293.59	419.74	1,155.76	5,272.43
Fe	OC-2	85.01	23.83	0.24	12,337.66	150.90	86.68	4,675.38	20,434.73	102.13	314.15*	41.45	9.47	1,867.82	8,548.00
	OC-4	1,164.71	4.38	0.52*	2,178.86	15.75	90.26	1,650.06	80,254.49	118.67*	279.54	28.41	3.69	2,079.14	23,015.35
	OC-5	24.44	13.97	0.06	1,149.75	47.61	3.61*	421.67	4,854.10	1.31	25.96	44.72	-	1,421.18	4,915.73
	OC-6	596.43	15.11	0.39	15,676.91	15.12	109.04	6,489.88	101,495.80	127.82	322.34	83.61	23.11	4,027.50	17,593.66

Table 4-5. ICP-MS data in ug/g of all solid samples. Triplicate samples were averaged and statistically insignificant results from the blank ($p < 0.05$) are denoted by *.

4.5.1 ICP-MS Analysis by Pipe Material

Aluminum levels in each distribution system were also affected by the pipe material. Aluminum concentrations in Milwaukee and Waukesha lead pipes were significantly higher than in iron pipes ($p < 0.05$). Although not seen in these samples, aluminosilicate/aluminum hydroxide deposition on pipe walls has been observed as a side effect of aluminum sulfate use (Kvech & Edwards, 2001). Despite the high concentrations of aluminum, aluminum solids were likely amorphous and not observable. Arsenic concentrations were significantly higher in copper pipes than iron or lead pipes ($p < 0.01$). This may be attributed to an impurity in the processing of copper pipes. Arsenic could be an inclusion during pyrometallurgy formation of copper pipes, but it is unknown if this is how these pipes were formed. Manganese concentrations were considerably higher in copper and iron pipes, although they were not statistically significant due to a much higher value in the lone Waukesha lead pipe. Manganese has the potential to sorb trace metals which will be examined in more detail in section 4.6.

Lead accumulation within copper pipes was significantly higher than in iron pipes ($p < 0.01$). Galvanized connections between lead and copper could result in corrosive action of the lead as it has a higher half-reaction standard potential in aqueous systems (table 2-2). The only known connection between copper and lead was within sample MKE-9. The connection location of these pipes was not known and would be vital to determine the extent of corrosion accumulation. For instance, if the lead pipe was upstream of the copper pipe, the destabilized lead may accumulate within the copper pipe. If the inverse were true, the lead would not be able to accumulate in the copper scale. There was not enough powdered sample of the copper

section for ICP-MS analysis, so it is not possible to determine the extent of lead release that may have been accumulated in the copper scale.

Chloride to sulfate mass ratio is a very important factor in the galvanic corrosion of lead. Sulfate alone has demonstrated the ability to prevent lead dissolution in these galvanic couples, but chloride may attack the lead (Edwards & Triantafyllidou, 2007). Increasing the chloride to sulfate mass ratio as well as alkalinity has been shown to increase the galvanic corrosion of lead (Edwards et al. 1999; Nguyen et al. 2011). The particulate or dissolved lead may then be in contact with the copper for long periods of time in stagnant conditions when the water line is not being used, adsorbing to the corrosion scale. Alkalinity, chloride, and sulfate were not measured in the water samples at the time of pipe harvesting, but the hardness of the water was sufficiently high (> 180 mg/L as $CaCO_3$) and sulfate would have been present as a by-product of adding aluminum sulfate as a coagulant in Milwaukee.

Lateral pipes WK2-Fe and WK2-Pb were galvanically connected. In this system, the cast iron pipe becomes anodic to the lead section and will preferentially corrode. Depending on the connection type, there may not be any direct contact between the dissimilar metals. The corrosion and release of iron from the pipe could potentially re-deposit onto the lead scale by supersaturation precipitation or other mechanisms. The lead pipe had elevated levels of iron, found at 114,864 μg/g. This was the highest among any lead pipe samples. Conversely, there were high concentrations of lead within the iron scale, at 2,161 μg/g. This was the highest concentration of lead within iron pipe sections.

Although not majorly seen in this study, lead accumulation within iron pipes has been substantially documented. This association can be explained by the hypothesis of lead

adsorbing to iron oxide particulates within water. This has been proven in natural systems (Erel & Morgan, 1992), and simulated plumbing systems with iron and lead connections (McFadden et al. 2011; Camara & Gagnon, 2012; Masters & Edwards, 2015). In this mechanism, particulate lead should adsorb to the surface of the iron oxide scales, such as goethite, which has been tested in lab-scale distribution systems (Camara & Gagnon, 2012). The corrosion and disturbance of the iron thus controls the release of the lead, which can become a persistent problem for years after partial or full lead service line replacement (McFadden et al. 2011, Camara et al. 2013).

For the three iron lateral samples (2 cast iron, 1 ductile) the accumulation of lead is explainable by possible lead laterals upstream in the distribution system. The correlation between lead and iron concentrations was mediocre at $R^2 = 0.5825$. This trend worsened when mains were studied. An R^2 of 0.0748 was calculated between lead and iron concentrations in all mains samples. This makes sense because iron mains are upstream of the lead and prevent lead adsorption onto the surface of the corrosion scales. Long stagnation times in laterals increases the contact time between dissolved or particulates in the water and could also increase the likelihood of deposition.

Lead pipes had higher correlations of copper and vanadium ($R^2 = 0.6033$), arsenic and vanadium ($R^2 = 0.7633$), and magnesium and calcium ($R^2 = 0.6505$). Magnesium and calcium correlation is expected in correspondence with the observation of dolomite and calcite minerals in corrosion scales. The sources of vanadium and arsenic are unknown and require further research. Copper incorporated into lead scales could be due to the galvanic mechanism discussed previously.

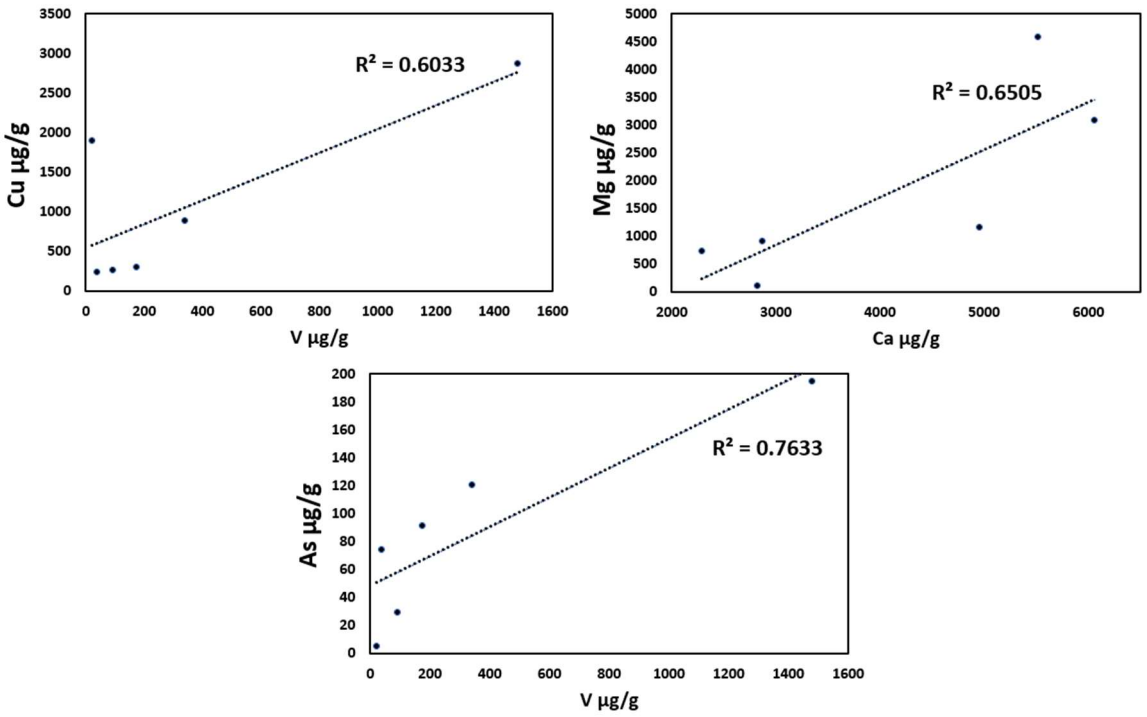

Figure 4-21. Elemental association trends observed in lead pipes between V and Cu, Ca and Mg, and V and As.

4.5.2 ICP-MS Analysis by Distribution System

The varying water quality of each distribution system can contribute different factors to metal contamination within the pipe scales. As previously stated, Milwaukee utilizes aluminum sulfate as a coagulant, and has significant accumulation of aluminum within its corrosion scales compared to Oak Creek and Waukesha ($p < 0.01$). Oak Creek uses a proprietary blend of poly aluminum chloride as coagulant and has an average aluminum concentration of 13,336.31 µg/g compared to Waukesha's 538.23 µg/g, although it is not statistically significant at $p > 0.05$ due to concentration variance between samples. For reference, Milwaukee has an average aluminum concentration in its corrosion scales of 11,836.60 µg/g.

Waukesha had the hardest water of the three distribution systems yet trailed just behind Oak Creek in average calcium concentration, independent of pipe material. Dolomite or calcite were found in almost all Oak Creek samples, and calcium and magnesium concentrations were present at 11,869.03 and 1,082.15 μg/g respectively. The formation of carbonate scales on pipe walls can be a function of time as well as concentration. Since both distribution systems identified carbonate minerals in the corrosion scales, it's important to recognize the relevance of the specific minerals. In WK2-Pb, the lead carbonate mineral cerussite was partially or completely covered by plattnerite, inhibiting further incorporation of carbonate minerals. This could decrease the activity of calcium to exchange with carbonates.

Milwaukee had more samples that could be analyzed via ICP-MS, but also had some statistical variance that led to potential outliers. For example, Milwaukee had the highest average concentrations of toxic trace metals arsenic (162.03 μg/g), chromium (119.40 μg/g), barium (913.95 μg/g), uranium (184.71 μg/g), and vanadium (263.66 μg/g). Concentrations within Oak Creek and Waukesha samples were consistently at least half as high, and in the case of uranium, Waukesha and Oak Creek had concentrations of 1.21 and 1.28 μg/g. Lead sample MKE-10 had a uranium concentration of 2,605.33 μg/g which was deemed statistically significant from the blanks. Even factoring this sample out of the average, Milwaukee had a surprisingly high uranium concentration at 23.34 μg/g. Milwaukee lead pipes average uranium level was 539.72 μg/g (or 23.32 μg/g taking out MKE-10). Comparatively, iron pipes had concentrations far below this at 4.94 μg/g. These concentrations are a few orders of magnitude higher than would be found in any treated water. This is a product of accumulation over the long service life of the pipes. Many of these samples could violate the EPA's drinking water

quality standards if they were to mass release the trace metals back to the water. While it isn't likely that mass release would occur, it is best to be aware of all scenarios, including slow release over time (a counter action to the slow accumulation and integration into the corrosion scales).

4.5.3 ICP-MS Analysis by Pipe Type

Most published field studies sample and analyze internal corrosion of drinking water pipes from a single distribution system or many distribution systems but one pipe material. This work is novel in that three distribution systems with different finished water qualities were examined, and three pipe materials were examined serving different purposes. The effect of water mains or laterals from different distribution systems with the same pipe material has not been reported to the knowledge of the researcher. Differences in contaminant accumulation is not only driven by pipe material, but also by mechanical forces such as water pressure and stagnation time.

Milwaukee mains are comprised of unlined cast iron pipes that range in service age from 66 – 69 years. Oak Creek mains are constructed of ductile iron and are younger, between 33 – 38 years. The only iron pipes from Waukesha were laterals and were not considered despite them being unlined cast iron. Despite the age difference in service use, the cast iron pipes experienced significantly more iron corrosion, both visually and through ICP-MS analysis of iron accumulation ($p < 0.01$). Figure 4-22 shows the iron accumulation within Oak Creek and Milwaukee mains with respect to age. Despite the discrepancy of service length between the

two types, it is clear that the ductile iron pipes withstood corrosion better, even without an added corrosion inhibitor.

Cast iron pipes from Milwaukee had an average iron concentration of 314,873.4 µg/g, compared to 94,195.01 µg/g in Oak Creek ductile iron pipes. Even the copper pipe from Oak Creek had higher iron accumulation at 121,297.50 µg/g. In total, cast iron pipes had an average iron concentration of 362,508.90 µg/g. The iron corrosion scaling relationship with pipe age was better for mains than laterals (R^2 = 0.829 for mains, R^2 = 0.509 for laterals) shown in figure 4-23. Mains may accumulate trace metals and corrode slowly over time due to constant flow conditions, while laterals have transient conditions that do not allow for consistent accumulation. Regardless of service type, pipe material, and distribution system, an R^2 of 0.480 for iron concentration was calculated with respect to age. This data only represents the pipes for which the service age was known. Ductile iron corrosion had the most linear relationship with respect to age, with R^2 = 0.871.

Corrosion of cast iron pipes were visually and analytically different for Milwaukee and Waukesha. Milwaukee pipes did not form as pronounced of tubercles as Waukesha pipes and had visibly less corrosion layer buildup. Layering effects were not considered in this study, and the primary minerals detected in all scales were in the +3-oxidation state. The average iron concentration within the Milwaukee scales was 309,213.68 µg/g, compared to 553,050.90 µg/g within Waukesha. Albeit from a smaller sample size, the maximum value from Milwaukee was still dwarfed by the average Waukesha concentration, at 474,960.94 µg/g. Corrosion appears to increase linearly with service age as shown in figure 4-23. This could be explained by the absence of main samples from Waukesha, as the laterals generally had higher corrosion of iron.

Iron laterals had higher concentration levels of iron than iron mains for both material types. Cast iron mains had an average iron concentration of 314,873.40 µg/g, while cast iron laterals had an average of 553,050.90 µg/g. For ductile iron, mains had an average iron concentration of 98,102.15 µg/g, while laterals had an average of 263,935.93 µg/g (albeit only one sample from Milwaukee). The high pressure within laterals to force water vertically throughout a building and around corners may enable mechanical detachment of the corrosion scales after long periods of stagnation, wherein the pipe scale may accumulate. Non-lead-based laterals also had significant levels of lead compared to the iron mains, with the iron laterals being upwards of 40x higher in lead concentration ($p < 0.01$).

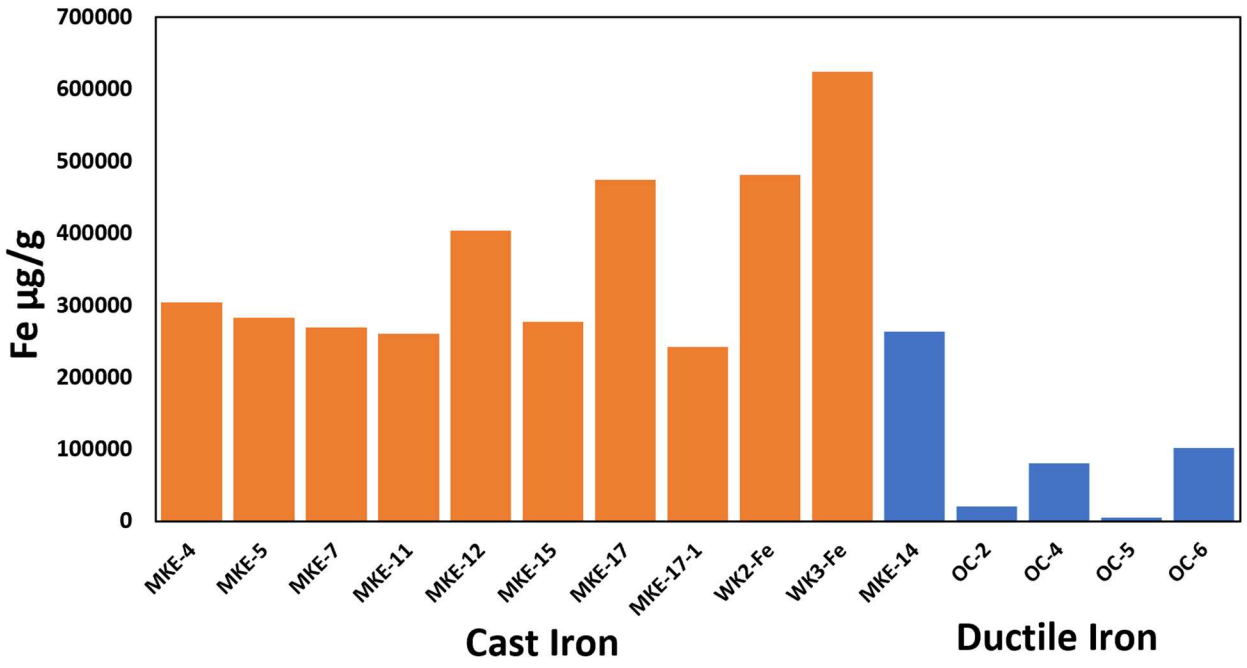

Figure 4-22. Iron accumulation within corrosion scales of Milwaukee cast iron mains, and Oak Creek ductile iron mains.

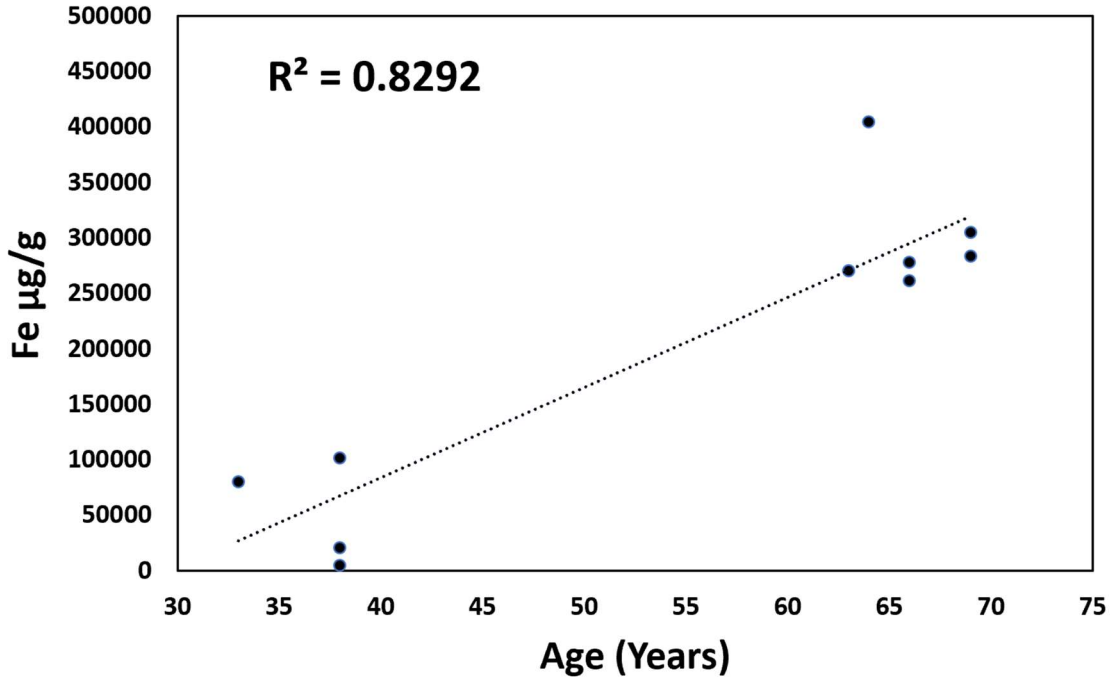

Figure 4-23. Iron corrosion increases as pipe age increases ductile and cast iron mains.

Trace metal accumulation of aluminum, vanadium, arsenic, and manganese was statistically significant in laterals compared to mains ($p < 0.05$). The abundance of these trace metals may be just as much a factor of water quality as physical forces. Stagnation within the pipes in between water use results in high contact time with dissolved species in the water and the surrounding pipe wall. Interactions such as adsorption of arsenic onto iron corrosion solids is a well-documented phenomenon (Lytle et al. 2004; Copeland et al. 2007; Kim & Herrera, 2010). One study even correlated aluminum and arsenic concentrations within lead laterals, although that was not reproducible in this study despite both being statistically significant in the laterals ($R^2 = 0.029$) (Kim & Herrera, 2010).

Magnesium was the only non-base material that was significantly higher in the mains ($p < 0.05$). Dolomite was detected in 7 of the 14 mains samples and was not detected in any iron laterals. Calcite was observed in 1 of 2 iron laterals as well as 5 of the 14 mains. The formation pathways for these minerals are simple precipitation due to supersaturation, and ion exchange or substitution may occur between calcium and magnesium. Magnesium would be higher in concentration in the mains as they are closer upstream in the plumbing system and may be precipitated out of solution early, whereas calcium concentrations were typically greater than twice as high and can continue to precipitate further downstream in the laterals.

4.6 Sequential Extraction Results and Discussion

Sequential extraction experiments have been scarcely conducted for corrosion scales from drinking water pipes. The original method proposed by Tessier in 1979 was developed for trace metal analysis within sediments (Tessier et al. 1979). To date, two studies have adapted this method for analysis of metal speciation within iron pipes (Peng & Korshin, 2011; Gao et al. 2019). No prior studies have published the speciation of metals within copper and lead pipes. This study maintains the original 5 fractions proposed by Tessier, in order from easiest to be re-released: Exchangeable, Bound to Carbonates, Bound to Iron/Manganese Oxides, Bound to Organic Matter, and Residual (Tessier et al. 1979). The metals found within each fraction can be an important key to informing water engineers about how to limit availability for re-release of trace metals back into water.

Sediment and soil studies performing the sequential extraction method typically use greater than 1 g of solid per sample. Due to the limited amount of solid per each corrosion

sample, 200 mg was chosen, and triplicates were used. All reactions were completed within 50 mL centrifuge tubes that were clean of any prior metal contamination. The full suite of metals measured by ICP-MS were also analyzed here, but the main focus was on toxic metals and some of the most abundant metals found in every sample in ICP-MS analysis (Al, Mn, Fe, Cu, Zn, As, Pb, Ba). Four iron samples (three from Milwaukee and one from Waukesha) were analyzed, as well as three lead samples (two from Milwaukee, one from Waukesha). Owing to the small sample size of the copper corrosion solids, only one sample from Milwaukee had enough to run a single test.

4.6.1 Sequential Extraction of Iron Results

Iron was found majorly in two fractions which may be explicable by the distribution system the sample was from. For the three Milwaukee samples the dominant fraction was the residual and least mobile fraction. This is in contrast to the lone Waukesha sample which was a lateral and not a drinking water main, and the dominant fraction was the iron/manganese oxides. Gao et al. reported similar results with the top two fractions being residual and iron/manganese oxides and assumed the residual fraction consisted of mostly well-formed crystalline iron oxides and primary silicate minerals (Li & Thornton, 2001; Gao et al. 2019). It has also been speculated that the iron/manganese oxide fraction consists of easy to be reduced forms of these elements and poorly crystalline structures, giving way to amorphous iron oxides (Kim & Fergusson, 1991). This was not seen in this study, as XRD could not identify a crystalline iron form in sample MKE-17, yet it had the highest distribution in the residual fraction (91.5%) and a low percentage in the iron/manganese oxides (7.0%). Whether or not the sample was

from a pipe scraping or a loose pipe deposit scale has been examined in past literature and did not make a difference in this study, although it should be noted that the lone Waukesha sample had the only non-residual dominant fraction (Gao et al. 2019). Not enough sample material was available to explore this further.

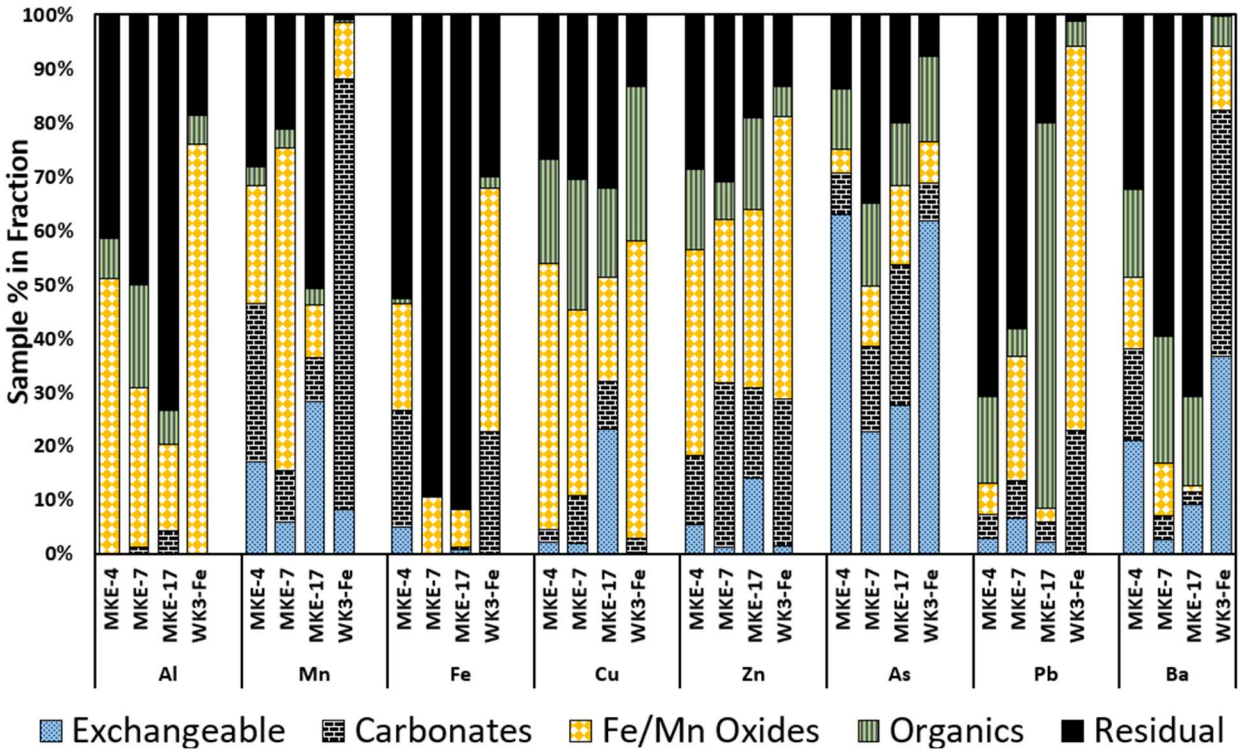

Figure 4-24. Average fraction percentage of heavy metal binding in iron corrosion scales.

Aluminum was found between iron/manganese oxide fraction and the residual fraction. Two samples had aluminum predominantly in the residual fraction and second highest in the oxides fraction, and vice versa. These agree with the literature from the only other study of iron pipe trace metal partitioning (Gao et al. 2019). As the second highest metal by concentration in these experiments, manganese was split between the bound to carbonates fraction (2 of 4

samples), and the residual and iron/manganese oxides fraction. In every sample these were the top three binding fractions, except for MKE-17 which had 28.2% in the exchangeable fraction.

The dominant fraction for copper was in the iron/manganese oxides in 3 of the 4 samples. These results compare well with previous studies as copper is known to become adsorbed by iron and manganese oxide minerals (Gao et al. 2019). The second highest fraction was the residual fraction which was the main fraction for copper in sample MKE-17. By virtue of copper binding in these fractions, changes in redox potential or pH could cause mobility of the copper into water sources (Balasoui et al. 2001). Still relatively high, the bound to organics fraction was the third highest fraction (22% average). Copper can form very stable complexes with organic matter and are seen as one of the highest fractions for copper partitioning in soils (Balasoui et al. 2001; Papafilippaki et al. 2007; Iwegbue, 2013; Gao et al. 2019).

Zinc concentrations were highest in the iron/manganese oxides (38.5%), followed by the residual fraction (23.1%), and the bound to carbonates fraction (21.9%). Barium was present mainly in the residuals (40.1%) and the rest mixed between the carbonates (17.3%), exchangeable (17.3%) and organics (15.5%). Barium can pose a health threat upon ingestion but was found to be mostly in the immobile fraction of residuals. Lead was measured highest in the residual fraction in 2 of the 4 samples (37.7% total), while also occurring the highest in the organics fraction and the iron/manganese oxides fraction in the remaining two (24.2% and 25.7% respectively). This may partially support other studies which have found lead adsorption onto iron oxide surfaces. Elements that are found in the iron and manganese oxide fraction are controlled by the sorption processes of those metal complexes, which then control their

release. Lead concentrations were lowest within the exchangeable fraction which indicated it would not be easily released from iron corrosion scales.

The majority of arsenic was found present in the easily released exchangeable fraction (43.7%). The implications for this are that changing water quality conditions could increase the release of arsenic into drinking water, which could have potentially serious adverse health effects. Interestingly, the second highest source of arsenic was in the residual fraction which are considered very inert under most drinking water conditions (Peng & Korshin, 2011). This fraction of arsenic would be protected and would be very difficult to be released into the drinking water. The carbonates and organics were the next two highest sources of arsenic (14.1% and 13.5% respectively). Sample MKE-17 had arsenic at 26.1% within the carbonate fraction, which may be explained by the ability of arsenic to substitute for carbon within carbonate minerals such as calcite (Lin et al. 2018).

4.6.2 Sequential Extraction of Lead Results

The same trace metals were analyzed for lead pipes which were all pipe scrapings from service lines. To date, there have not been any known publications investigating the partitioning of trace metals within lead pipes, or lead-containing sediments. Two samples from Milwaukee and one from Waukesha were examined. Lead concentrations were highest in the carbonates fraction for every sample (65.5% average). XRD results for all of these samples indicated the abundance of carbonate minerals in these corrosion scales (hydrocerussite, plumbonacrite, calcite, and dolomite). The lone Waukesha sample also detected plattnerite co-

existence with cerussite. The second highest concentration of lead within this sample was in the iron/manganese oxides.

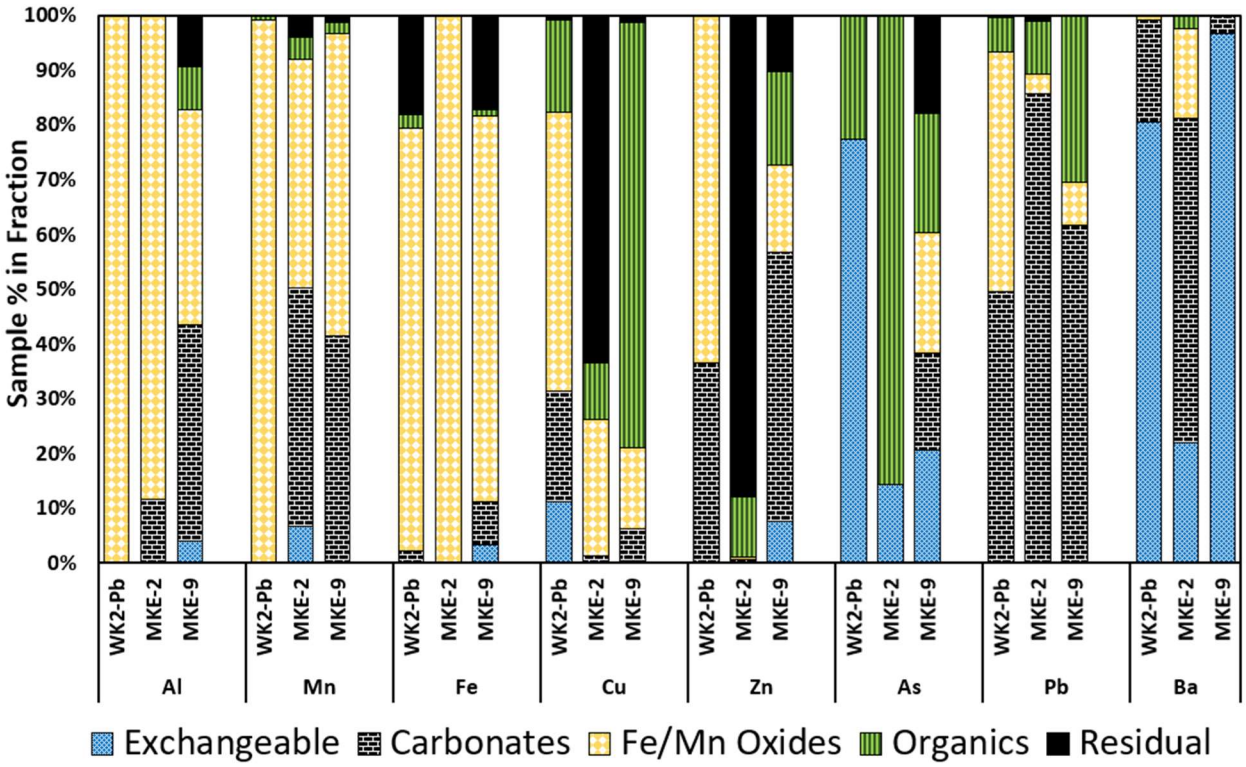

Figure 4-25. Average fraction percentage of heavy metal binding in lead corrosion scales.

Aluminum was found highest within the iron/manganese oxides (75.8% average across three samples). For the lone Waukesha sample, this fraction represented the only source of aluminum binding as it was not detected in any other fraction. The second highest fraction was the bound to carbonates, and this was the highest level of aluminum within sample MKE-9 by a narrow margin over the iron/manganese oxides (39.6% to 39.3%). Manganese exhibited similar trends with the abundance of the metal being found in the iron/manganese oxides (65.4%

average) with the next highest level being the carbonates (28.3%). Iron had the best consistency across samples with the majority of the metal being in the iron/manganese oxides (82.5% average). Comparable to the iron pipe sequential extraction results, iron found in this phase is expected to have poorly formed crystalline structure, and could be amorphous (Kim & Fergusson, 1991). Iron was the second highest element within the lead corrosion scales via ICP-MS, although there were no distinct iron phases detected by XRD.

The top two fractions for barium were the exchangeable (66.5% average) and carbonates (27.0%). The remaining elements displayed poor trends due to the small sample size of lead pipes that could be featured in this experiment. The dominant copper fraction was split across the three samples. Within the Waukesha sample, the iron/manganese oxides were the highest source (51.1%), and the two Milwaukee samples had copper majorities in the residual and organics phase (MKE-2 and MKE-9). Overall, the most copper was found in the bound to organics phase (35.0%), followed by the reduceable iron/manganese oxide fraction (30.3%), and finally the residual phase (21.7%). All samples were in agreement that the lowest fraction was the exchangeable binding fraction.

The residual fraction measured the highest average levels of zinc across all samples but was only the dominant fraction for sample MKE-2 (32.7% average across all samples). The Waukesha sample had a highest fraction within the iron/manganese oxides (63.5%), while the MKE-9 sample had the highest zinc concentration in the carbonates group (49.0%). The carbonates were the second highest source of zinc (28.7% average) followed by the iron/manganese oxides (26.7% average). Similarly, arsenic did not have any outlying trends

such as in iron pipe corrosion scales. All three samples had varying dominant fractions such as exchangeable, iron/manganese oxides, and organics. The organics fraction was the highest on a per-sample basis, at 43.3% average. The only other significant fraction was the exchangeable fraction at 37.6% average. This was the dominant fraction for the Waukesha sample which featured PbO_2 phase plattnerite. Arsenic present in this binding fraction could indicate that accumulation of arsenic occurred after deposition of the PbO_2 film and could be released into the water by simple changes in potential or pH, not directly related to PbO_2 stability.

To quantify the extent that organic matter may be present in the corrosion scale, either as a biofilm or other organic/inorganic complexes, the total carbon was measured analytically via Carlo Erba NA 1500 Elemental Analyzer. This is not a direct calculation of the organic matter, as some of the carbon is likely in the inorganic form. For instance, in table 4-6, sample OC-5 did not have any distinguishable iron minerals but had dolomite. OC-1 was another sample from Oak Creek that had copper carbonate mineral malachite but had a 10x lower carbon weight percentage. There was minimal difference in carbon percent from Milwaukee as MKE-4 did not have carbonate minerals and MKE-17 did. Carbon content was slightly higher for lead samples, of which all samples had carbonate-complexes. From this data it can be speculated that organic matter content within Milwaukee is low but could still be significant in complexation for trace metals. Oak Creek and Waukesha had higher carbon but weight percentage which could present more opportunity for organic matter complexes.

Table 4-6. Total carbon weight % of various samples.

Sample	Total Carbon (weight %)
MKE-4 (Cast Iron)	1.03%
MKE-17 (Cast Iron)	0.93%
WK2-Fe (Cast Iron)	3.60%
WK3-Fe (Cast Iron)	8.83%
OC-5 (Ductile Iron)	53.86%
MKE-13 (Copper)	1.18%
OC-1 (Copper)	4.99%
MKE-6 (Lead)	2.38%
WK2-Pb (Lead)	1.04%

4.6.3 Sequential Extraction Copper Results

Only one copper sample from Milwaukee could be analyzed due to the limited corrosion exhibited by copper pipes. It is important to note that the only crystalline phase identified in this sample was cuprous oxide (Cu_2O), so there were no other elements detected in associated minerals or complexes with copper. In summary, limited trends could be deduced from the data due to a single data point from a single municipality. Similar to lead, to the knowledge of the researcher there have been no reports or studies conducted on sequential extraction techniques of copper corrosion scales.

The highest concentration of copper was found in the bound to organics fraction (46.5% total). Copper can form stable complexes with organic matter within soil and has been found in abundance within this fraction in sequential extraction results of soil (Balasoui et al. 2001; Papafilippaki et al. 2007; Iwegbue, 2013). The next highest fraction was the residuals (28.3%) belying the notion that copper mobility from these scales would be quite difficult.

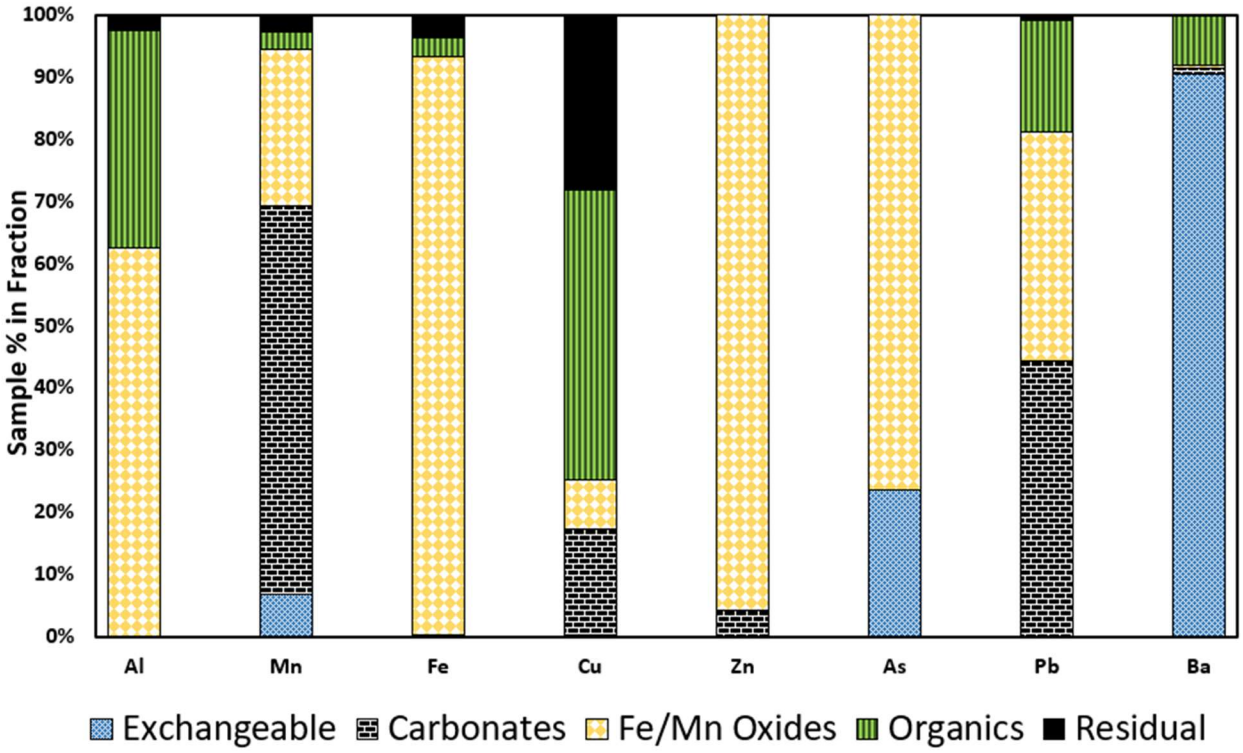

Figure 4-26. Average fraction percentage of heavy metal binding in copper corrosion scale MKE-13.

The remaining trace metals were found above the bound to organics fraction, indicating an increase in mobility. Aluminum (62.5%), iron (92.8%), arsenic (76.2%) and zinc (95.6%) were found within the reduceable iron/manganese oxides phase. From the ICP-MS elemental analysis it was determined iron was the second most abundant metal within the copper corrosion

scales, albeit at 5.69% by weight. Aluminum and manganese were the second and third most abundant at 1.69% and 0.77%. Despite the presence of these metals, they were not observed in crystalline form to suggest copper complexation or associated minerals. Manganese (62.5%) and lead (44.2%) were observed highest in the carbonates fraction, likely forming amorphous carbonate complexes that could not be detected by XRD. Barium was measured at 90.3% in the exchangeable fraction, a comparable level to that shown in the lead samples.

4.6.4 Sequential Extraction General Trends

General trends independent of pipe material and distribution system were distinguishable for a few trace metals. For instance, the top two fractions for aluminum within 7 of the 8 samples were heavily associated with iron/manganese oxides, and the mobilization resistant residual fraction. The outlier was sample MKE-9 which found aluminum in the carbonates fraction at 39.6% compared to 39.3% within the reduceable oxides.

Milwaukee iron pipes main source of iron was within the residual fraction, whereas a single Waukesha pipe had highest levels in the iron/manganese oxides. Past studies have demonstrated that the primary source of arsenic was in the residuals, while this research found arsenic in the exchangeable fraction, followed by the residual fraction (Peng & Korshin, 2011; Gao et al. 2019). Arsenic in the +5-chemical state is known to have moderate affinity to adsorb to iron mineral surfaces such as goethite, but the chemical state was not examined in this work (Wilkie & Hering 1996; Dixit & Hering, 2003). Prior research found As(V) associated mainly with the mobilization resistant fraction, as As(V) is less mobile than As(III) (Dexit & Hering, 2003; Peng & Korshin, 2011). As(III) had higher affinity for iron minerals such as goethite, but that was

not seen in the present study as goethite was found in 3 of the 4 samples. Phosphates from orthophosphate corrosion inhibition in Milwaukee could compete with As(V) for binding sites, allowing As(III) to dominate (Dixit & Hering, 2003).

Chapter 5: Conclusions and Future Work

5.1 Conclusions

This study aimed to uncover the internal corrosion makeup of three distribution systems in South-Eastern Wisconsin. Despite what could be attributed as a localized study, the different source water and pipe materials have potential implications for other distribution systems. Mains from two distribution systems were compared, of which ductile iron and cast iron pipe corrosion were scrutinized for the first time to the knowledge of the researcher. Ductile iron pipes were observed to be significantly more resistant to corrosion, through the absence of a distinguishable iron corrosion mineral, and in accumulation of iron deposited at the pipe-water interface. Iron mains had a positive correlation of iron accumulation with respect to age (R^2 = 0.8292) indicating uniform corrosion. Of all the iron samples, goethite and lepidocrocite were the only iron-bearing minerals observed.

Accumulation of major and trace metals were mostly significantly higher in laterals compared to water mains. This is attributed to the stagnation periods when water is not in use that leads to high contact time between the bulk water, ions in solution, and the pipe wall that can lead to adsorption, deposition, or other accumulation mechanisms. Iron was the most abundant metal in all pipe materials following the base metal, followed by a top five trend of calcium, manganese, magnesium, and aluminum.

This study was the first to perform an adapted sequential extraction experiment on copper and lead pipes. Within iron pipes, iron accumulation was mostly localized to the mobilization resistant residual fraction. Due to the overwhelming majority of lead-carbonate

minerals present in the lead pipes, the extent of lead speciation was mainly in the carbonates fraction. Lastly for copper pipes, the ability of copper to form stable complexes with organic matter resulted in a dominant fraction of the bound to organics. The speciation of other toxic metals largely depended on the pipe material, yet only aluminum could be ascertained within the iron and manganese oxide/reducible fraction for all pipe materials.

5.2 Future Work

It should be noted that although these results may be non-unique to this region, care should be taken when implicating the results to other distribution systems. Theory developed in lab may tell us how corrosion should develop over time, but observations in the field usually have outliers. Distribution systems that have identical water quality may find different corrosion minerals or trace element accumulation within their drinking water pipes. Disruptions in service, changes in disinfectant/pH/alkalinity and more are possible reasons that formation may be hindered and changed from what was found in this study.

Despite this, more work should be focused on identifying minerals in copper and lead pipes, and connected to the water quality of the distribution systems that they were surveyed in. Sequential extraction experiments should be used to verify the mobility of toxic heavy metals to prevent their release back into the drinking water. More work should also be conducted on naturally occurring organic material in the distribution system such as biofilms that can create localized reduced or oxidized regions. Biofilms can also be a source or sink for trace metals and could be a source for accumulation into corrosion scales.

References

[1] Bae, Yeunook., Pateris, Jill D., and Giammar, Daniel E. (2019). “The ability of phosphate to prevent lead release from pipe scale when switching from free chlorine to monochloramine”. Environmental Science & Technology 52(2): 879 – 888.

[2] Balasoiu, Cristina F., Zagury, Gerald J., and Deschenes, Louise. (2001). “Partitioning and speciation of chromium, copper, and arsenic in CCA-contaminated soils: influencing of soil composition. The Science of the Total Environment 280(1-3): 239 – 255.

[3] Boulay, Nicolle., and Edwards, Marc. (2001). “Role of temperature, chlorine, and organic matter in copper corrosion by-product release in soft water”. Water Research 35(3): 683 – 690.

[4] Brown, Dennis G., and Weser, Ulrich. (1979). “XPS spectra of copper and nickel biuret complexes – observations of intense satellite structure in the 2p spectrum of a copper(III) system”. Zeitschrift Fur Naturforschung B 34(7): 989 – 994.

[5] Camara, Eliman., Montreuil, Krysta, R., Knowles, Alisha K., Gagnon, Graham A. (2013). “Role of the water main in lead service line replacement: a utility case study”. Journal – American Water Works Association 105(8): E423 – E431.

[6] Cantor, Abigail F., Denig-Chakroff, David., Vela, Richard R., Oleinik, Mark G., and Lynch, Daniel L. (2000). “Use of polyphosphate in corrosion control”. Journal – American Water Works Association 92(2): 95 – 102.

[7] CDC.gov (2022). “Health Effects of Lead Exposure”. Retrieved September 2, 2022, from https://www.cdc.gov/nceh/lead/prevention/health-effects.htm

[8] Chusuei, C. C., Brookshier, M. A., and Goodman, D. W. (1999). “Correlation of relative x-ray photoelectron spectroscopy shake-up intensity with CuO particle size”. Langmuir 15(8): 2806 – 2808.

[9] Congress.gov. S.3874 – Reduction of Lead in Drinking Water Act. Retrieved September 9, 2022, from https://www.congress.gov/bill/111th-congress/senate-bill/3874

[10] Copeland, Rachel C., Lytle, Darren A., and Dionysiou, Dionysios, D. (2007). "Desorption of arsenic from drinking water distribution system solids". Environmental Monitoring Assessment 123(1-3): 523 - 535.

[11] Das, Soumya., Hendry, Jim M., and Essilfie-Dughan, Joseph. (2013). “Adsorption of selenate onto ferrihydrite, goethite, and lepidocrocite under neutral pH conditions”. Applied Geochemistry 28: 185 – 193.

[12] Davidson, C. M., Peters, N. J., Britton, A., Brady, L., Gardiner, P. H. E., and Lewis, B. D. (2004). “Surface analysis and depth profiling of corrosion products formed in lead pipes used to supply low alkalinity drinking water”. Water Science & Technology 49(2): 49 – 54.

[13] Denig-Chakroff, D. (2001). “If the regulation fits, wear it ---If not, stretch it: A case study of compliance with the lead and copper rule”. Proc. AWWA Annual Conference and Exhibition, Washington.

[14] DeSantis, Michael K., Triantafyllidou, Simoni., Schock, Michael R., and Lytle, Darren A. (2018). “Mineralogical evidence of galvanic corrosion in drinking water lead pipe joints”. Environmental Science & Technology 52(6): 3365 – 3374.

[15] DeSantis, Michael K., Schock, Michael R., Tully, Jennifer., and Bennett-Stamper, Christina. (2020). “Orthophosphate interactions with destabilized PbO2 scales”. Environmental Science & technology 54(22): 14302 – 14311.
[16] Dhineshbabu, N. R., Rajendran, V., Nithyavathy, N., and Vetumperumal, R. (2016). “Study of structural and optical properties of cupric oxide nanoparticles”. Applied Nanoscience 6: 933 – 939.
[17] Dryer, Deborah, J., and Korshin, Gregory V. (2007). “Investigatio of the reduction of lead dioxide by natural organic matter”. Environmental Science & Technology 41(15): 5510 – 5514.
[18] Edwards, Marc., and Ferguson, John F. (1993). “Accelerated testing of copper corrosion”. Journal – American Water Works Association 85(10): 105 – 113.
[19] Edwards, Marc., Jacobs, Sara., and Dodrill, Donna. (1999). “Desktop guidance for mitigating Pb and Cu corrosion by-products”. Journal – American Water Works Association 91(5): 66 – 77.
[20] Edwards M., Powers, K., Hidmi, L., and Schock, Michael R. (2001). “The role of pipe ageing in copper corrosion by-product release”. Water Science and Technology: Water Supply 1(3): 25 – 32.
[21] Edwards, Marc, and Dudi, Abhijeet. (2004). "Role of chlorine and chloramine in corrosion of lead-bearing plumbing materials". Journal- American Water Works Association 96(10): 69 - 81.
[22] Edwards, Marc., and Triantafyllidou, Simoni. (2007). “Chloride-to-sulfate mass ratio and lead leaching to water”. Journal – American Water Works Association 99(7): 96 – 109.
[23] EPA.gov[1] (2021). “Lead and Copper Rule”. Retrieved September 23, 2022, from https://www.epa.gov/dwreginfo/lead-and-copper-rule
[24] EPA.gov[2] (2022). “National Primary Drinking Water Regulations”. Retrieved September 23, 2022, from https://www.epa.gov/ground-water-and-drinking-water/national-primary-drinking-water-regulations
[25] EPA.gov[3] (2020). “Safe Drinking Water Act”. Retrieved September 23, 2022, from https://www.epa.gov/sites/default/files/2020-05/documents/safe_drinking_water_act-title_xiv_of_public_health_service_act.pdf
[26] EPA.gov[4] (2022). “Lead Service Line Replacement”. Retrieved September 9, 2022, from https://www.epa.gov/ground-water-and-drinking-water/lead-service-line-replacement
[27] EPA.gov[5] (2022). “Secondary drinking water standards: guidance for nuisance chemicals”. Retrieved September 8, 2022, from https://www.epa.gov/sdwa/secondary-drinking-water-standards-guidance-nuisance-chemicals
[28] Erel, Yigal, and Morgan, James J. (1992). “The relationship between rock-derived lead and iron in natural waters”. Geochemica et Cosmochimica Acta 56(12): 4157 – 4167.
[29] Feng, Q. L., Pu, G., Pei, Y., Cui, F. Z., Li, H. D., and Kim, T. N. (2000). “Polymorph and morphology of calcium carbonate crystals induced by proteins extracted from mollusk shell”. Journal of Crystal Growth 216(1-4): 459 – 465.
[30] Gao, Jiali., Liu, Quanli, Song, Laizhou., and Shi, Baoyou. (2019). “Risk assessment of heavy metals in pipe scales and loose deposits formed in drinking water distribution systems”. Science of the Total Environment 652(20): 1387 – 1395.

[31] Gerke, Tammie L., Maynard, J. Barry., Schock, Michael R., and Lytle, Darren L. (2008). "Physiochemical characterization of five iron tubercles from a single drinking water distribution system: possible new insights on their formation and growth". Corrosion Science 50(7): 2030 – 2039.
[32] Gerke Tammie L., Scheckel, Kirk G., and Shock, Michael R. (2009). "Identification and distribution of vanadinite (Pb5(V5+O4)3Cl) in lead pipe corrosion by-products". Environmental Science & Technology 43(12): 4412 – 4418.
[33] Gerke, Tammie L., Little, Brenda J., and Maynard, J Barry. (2016). "Manganese deposition in drinking water distribution systems". Science of the Total Environment 541: 184 – 193.
[34] Ghodselahi, T., Vesaghi, M. A., Shafiekhani, A., Baghizadeh, A., and Lameii, M. (2008). "XPS study of the Cu@Cu_2O core-shell nanoparticles". Applied Surface Science 255(5): 2730 – 2734.
[35] Guo, Daoping, and Herrera, Jose E. (2021). "Influence of drinking water quality on the formation of corrosion scales in lead-bearing drinking water distribution systems". Journal of Environmental Science and Health, Part A: 1-12.
[36] Gupta, S, and Chen, K. (1975). "Partitioning of trace metals in selective chemical fractions of nearshore sediments". *Environmental Letters* 10: 129 – 158
[37] Hayes, Colin R., Croft, Nick., Phillips, Edith., Craik, Steve., and Schock, Michael R. (2016). "An evaluation of sampling methods and supporting techniques for tackling lead in drinking water in Alberta Province". Journal of Water Supply 65(5): 373 – 383.
[38] Hanna-Attisha, Mona., LaChance, Jenny., Sadler, Richard C., and Schnepp, Allison C. (2016). "Elevated blood lead levels in children associated with the Flint drinking water crisis: a spatial analysis of risk and public health response". American Journal of Public Health 106: 283 – 290
[39] Heyer, C. (1888). "Ursache und beseitigung des bleiangriffs durch leitungswasser, verlag Paul Baumann, Dessau. Publishing house of Paul Baumann.
[40] Hopwood, Jeremy D., Derrick, Glyn R., Brown, David R., Newman, Christopher D., Haley, John., Kershaw, Richard., and Collinge, Mike. (2016). "The identification and synthesis of lead apatite minerals formed in lead water pipes". Journal of Chemistry.
[41] ICDD.com (2022). "International Center for Diffraction Data". Retried September 14, 2022, from https://www.icdd.com/
[42] Itamiya, Hiromi., Sugita, Ritsuko., and Sugai, Toshihiko. (2019). "Analysis of the surface microtextures and morphologies of beach quartz grains in Japan and implications for provenance research". Progress in Earth and Planetary Science 6(43):
[43] Iwegbue, Chukwujindu M. A. (2013). "Chemical fractionation and mobility of heavy metals in soils in the vicinity of asphalt plants in Delta State, Nigera". Environmental Forensics 14(3): 248 – 259.
[44] Jones, D.A. (1996). "Principles and Prevention of Corrosion, 2nd edition". Prentice-Hall, Inc. ISBN 0-13-359993-0.
[45] Kim, N.D., and Fergusson, J.E. (1991). "Effectiveness of a commonly used sequential extraction technique in determining the speciation of cadmium in soils". The Science of the Total Environment 105: 191 – 209.

[46] Kim, Eun Jung, and Jose E. Herrera. (2010). "Characteristics of lead corrosion scales formed during drinking water distribution and their potential influence on the release of lead and other contaminants." Environmental science & technology 44(16): 6054-6061.
[47] King, Fraser. (2010). “Critical review of the literature on the corrosion of copper by water”. Integrity Corrosion Consulting Limited, Technical Report TR-10-69.
[48] Klueh, Kevin G., and Robinson, R. Bruce. (1988). “Sequestration of iron in groundwater by polyphosphates”. Journal of Environmental Engineering 114(5): 1192 – 1199.
[49] Knobeloch, L., Schubert, C., Hayes, J., Clark, J., Fitzgerald, C., and Fraundorff, A. (1998). “Gastrointestinal upsets and new copper plumbing – is there a connection?”. Wisconsin Medical Journal 97(1): 49 – 53.
[50] Knowles, Alisha D., Nguyen, Caroline K., Edwards, Marc A., Stoddart, Amina., McIlwain, Brad., and Gagnon, Graham A. (2015). “Role of iron and aluminum coagulant metal residuals and lead release from drinking water pipe materials”. Journal of Environmental Science and Health 50(4): 414 – 423.
[51] Kosmulski, Marek., Durand-Vidal, Serge., Maczka, Edward., and Rosenholm, Jarl B. (2004). “Morphology of synthetic goethite particles”. Journal of Colloid and Interface Science 271(2): 261 – 269.
[52] Kvech, Steven., and Edwards, Marc. (2001). “Role of aluminosilicate deposits in lead and copper corrosion”. Journal – American Water Works Association 93(11): 104 – 112.
[53] Lagos, Gustavo E., Cuadrado, Claudia A., Letelier, Victoria M. (2000). “Aging of copper pipes by drinking water”. Journal – American Water Works Association 93(11): 94 – 103.
[54] Lane, Russell W. (1993). “Control of scale and corrosion in building water systems”. McGraw Hill.
[55] Larson, Thurston, E., and Skold, R. V. (1957). “Corrosion and Tuberculation of Cast Iron”. Journal – American Water Works Association 49(10): 1294 – 1302.
[56] Larson, T. E., and Skold, R. V. (1958). “Laboratory studies relating mineral quality of water to corrosion of steel and cast iron”. Corrosion 14(6): 285 – 288.
[57] LeChevallier, Mark W., Lowry, Cheryl D., Lee, Ramon G., and Gibbon, Donald L. (1993). “Examining the relationship between iron corrosion and the disinfection of biofilm bacteria”. Journal – American Water Works Association 85(7): 111 – 123.
[58] Lee, Sai H., O’Connor, John T., and Banerji, Shankha K. (1980). “Biologically mediated corrosion and its effects on water quality in distribution systems”. Journal – American Water Works Association 72(11): 636 – 645.
[59] Legodi, M. A. and D. de Waal. (2007). “The preparation of magnetite, goethite, hematite and maghemite of pigment quality from mill scale iron waste”. Dyes and Pigments 74(1): 161 – 168.
[60] Lehrman, Leo., and Shuldener L, Henry. (1952). "Action of sodium silicate as a corrosion inhibitor in water piping". Industrial and Engineering Chemistry: 1765 - 1769.
[61] Lehrman, Leo., and Shuldener L, Henry. (1959). "Thirty years' experience with silicate as a corrosion inhibitor in water systems". Corrosion, 16(7): 354 - 358.
[62] Li Xiangdong, Li., and Thornton, Iain. (2001). “Chemical Partitioning of trace and major elements in soils contaminated by mining and smelting activities”. Applied Geochemistry 16(15): 1693 – 1706.

[63] Li, Manjie., Liu, Zhaowei., Chen, Yongcan., and Hai, Yang. (2016). “Characteristics of iron corrosion scales and water quality variations in drinking water distribution systems of different pipe materials”. Water Research 106: 593 – 603.
[64] Li, Bofu., Trueman, Benjamin F., Munoz, Sebastian., Locsin, Javier A., and Gagnon, Graham A. (2021). “Impact of sodium silicate on lead release and colloid size distributions in drinking water”. Water Research 190.
[65] Lin, Jianping., Ellaway, Mark., and Adrien, Robert. (2001). “Study of corrosion material accumulated on the inner wall of steel water pipe”. Corrosion Science 43(11): 2065 – 2081.
[66] Lin, Yi-Pin., and Valentine, Richard L. (2007). “The release of lead from the reduction of lead oxide (PbO_2) by natural organic matter”. Environmental Science & Technology 42(3): 760 – 765.
[67] Lin, Yi-Pin., and Valentine, Richard L. (2008). “Release of Pb(II) from monochloramine-mediated reduction of lead oxide (PbO_2)”. Environmental Science & Technology 42(24): 9137 – 9143.
[68] Lin, Yi-Pin., and Valentine, Richard L. (2009). “Reduction of lead oxide (PbO_2) and release of Pb(II) in mixtures of natural organic matter, free chlorine and monochloramine”. Environmental Science & Technology 43(10): 3872 – 3877.
[69] Lin, Junjie., Zhang, Shuai., Liu, Dan., Yu, Zhiguo., Zhang, Liuyi., Cui, Jian., Xie, Kun., Li, Tingzhen., and Fu, Chuan. (2018). “Mobility and potential risk of sediment-associated heavy metal fractions under continuous drought-rewetting cycles”. Science of the Total Environment 625: 79 – 86.
[70] Lintereur, Phillip A., Duranceau, Steven J., Taylor, James S., and Stone, Erica D. (2010). “Sodium silicate impacts on lead release in a blended potable water distribution system”. Desalination and Water Treatment 16(1-3): 427 – 438.
[71] Liu, J. H., Hao, X. Y., Li, G. L., Liu, G. S. (2002). “Microvoid evaluation of ferrite ductile iron under strain”. Materials Letters 56(5): 748 – 755.
[72] Liu, Haizhou., Korshin, Gregory V., and Ferguson, John F. (2008). “Investigation of the Kinetics and Mechanisms of the oxidation of cerussite and hydrocerussite by chlorine”. Environmental Science & Technology 42(9): 3241 – 3247.
[73] Liu, Ruyin., Zhu, Junge., Yu, Zhisheng., Joshi, DevRaj., Zhang, Hongxun., Lin, Wenfang., and Yang, Min. (2014). “Molecular analysis of long-term biofilm formation on PVC and cast iron surfaces in drinking water distribution system”. Journal of Environmental Sciences 26: 865 – 874.
[74] Lyon, S.B. (2010). “Corrosion of Lead and its Alloys”. Shreir’s Corrosion. 2053 – 2067.
[75] Lytle, Darren A., Sorg, Thomas J, and Frietch, Christy. (2004). "Accumulation of Arsenic in Drinking Water Distribution Systems". Environmental Science & Technology 38(20): 5365 - 5372.
[76] Lytle, Darren A, and Schock, Michael R. (2005). “Formation of Pb(IV) oxides in chlorinated water”. Journal – American Water Works Association 97(11): 102- 114.
[77] Lytle, Darren A., Schock, Michael R., and Scheckel, Kirk. (2009). “The inhibition of Pb(IV) oxide formation in chlorinated water by orthophosphate”. Environmental Science & Technology 43(17): 6624 – 6631.

[78] Lytle, Darren A., Schock, Michael R., Formal, Casey., Bennett-Stamper, Christina., Harmon, Stephen., Nadagouda, Mallikarjuna N., Williams, Daniel., Desantis, Michael K., Tully, Jennifer., and Pham, Maily. (2020). "Lead particle size fractionation and identification in Newark, New Jersey's drinking water". Environmental Science & Technology 54(21): 13672 – 13679.

[79] Madison Water Utility. "Lead & Copper in Water". Retrieved September 14, 2022, from https://www.cityofmadison.com/water/water-quality/water-quality-testing/lead-copper-in-water#:~:text=Replacing%20Lead%20Services&text=If%20you%20have%20a%20lead,email%20water%40madisonwater.org.

[80] Masters, Sheldon., and Edwards, Marc. (2015). "Increased lead in water associated with iron corrosion". Environmental Engineering Science 32(5): 361 – 369.

[81] Maynard, Barry J. (2008). "Overview of lead scale formation and solubility". University of Cincinnati.

[82] McFadden, Matthew., Giani, Richard., Kwan, Pierre., and Reiber, Steven H. (2011). "Contributions to drinking water lead from galvanized iron corrosion scales". Journal – American Water Works Association 103(4): 76 – 89.

[83] McGill, Sarah M. (2012). "Peak phosphorus? The implications of phosphate scarcity for sustainable investors". Journal of Sustainable Finance & Investment 2(3-4): 222 – 239.

[84] McNeill, Laurie S., and Edwards, Marc. (2001). "Iron pipe corrosion in distribution systems". Journal – American Water Works Association 93(7): 88 – 100.

[85] Mendoza-Flores, Arturo., Villalobos, Mario., Pi-Puig, Teresa., and Martinez, Nadia V. (2017). "Revised aqueous solubility product constants and a simple laboratory synthesis of the Pb(II) hydroxycarbonates: plumbonacrite and hydrocerussite". Geochemical Journal 51: 315 – 328.

[86] Milwaukee Water Works. "Water Treatment". Retrieved September 7, 2022, from https://city.milwaukee.gov/water/about/WaterTreatment

[87] Mohammadzadeh, Maryam., Basu, Onita D., and Herrera, Jose E. (2015). "Impact of water chemistry on lead carbonate dissolution in drinking water distribution systems". Journal of Water Resource and Protection 7(5): 389 – 397.

[88] Mohebbi, H., and Li, C. Q. (2011). "Experimental investigation on corrosion of cast iron pipes". International Journal of Corrosion 2011: 1 – 17.

[89] Nancollas, George H., Kazmierczak, Thomas F., and Schruttringer, Eric. (1981). "A controlled composition study of calcium carbonate crystal growth: the influence of scale inhibitors". Corrosion 37(2): 76 – 81.

[90] Ng, Ding-quan., Strathmann, Timothy J., and Lin, Yi-Pin. (2012). "Role of orthophosphate as a corrosion inhibitor in chloraminated solutions containing tetravalent lead corrosion product PbO_2". Environmental Science & Technology 46(20): 11062 – 11069.

[91] Ng, Ding-Quan., Lin, Jun-Kai., and Lin, Yi-Pin. (2020). "Lead release in drinking water resulting from galvanic corrosion in three-metal systems consisting of lead, copper and stainless steel". Journal of Hazardous Materials 398.

[92] Nguyen, C.K., Clark, B.N., Stone, K.R., and Edwards., M.A. (2011). "Role of chloride, sulfate, and alkalinity on galvanic lead corrosion". Corrosion 67(6): 065005-1 – 065005-9.

[93] NIST Standard Reference Database 20, Version 4.1. (2012). Retrieved October 9, 2022, from https://srdata.nist.gov/xps/Default.aspx
[94] Noel, James D., Wang, Yin., and Giammar, Daniel E. (2014). “Effect of water chemistry on the dissolution rate of the lead carbonate product hydrocerussite”. Water Research 54: 237 – 246.
[95] Oak Creek Water and Sewer Utility. “2022 Water Quality Report”. Retrieved September 7, 2022, from https://www.oakcreekwi.gov/home/showpublisheddocument/16684/637919980018270000
[96] Palit, Abhijit., and Pehkonen, Simo O. (2000). “Copper corrosion in distribution systems: evaluation of a homogenous Cu_2O film and a natural corrosion scale as corrosion inhibitors”. Corrosion Science 42(10): 1801 – 1822.
[97] Papafilippaki, Androniki., Stavroulakis, George., and Gasparatos, Dionisios. (2007). “Total and bioavailable forms of Cu, Zn, Pb, and Cr in agricultural soils: a study from the hydrological basin of Keritis, Chania, Greece”. GlobalNEST International Journal 9(3): 201 – 206.
[98] Patterson, James W., Boice, Richard E., and Marani, Darlo. (1991). “Alkaline precipitation and aging of copper from dilute cupric nitrate solution”. Environmental Science & Technology 25(10): 1780 – 1787.
[99] Pederson, L. R. (1982). “Two-dimensional chemical-state plot for lead using XPS”. Journal of Electron Spectroscopy and Related Phenomena 28(2): 203 – 209.
[100] Pieper, Kelsey J., Tang, Min., and Edwards, Marc A. (2017). "Flint water crisis caused by interrupted corrosion control: Investigating "Ground Zero" home". Environmental Science & Technology 51(4): 2007 – 2014.
[101] Peng, Ching-Yu., Korshin, Gregory V., Valentine, Richard L., Hill, Andrew S., Friedman, Melinda J., and Reiber, Steve H. (2010. “Characterization of elemental and structural composition of corrosion scales and deposits formed in drinking water distribution systems”. Water Research 44(15): 4570 – 4580.
[102] Peng, Ching-Yu., and Korshin, Gregory. (2011). “Speciation of trace inorganic contaminants in corrosion scales and deposits formed in drinking water distribution systems”. Water Research 17(1): 5553 – 5563.
[103] Philippini, Violaine., Naveau, Aude., Catelette, Hubert., and Leclercq, Stephanie. (2006). “Sorption of silicon on magnetite and other corrosion products of iron”. Journal of Nuclear Materials 348(1-2): 60 – 69.
[104] Prakash, I., Muralidharan, P., Nallamuthu, N., Venkateswarlu, M., and Satyanarayana, N. (2007). “Preparation and characterization of nanocrystallite size cuprous oxide”. Materials Research Bulletin 42(9): 1619 – 1624.
[105] Rajani, Balvant., and Makar, Jon. (2000). “A methodology to estimate the remaining service life of grey cast iron water mains”. Canadian Journal of Civil Engineering 27(6): 1259 – 1272.
[106] Renner, Rebecca. (2004). "Plumbing the depths of the D.C.'s drinking water crisis". Environmental Science & Technology 38(12): 224A – 227A.

[107] Robinson, R Bruce., Reed, Gregory D., and Frazier, Brett. (1992). “Iron and manganese sequestration facilities using sodium silicate”. Journal – American Water Works Association 84(2): 77 – 82.
[108] Rondon, Sonia, and Sherwood, Peter M. A. (1998) “Core level and valence band spectra of PbO by XPS”. Surface Science Spectra 5(97): 97 – 103.
[109] Sarin, P., Snoeyink, L., Bebee, J., Kriven, W. M., and Clement, J. A. (2001). “Physico-chemical characteristics of corrosion scales in old iron pipes”. Water Research 35(12): 2961 – 2969.
[110] Scaife, J. F. (1957). “The solubility of malachite”. Canadian Journal of Chemistry 35: 1332 – 1340.
[111] Shock, Michael R. (1980). “Response of lead solubility to dissolved carbonate in drinking water”. Journal – American Water Works Association 72(12): 695 – 704.
[112] Schock, Michael R., and Clement, Jonathan A. (1996). “Lead and copper control with non-zinc orthophosphate”. Journal of the New England Water Works Association 112(1): 20 – 33.
[113] Schock, Michael R., Wagner, I., and Oliphant, R.J. (1996). “Corrosion and solubility of lead in drinking water”. Internal Corrosion of Water Distribution Systems, Chapter 4. American Water Works Association.
[114] Shock, Michael R, and Giani, Richard. (2004). “Oxidant/Disinfectant chemistry and impacts on lead corrosion”. American Water Works Association.
[115] Schock, Michael R., Cantor, Abigail F., Triantafyllidou, Simoni., Desantis, Michael K., and Scheckel, Kirk G. (2014). "Importance of pipe deposits to Lead and Copper Rule compliance." Journal-American Water Works Association 106(7): E336-E349.
[116] Schroeder, Henry A., Nason, Alexis P., Tipton, Isabel H., and Balassa, Joseph J. (1966). “Essential trace metals in man: Copper”. Journal of Chronic Diseases 19(9): 1007 – 1034
[117] Simon, L., Genin, J. M. R., and Refair, P. H. (1997). “Standard free enthalpy of formation of Fe(II) – Fe(III) hydroxysulphite green rust one and its oxidation into hydroxysulphate green rust two”. Corrosion Science 39(9): 1673 – 1685.
[118] Sontheimer, Heinrich., Kolle, W., Snoeyink, Vernon L. (1981). “The siderite model of the formation of corrosion-resistant scales”. Journal – American Water Works Association 73(11): 572 – 579.
[119] Stericker, William. (1938). “Sodium silicates in water to prevent corrosion”. Industrial & Engineering Chemistry 30(3): 348 – 351.
[120] Swertgefer, J., Hartman, D.J., Shrive, C., Metz, D.H., and Demarco, J. (2006). “Water quality effect of partial lead line replacement”. AWWA Annual Conference. American Water Works Association, San Antonio, TX.
[121] Switlik, Joanna., Raczyk-Stanislawiak, Urszula., Piszora, Pawel., and Nawrocki, Jacek. (2012). “Corrosion in drinking water pipes: the importance of green rusts”. Water Research 46(1): 1 – 10.
[122] Szeliga, Michael J., and Simpson, Debra M. (2003). “Evaluating ductile iron pipe corrosion”. New Pipeline Technologies, Security, and Safety 115 – 129.
[123] Tavanpour, Nima., Noshadi, Masoud., and Tavanpour, Navid. (2016). “Scale formation and corrosion of drinking water pipes: a case study of drinking water distribution system of Shiraz City”. Modern Applied Science 10(3): 166 – 177.

[124] Teng, F., Guan, Y. T., and Zhu, W. P. (2008). “Effect of biofilm on cast iron pipe corrosion in drinking water distribution system: corrosion scales characterization and microbial community structure investigation”. Corrosion Science 50(10): 2816 – 2823.
[125] Tessier, A., Campbell, P. G. C., and Bisson, M. (1979). "Sequential Extraction Procedure for the Speciation of Particulate Trace Metals". Analytical Chemistry 51(7)
[126] Triantafyllidou, Simoni, and Edwards, Marc. (2011). “Galvanic corrosion after simulated small-scale partial lead service line replacements”. Journal – American Water Works Association 103(9): 85 – 99.
[127] Triantafyllidou, Simoni., Schock, Michael R., Desantis, Michael K., and White, Colin. (2015). “Low contribution of PbO2-coated lead service lines to water lead contamination at the tap”. Environmental Science & Technology 49(6): 3746 – 3754.
[128] Trueman, Benjamin F., Krkosek, Wendy H., and Gagnon, Benjamin A. (2018). “Effects of ortho-and polyphosphates on lead speciation in drinking water”. Environmental Science: Water Research & Technology 4(4): 505 – 512.
[129] Tully, Jennifer., Desantis, Michael K., and Schock, Michael R. (2019). “Water quality-pipe deposit relationships in midwestern lead pipes”. AWWA Water Science 1(2): e1127.
[130] Tuovinen, Olli H., Button, Kenneth S., Vuorinen, Antti., Carlson, Liisa., Mair, David M., and Yut, Lynn A. (1980). “Bacterial, chemical, and mineralogical characteristics of tubercles in distribution pipelines”. Journal – American Water Works Association 72(11): 626 – 635.
[131] Turek, Nadja F. (2006). “Investigation of copper contamination and corrosion scale mineralogy in aging drinking water distribution systems”. Master’s Thesis, Air Force Institute of Technology.
[132] Vasquez, Ferdinand A., Heaviside, Robert., Tang, Zhijian., and Taylor, James S. (2006). “Effect of free chorine and chloramines on lead release in a distribution system”. Journal – American Water Works 98(2): 144 – 154.
[133] Waines, Paul L., Moate, Roy., Moody, John A., Allen, Mike., and Bradley, Graham. (2011). “The effect of material choice on biofilm formation in a model warm water distribution system”. Biofouling 27(10): 1161 – 1174.
[134] Wang, Yin., Xie, Yanjiao., Li, Wenlu., Wang, Zimeng., and Giammar, Daniel E. (2010). “Formation of Lead(IV) oxides from Lead(II) compounds”. Environmental Science & Technology 44(23): 8950 – 8956.
[135] Wang, Yin., Jing, He., Mehta, Vrajesh., Welter, Gregory J., and Giammar, Daniel E. (2012). “Impact of galvanic corrosion on lead release from aged lead service lines”. Water Research 46(16): 5049 – 5060.
[136] Wang, Yin. (2012). “Redox reactions influencing lead concentrations in drinking water: formation and dissolution of lead(IV) oxide and impact of galvanic corrosion”. PhD Thesis, Washington University in St. Louis.
[137] Wang, Haibo., Hu, Chun., Hu, Wuexiang., Yang, Min., and Qu, Jiuhui. (2012). “Effects of disinfectant and biofilm on the corrosion of cast iron pipes in a reclaimed water distribution system”. Water Research 46(4): 1070 – 1078.
[138] Wang, Lin., and Giammar, Daniel E. (2015). “Effects of pH, dissolved oxygen, and aqueous Fe(II) on the adsorption of arsenic to lepidocrocite”. Journal of Colloid and Interface Science 448: 331 – 338.

[139] Wasserstrom, L., Miller, S., Triantafyllidou, S., Desantis, M., and Schock, M. (2017). “Scale formation under blended phosphate treatment for a utility with lead pipes”. American Water Works Association 109(11): E464 – E478.
[140] Waukesha Water Utility. “Water Quality”. Retrieved September 8, 2022, from https://waukesha-water.com/wq.html
[141] Whitehouse.gov (2021). “Fact Sheet: The Biden-Harris Lead Pipe and Paint Action Plan”. Retrieved September 12, 2022, from https://www.whitehouse.gov/briefing-room/statements-releases/2021/12/16/fact-sheet-the-biden-harris-lead-pipe-and-paint-action-plan/
[142] Wilkie, Jennifer A., Hering, Janet G. (1996). “Adsorption of arsenic onto hydrous ferric oxide: effects of adsorbate/adsorbent ratios and co-occurring solutes”. Colloids and Surfaces A: Physicochemical Engineering Aspects 107(20): 97 – 110.
[143] Winning, Lisa D. Gorczyca, Beata., and Brezinski, Kenneth. (2017). “Effect of total organic carbon and aquatic humic substances on the occurrence of lead at the tap”. Water Quality Research Journal 52(1): 2 – 10.
[144] Woszczynski, Meghan., Bergese, John., Payne, Sarah J., and Gagnon, Graham A. (2015). “Comparison of sodium silicate and phosphate for controlling lead release from copper pipe rigs”. Canadian Journal of Civil Engineering 42(11): 953 – 959.
[145] Wu, Chun-Kwei., Yin, Ming,. O’Brien, Stephen, and Koberstein, Jeffrey T. (2006). “Quantitative analysis of copper oxide nanoparticle composition and structure by x-ray photoelectron spectroscopy”. Chemistry of Materials 18(25): 6054 – 6058.
[146] Wulfsberg, Gary. (2000). “Inorganic Chemistry”. University Science Books.
[147] Xie, Yanjiao., Wang, Yin, and Giammar, Daniel E. (2010). “Impact of chlorine disinfectants on dissolution of the lead corrosion product PbO_2”. Environmental Science & Technology 44(18): 7082 – 7088.
[148] Xie, Yanjiao., and Giammar, Daniel E. (2011). “Effects of flow and water chemistry on lead release rates from pipe scales”. Water Research 45(19): 6525 – 6534.
[149] Yang, Fan., Shi, Baoyou., Gu, Junnong., Wang, Dongsheng., Yang, Min. (2012). “Morphological and physicochemical characteristics of iron corrosion scales formed under different water source histories in a drinking water distribution system”. Water Research 46(16): 5423 – 5433.
[150] Zacarias, Isabel., Yanez, Carmen G., Araya, Magdalena., Oraka, Chinwe., Olivares, Manuel., and Uauy, Ricardo. (2001). “Determination of the taste threshold of copper in water”. Chemical Senses 26(1): 85 – 89.
[151] Zhang, Lizhi., Yu, Jimmy C., Xu, An-Wu., Li, Quan., Kwong, Kwan Wai., and Yu, Shu-Hong. (2004). “Peanut-shaped nanoribbon bundle superstructures of malachite and copper oxide”. Journal of Crystal Growth 266(4): 545 – 551.

Appendix: Pipe Photographs and XRD/XPS Spectra

MKE-1 Copper Lateral (69 years old)

Figure A-1. Longitudinal cross-section of MKE-1 copper pipe.

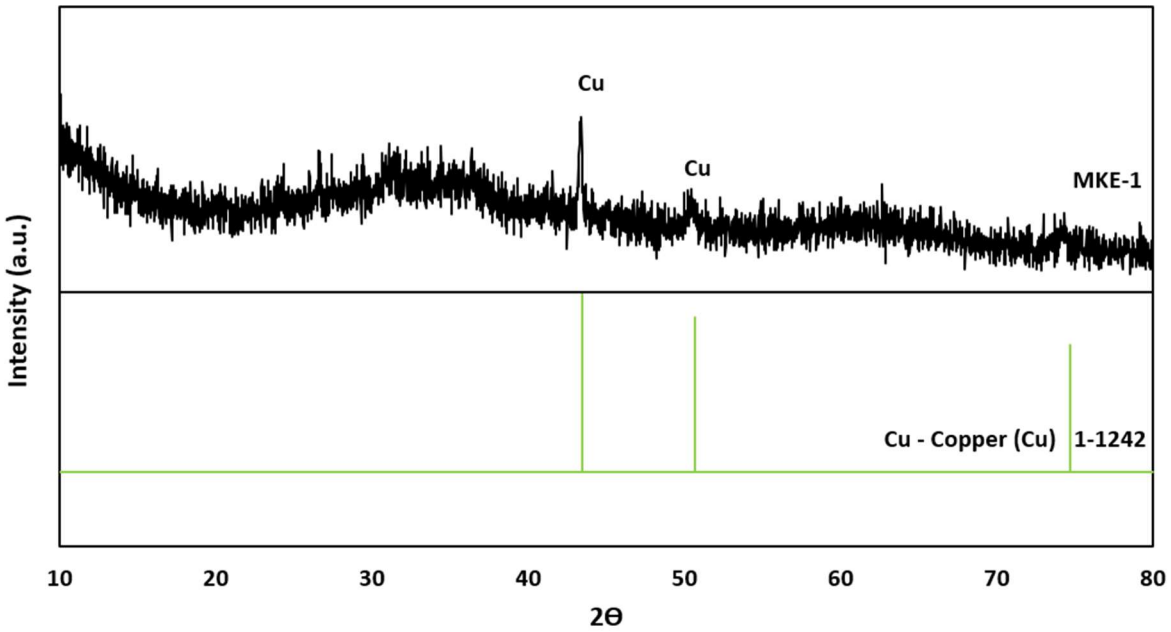

Figure A-2. XRD pattern for MKE-1 with reference patterns for elemental copper shown (JCPDS 00-001-1242).

MKE-2 Lead Lateral (74 years old)

Figure A-3. Longitudinal cross section of MKE-2 lead pipe.

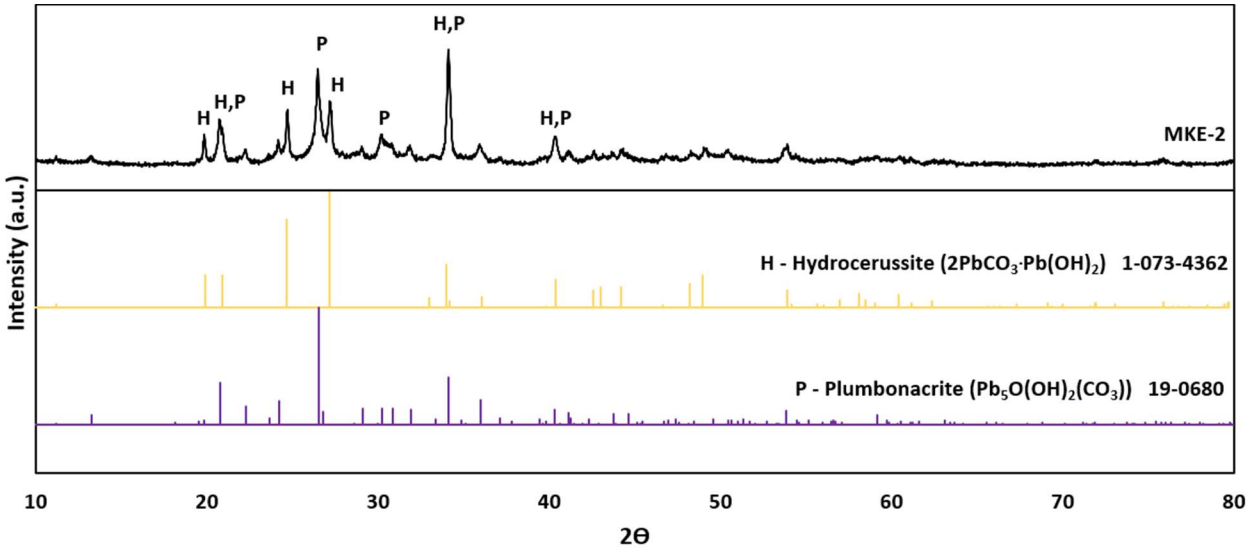

Figure A-4. XRD pattern for MKE-2 lead pipe with reference patterns for hydrocerussite (JCPDS 01-073-4362) and plumbonacrite (JCPDS 00-019-0680) shown.

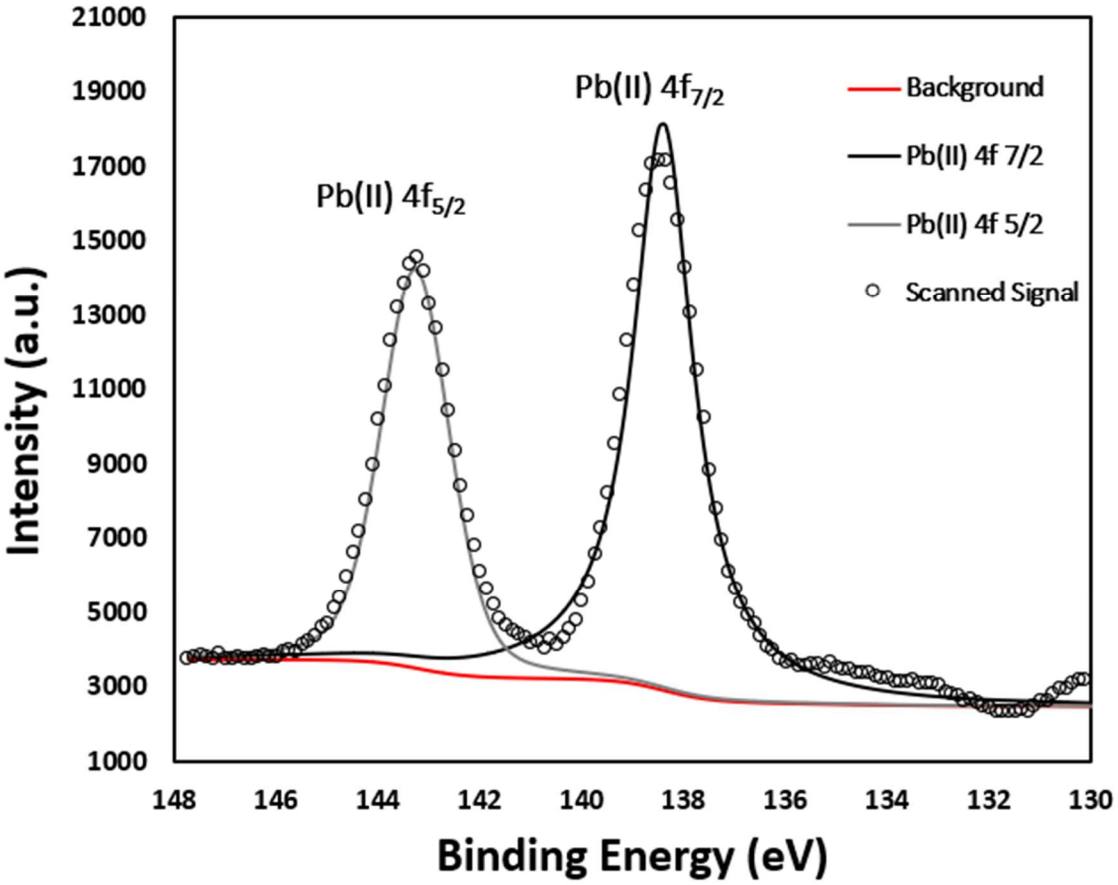

Figure A-5. XPS spectra for MKE-2 lead pipe. Lead 4f oxidation peaks matched well with Pb(II) to confirm the presence of Pb(II) corrosion products hydrocerussite and plumbonacrite.

MKE-3 Lead Lateral (89 years old)

Figure A-6. Longitudinal cross section of MKE-3 lead pipe. Inner walls of the pipe were a tan color, characteristic of lead carbonate minerals.

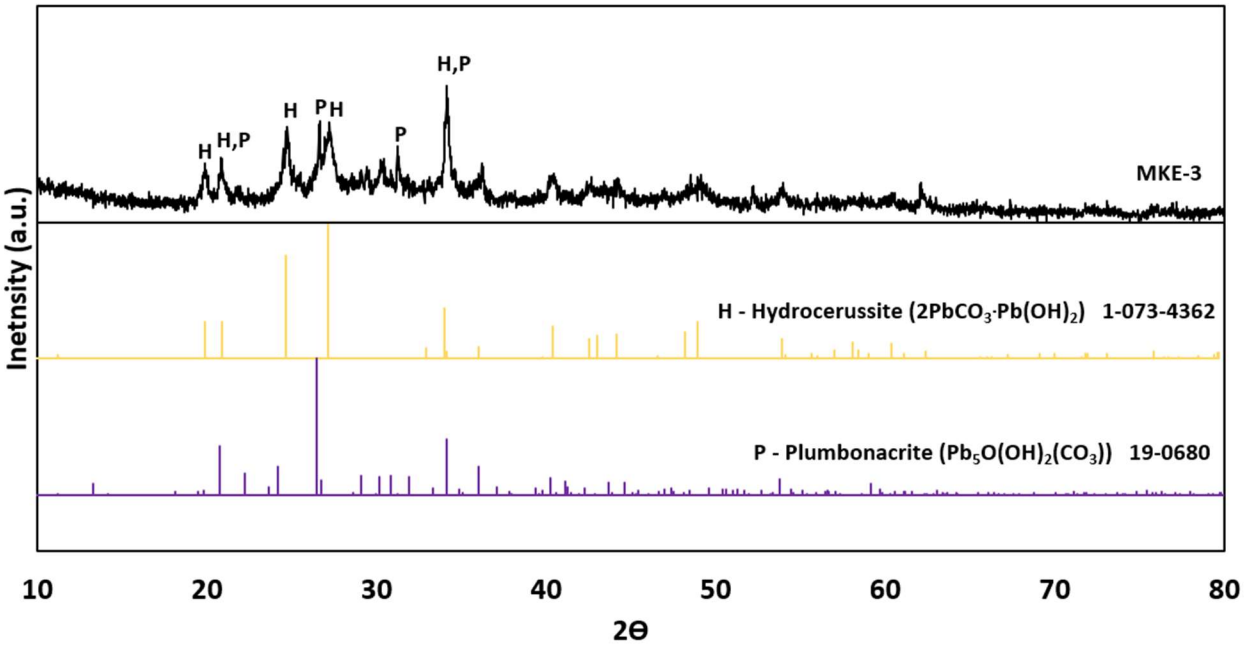

Figure A-7. XRD spectra of MKE-3 lead pipe, displaying two lead-carbonate minerals hydrocerussite (JCPDS 01-073-4362) and plumbonacrite (JCPDS 00-019-0680) which are shown for reference.

MKE-4 Cast Iron Main (66 years old)

Figure A-8. MKE-4 powder sample scraped from a cast iron corrosion scale on a Milwaukee drinking water pipe.

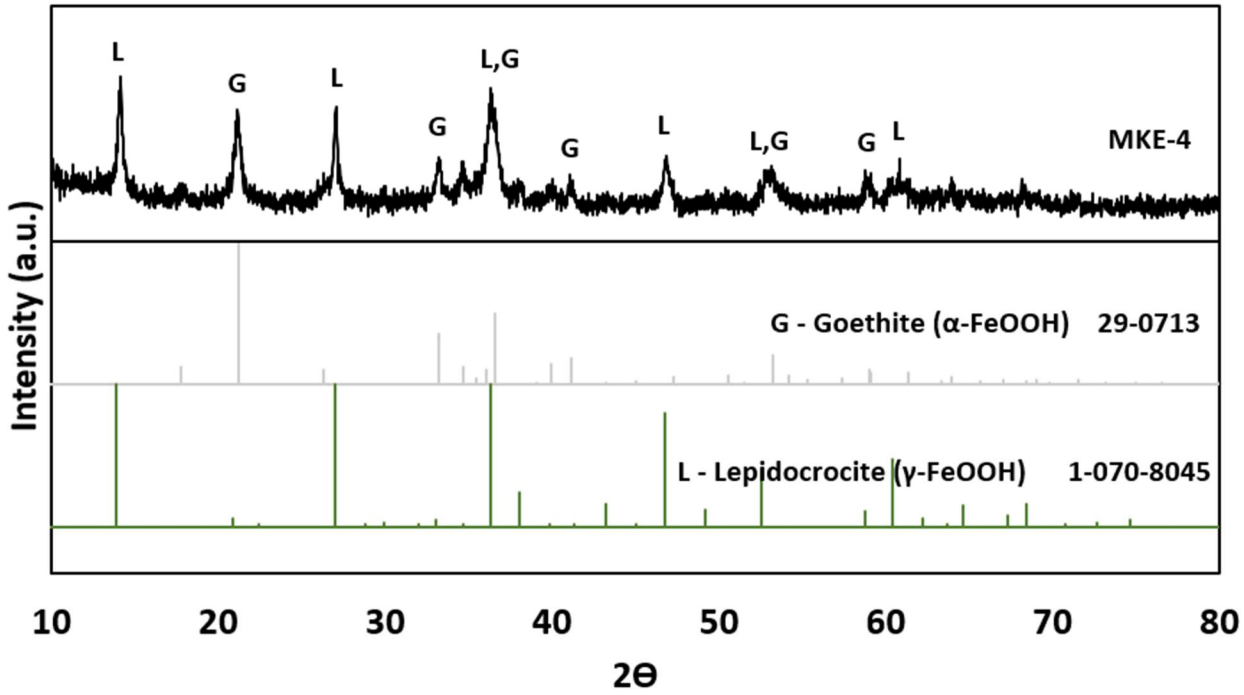

Figure A-9. XRD spectra for MKE-4 cast iron drinking water pipe corrosion scale. Sample data matches well with goethite (JCPDS 00-029-0713) and lepidocrocite (01-070-8045) which are shown for reference.

MKE-5 Cast Iron Main (69 years old)

Figure A-10. MKE-5 powder sample scraped from a cast iron drinking water pipe in Milwaukee.

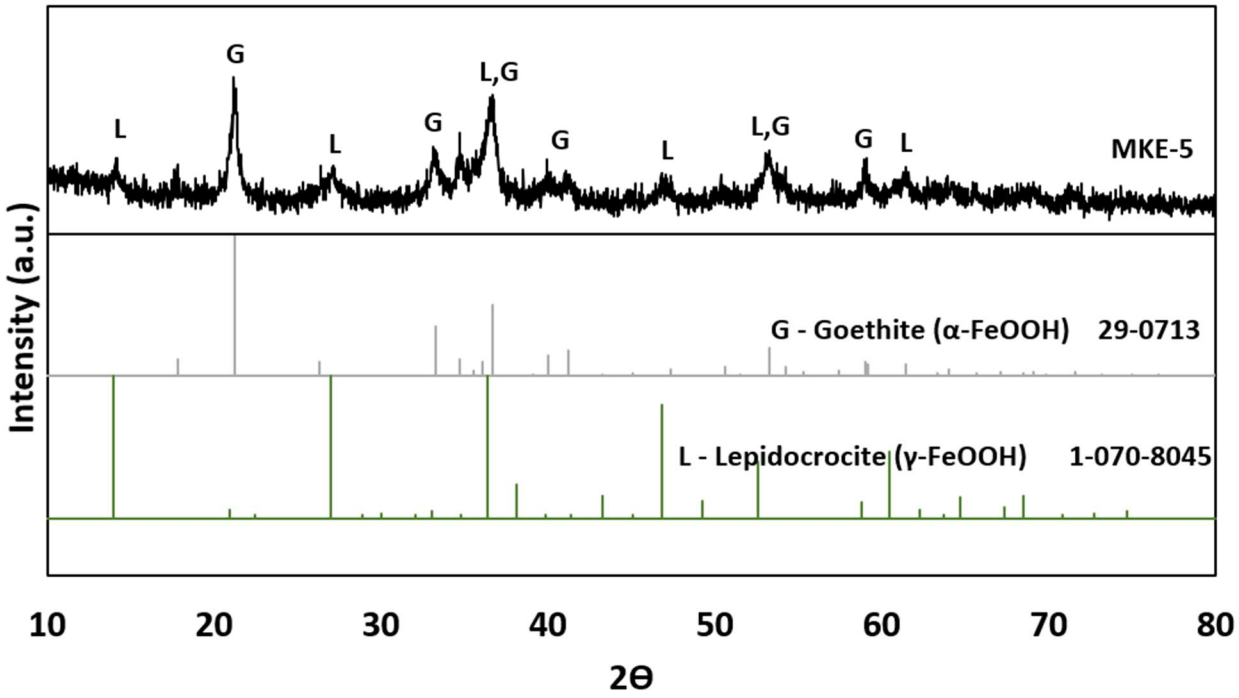

Figure A-11. XRD spectra of MKE-5 cast iron corrosion scale displaying good matches with goethite (JCPDS 00-029-0713) and lepidocrocite (JCPDS 01-070-8045) which are shown for reference.

MKE-6 Lead Lateral (79 years old)

Figure A-12. Longitudinal cross section of a lead pipe harvested from Milwaukee. The tan color of the corrosion scale is characteristic of lead carbonate minerals.

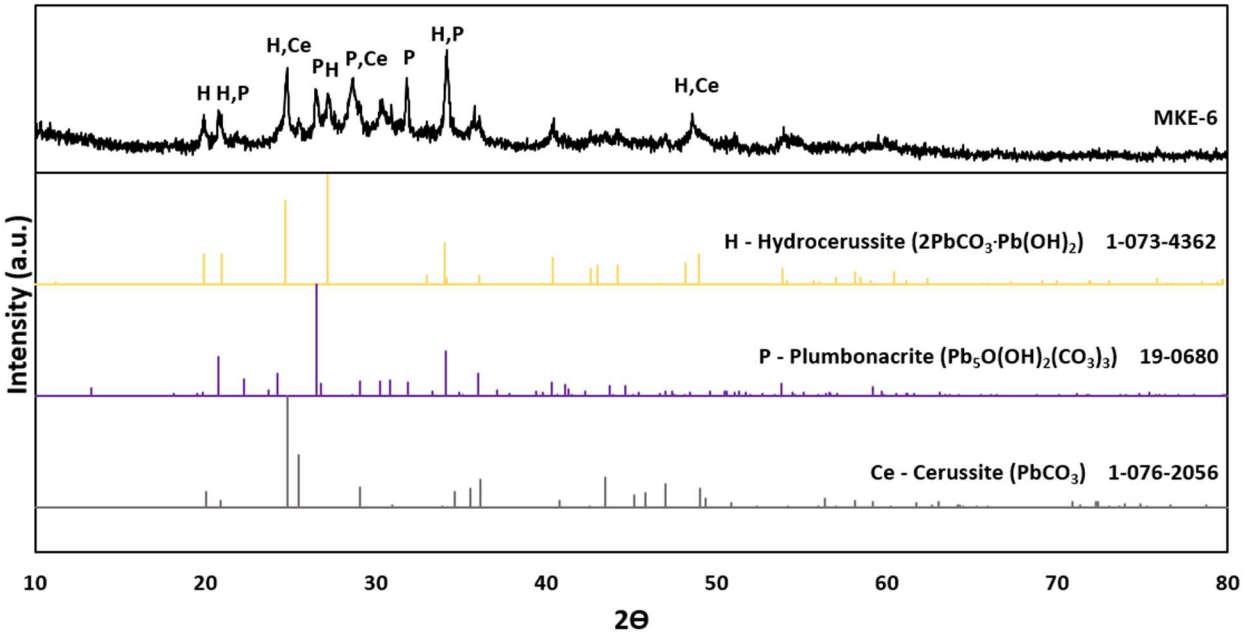

Figure A-13. XRD spectra of MKE-6 lead pipe sample. The reference patterns for cerussite (JCPDS 01-076-2056), hydrocerussite (JCPDS 01-073-4362) and plumbonacrite (JCPDS 00-019-0680) are shown.

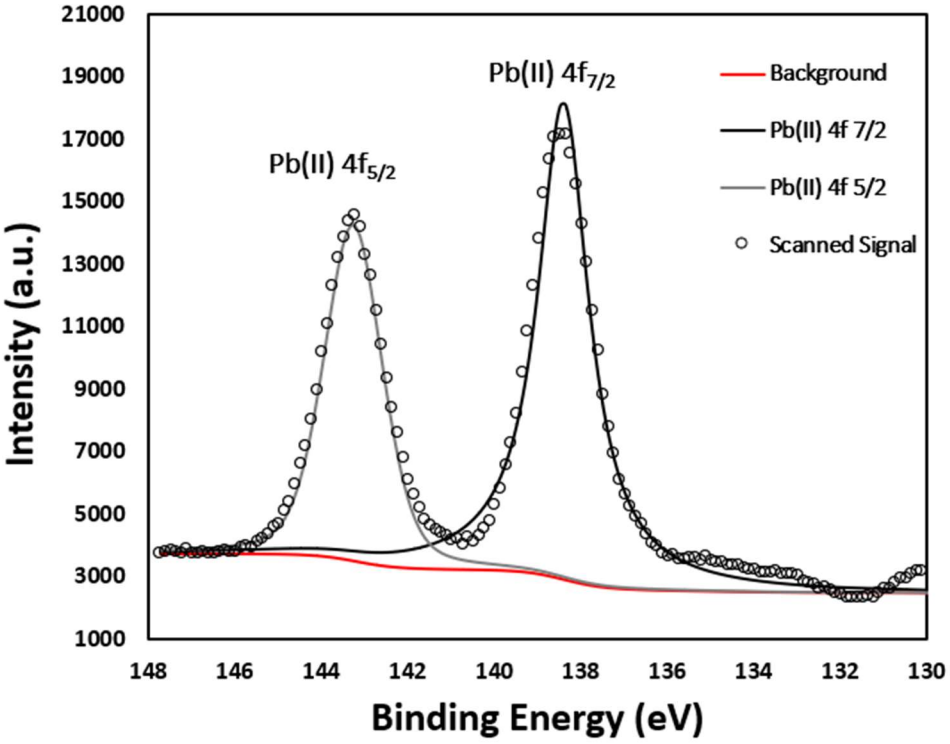

Figure A-14. XPS spectra for MKE-6 lead pipe sample displaying 4f peaks characterized as the Pb(II) oxidation state. This is complimentary to the XRD data indicating the presence of Pb(II) corrosion minerals.

MKE-7 Cast Iron Main (69 years old)

Figure A-15. MKE-7 powder sample scraping from a scale in a cast iron drinking water pipe from Milwaukee.

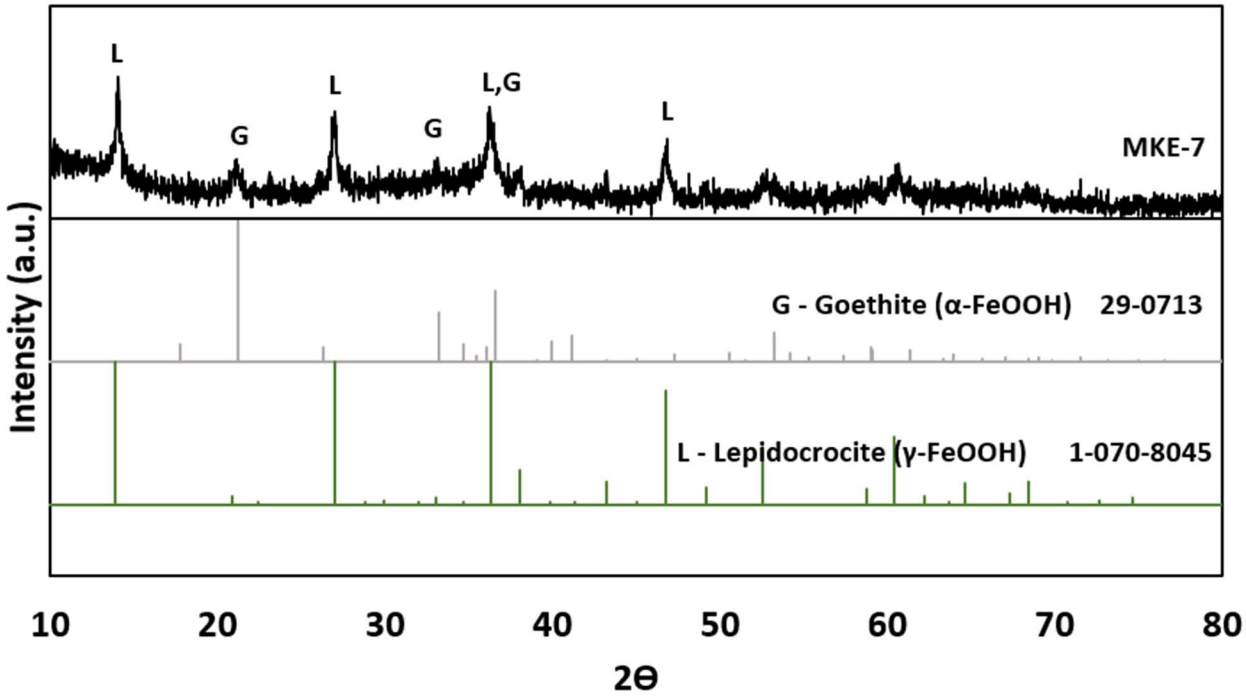

Figure A-16. XRD data for MKE-7 iron corrosion minerals. The sample data matches very well with goethite (JCPDS 00-029-0713) and lepidocrocite (JCPDS 01-070-8045) which are shown for reference.

MKE-9 Copper Lateral (100 years old)

Figure A-17. Longitudinal cross-section of a copper drinking water pipe from Milwaukee displaying minimal corrosion scaling.

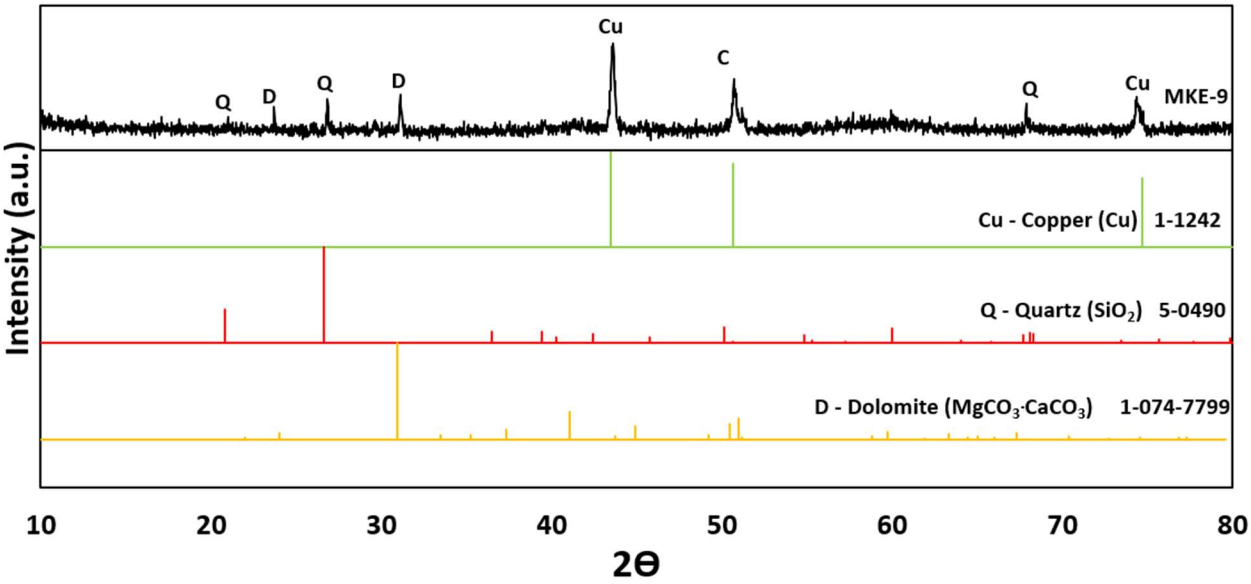

Figure A-18. XRD spectra for MKE-9 copper lateral. Elemental copper (JCPDS 00-001-1242) is the only copper-based material matching the data. Associated minerals quartz and dolomite are shown for reference (JCPDS 00-005-0490 and JCPDS 01-074-7799 respectively).

MKE-9 Lead Lateral (100 years old)

Figure A-19. Longitudinal cross-section of a lead pipe in Milwaukee (MKE-9-Pb). The pipe featured a goose-neck joint to attach to a copper pipe (MKE-9-Cu).

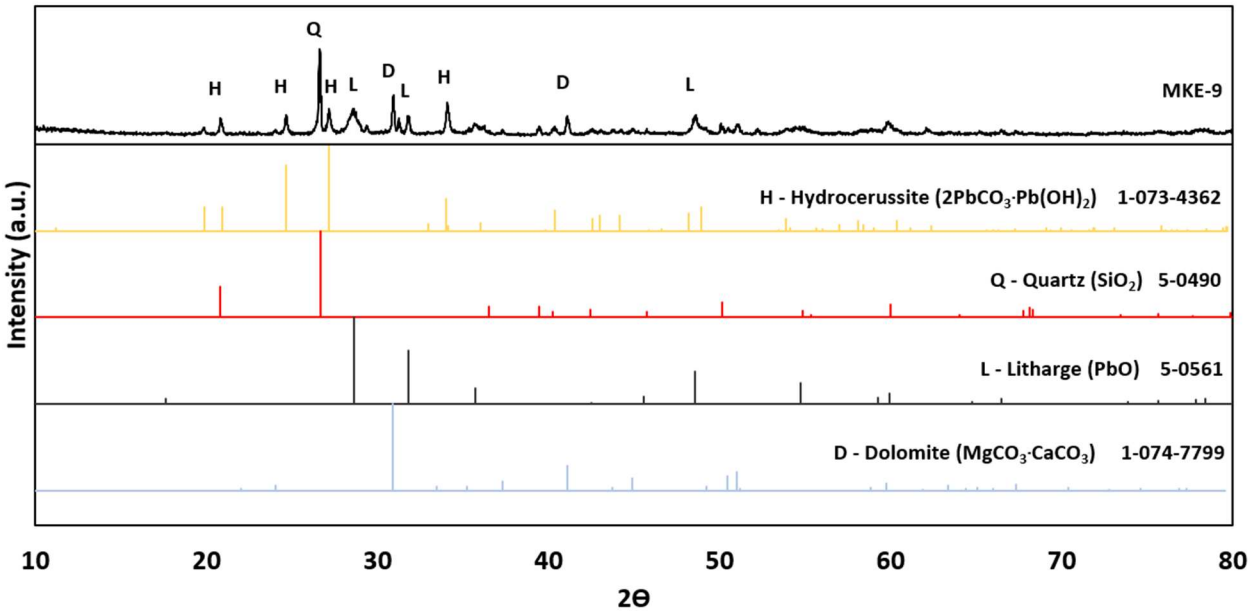

Figure A-20. XRD data for MKE-9 lead pipe. Lead-bearing minerals include hydrocerussite (JCDPS 01-073-4362) and litharge (JCPDS 00-005-0561). Associated minerals include quartz (JCPDS 00-005-0490) and dolomite (01-074-7799).

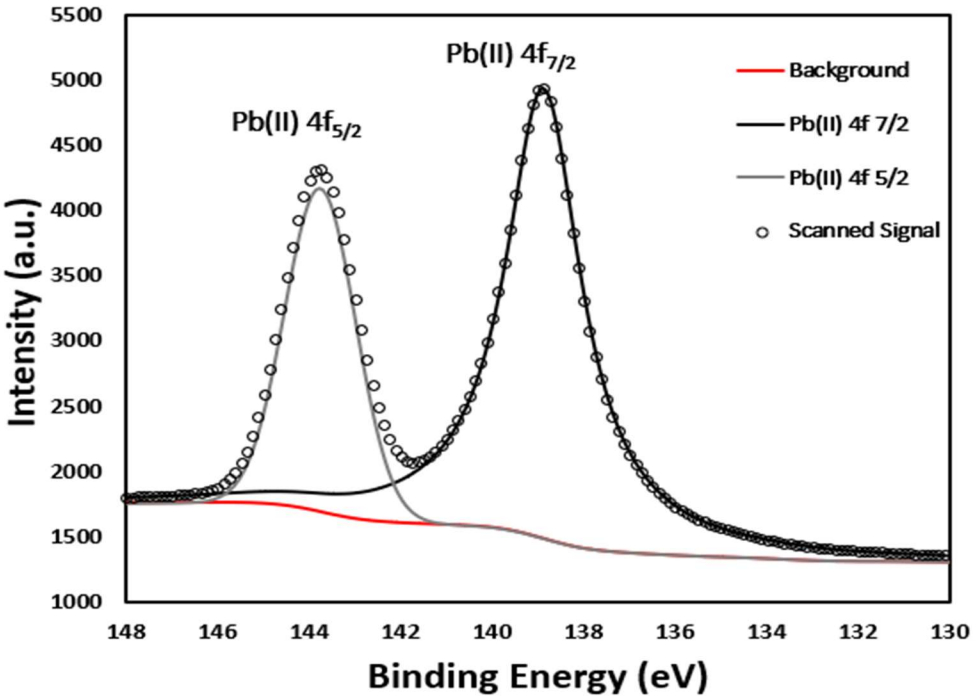

Figure A-21. XPS spectra for MKE-9 lead pipe utilized to confirm the absence of Pb(IV) oxidation state within the sample. XPSPeak41 software was used to fit the intensity values.

MKE-10 Lead Lateral (93 years old)

Figure A-22. Longitudinal cross-section of MKE-10 lead lateral pipe displaying tan colored corrosion scales on the inner pipe wall, which are common within lead carbonate minerals.

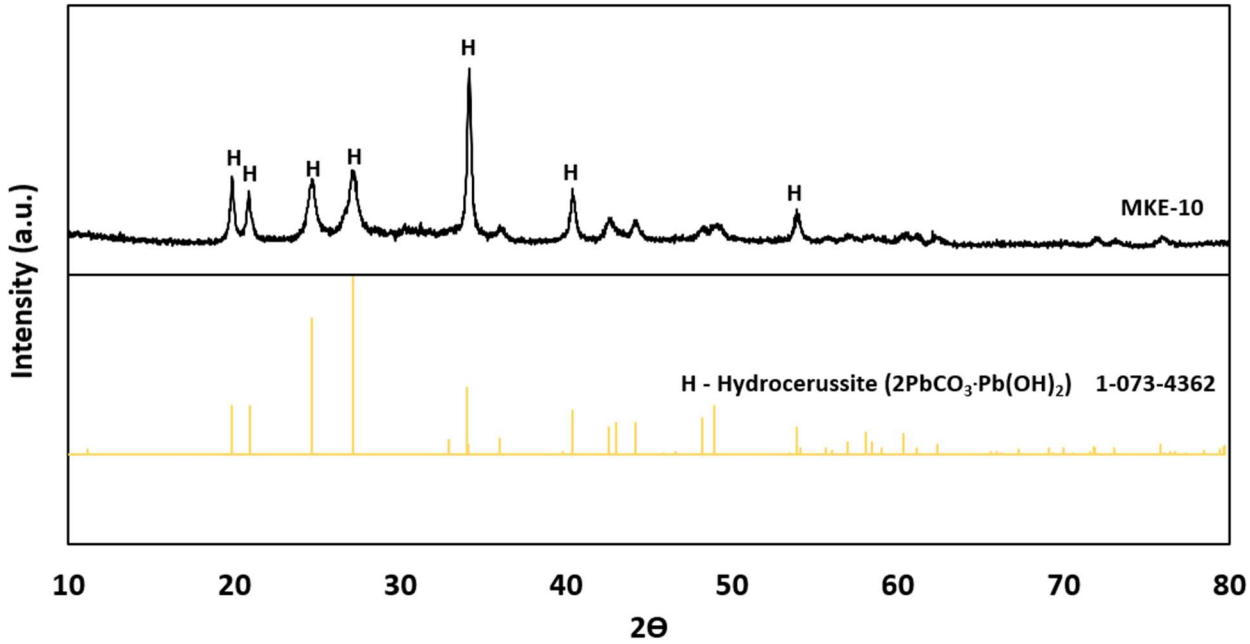

Figure A-23. XRD data for MKE-10 lead lateral which matches very well with the lead carbonate mineral hydrocerussite (JCPDS 01-073-4362) which is shown for reference.

MKE-11 Cast Iron Main (66 years old)

Figure A-24. Corrosion scale powder from a cast iron drinking water main in Milwaukee.

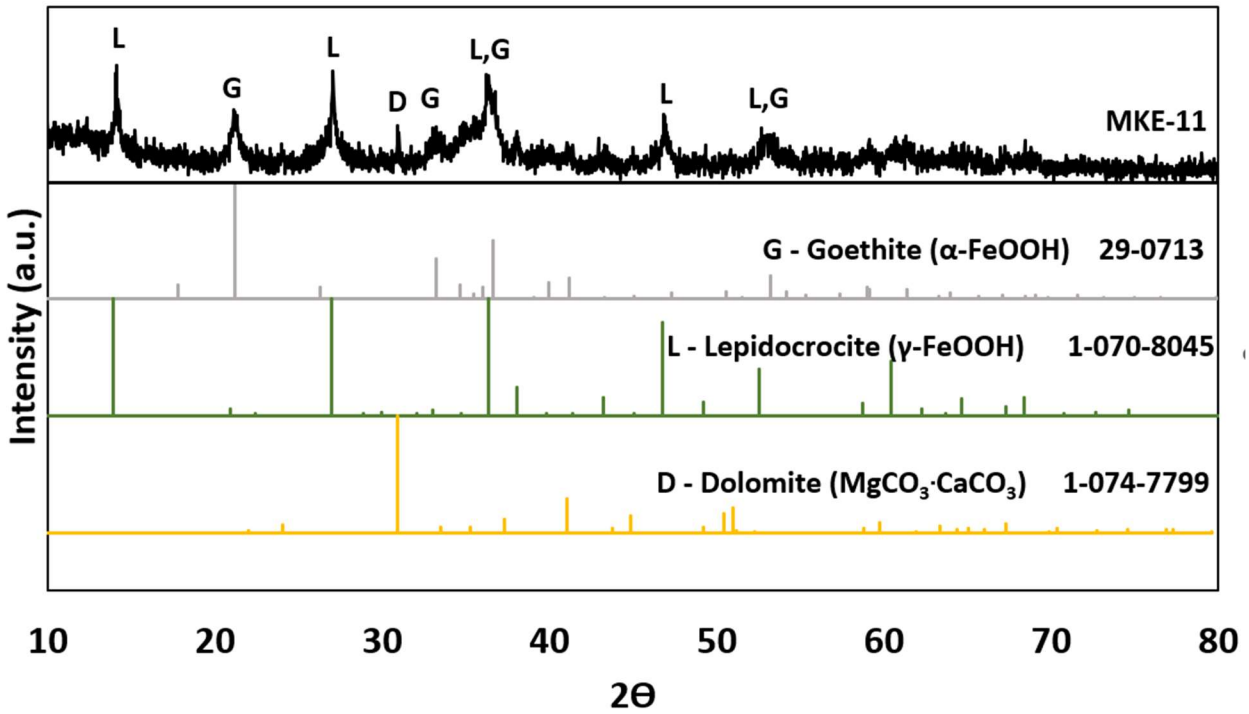

Figure A-25. XRD data for MKE-11 cast iron drinking water corrosion scale. The iron oxide-hydroxide minerals goethite and lepidocrocite (JCPDS 00-029-0713 and 01-070-8045 respectively) are shown as matches. Associated mineral dolomite is also selected as a match with its dominant peak exhibited at ~32°.

MKE-12 Cast Iron Main (64 years old)

Figure A-26. Corrosion scale powder scraped from the inside pipe wall of a cast iron drinking water main in Milwaukee.

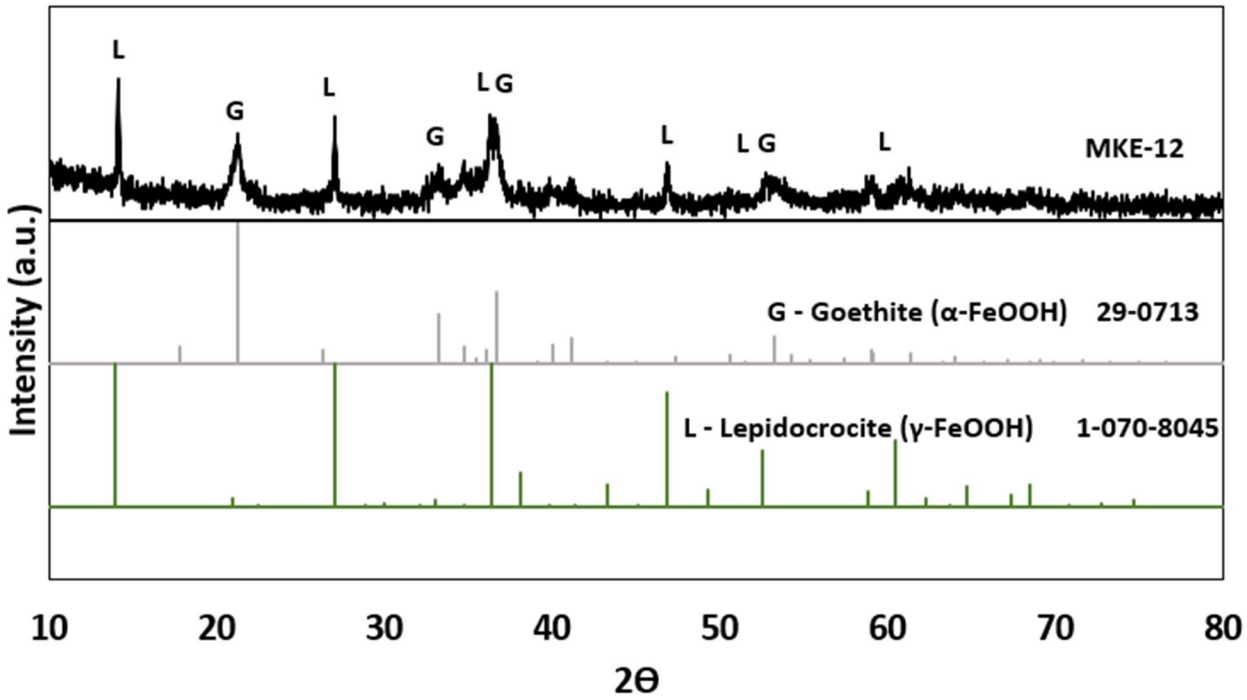

Figure A-27. XRD spectra from MKE-12 iron corrosion scale matching iron oxide-hydroxide minerals goethite and lepidocrocite (JCPDS 00-029-0713 and 01-070-8045 respectively).

MKE-13 Copper Lateral

Figure A-28. Longitudinal cross section of a copper lateral harvested from Milwaukee. Corrosion accumulation is shown as green-blue buildup on the inside of the pipe walls.

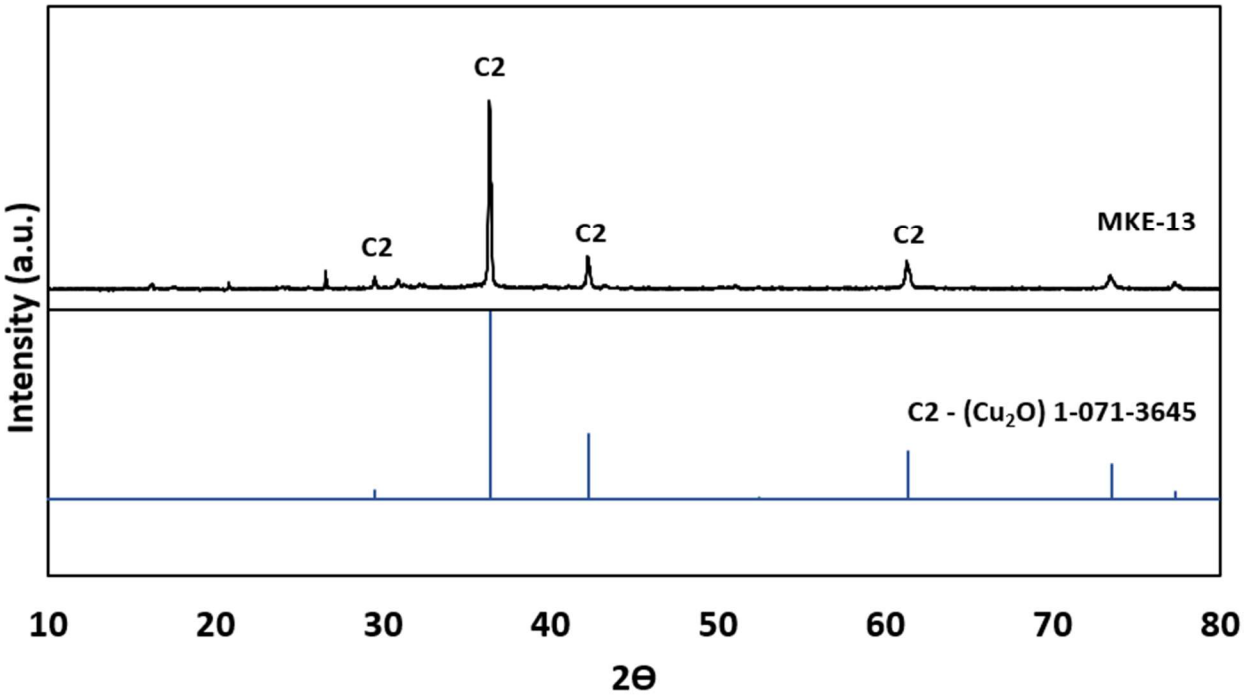

Figure A-29. XRD data from Milwaukee copper pipe MKE-13. A singular mineral match was determined to be cupric oxide (JCPDS 01-071-3645), while earlier peaks in the range of 15 – 28° could not be accurately supported by reference patterns.

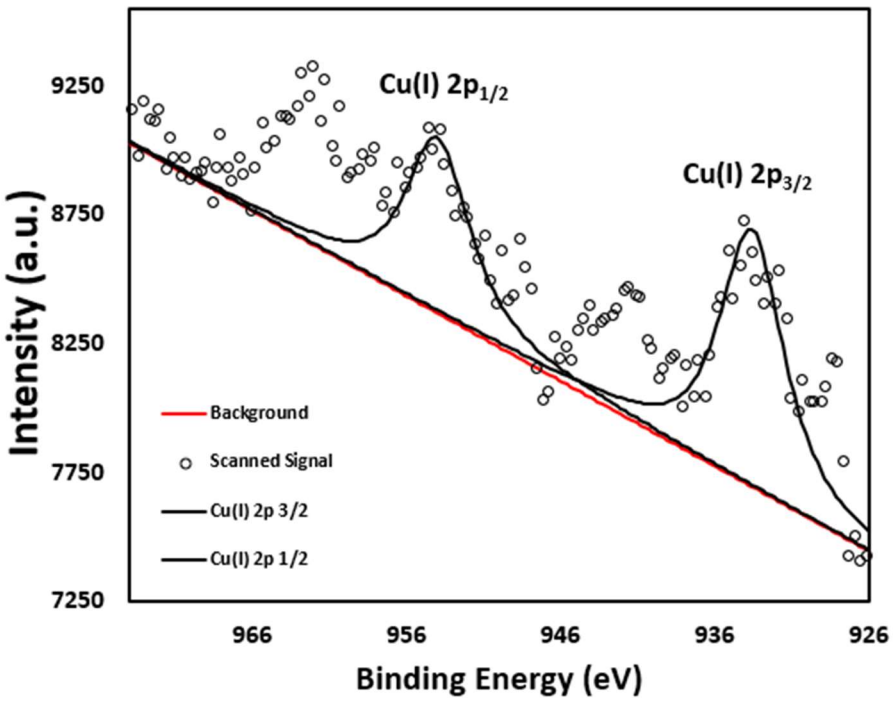

Figure A-30. XPS spectra of copper pipe MKE-13. XPSpeak41 software was used to fit the peak intensity and location to determine the chemical state of copper.

MKE-14 Ductile Iron Lateral (15 years old)

Figure A-31. Powderized corrosion scale scraped from the inside of a ductile iron drinking water lateral harvested from Milwaukee.

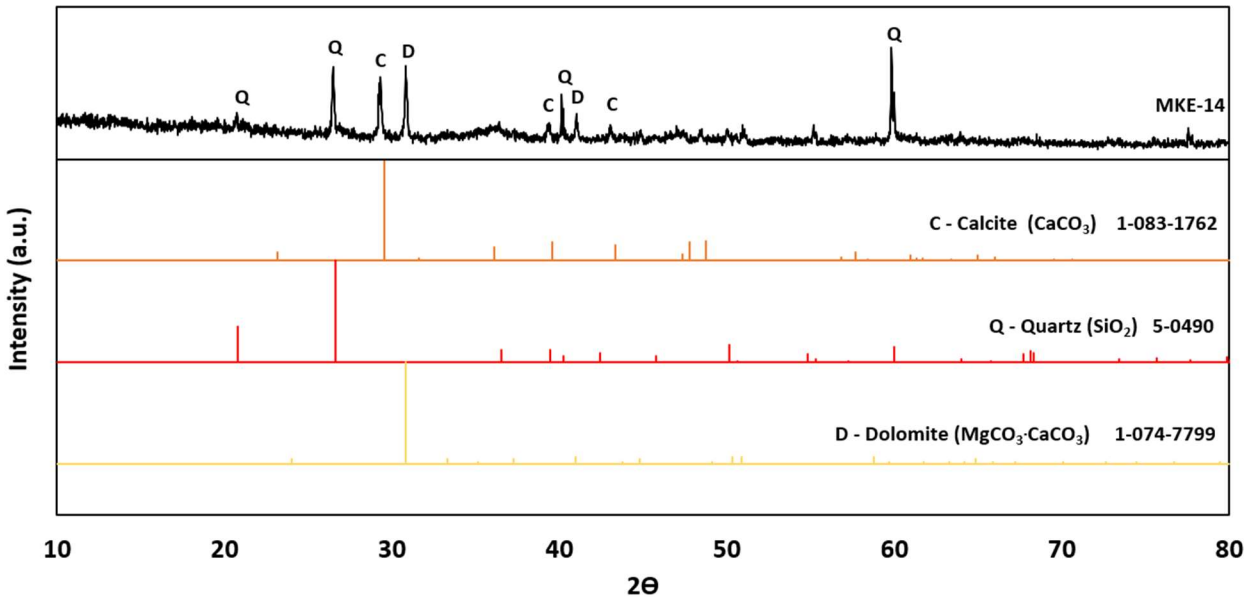

Figure A-32. XRD spectra for iron corrosion scale MKE-14. Calcite, dolomite, and quartz were the only observable crystalline constituents (JCPDS 01-083-1762, 01-074-7799, and 00-005-0490 respectively) in the scale. The non-uniform bulk before 20° may be a possible amorphous iron phase.

MKE-15 Cast Iron Main (66 years old)

Figure A-33. Powderized corrosion scale scraped from the inside of a cast iron main in Milwaukee.

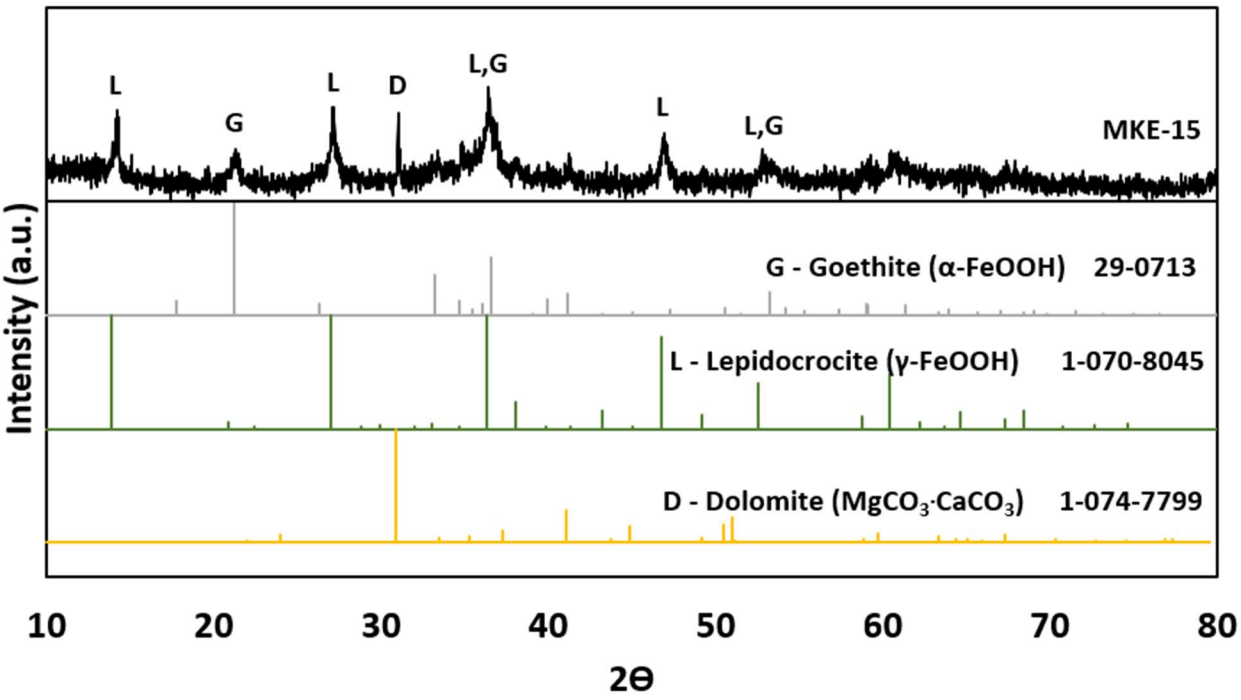

Figure A-34. XRD spectra of a cast iron main from Milwaukee matching iron oxide-hydroxide phases goethite and lepidocrocite with references plotted. Another non-iron phase was also detected as dolomite.

MKE-17 Cast Iron Main

Figure A-35. Powder obtained from scraping the corrosion scale from a cast iron main in Milwaukee.

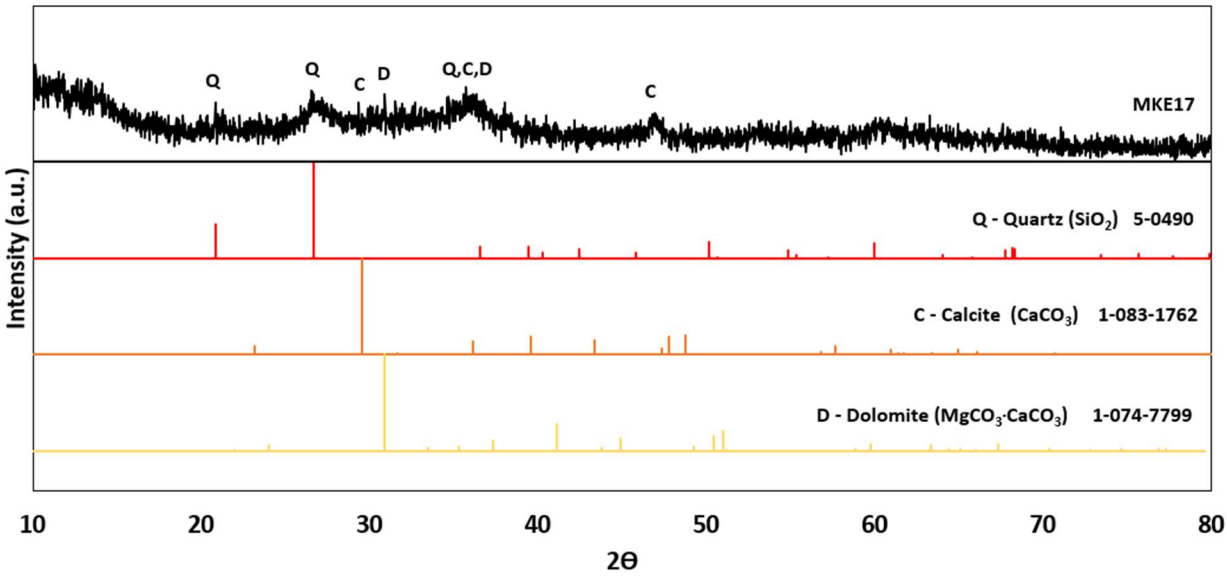

Figure A-36. XRD sample instrument readings for a cast iron main from Milwaukee. No well-defined peaks were detected for iron minerals. Associated minerals included quartz, calcite, and dolomite and their respective reference spectra were included.

MKE-17-1 Cast Iron Main

Figure A-37. Powder scraped from the inside pipe wall of a cast iron main in Milwaukee. A chunk deposit is shown on the right.

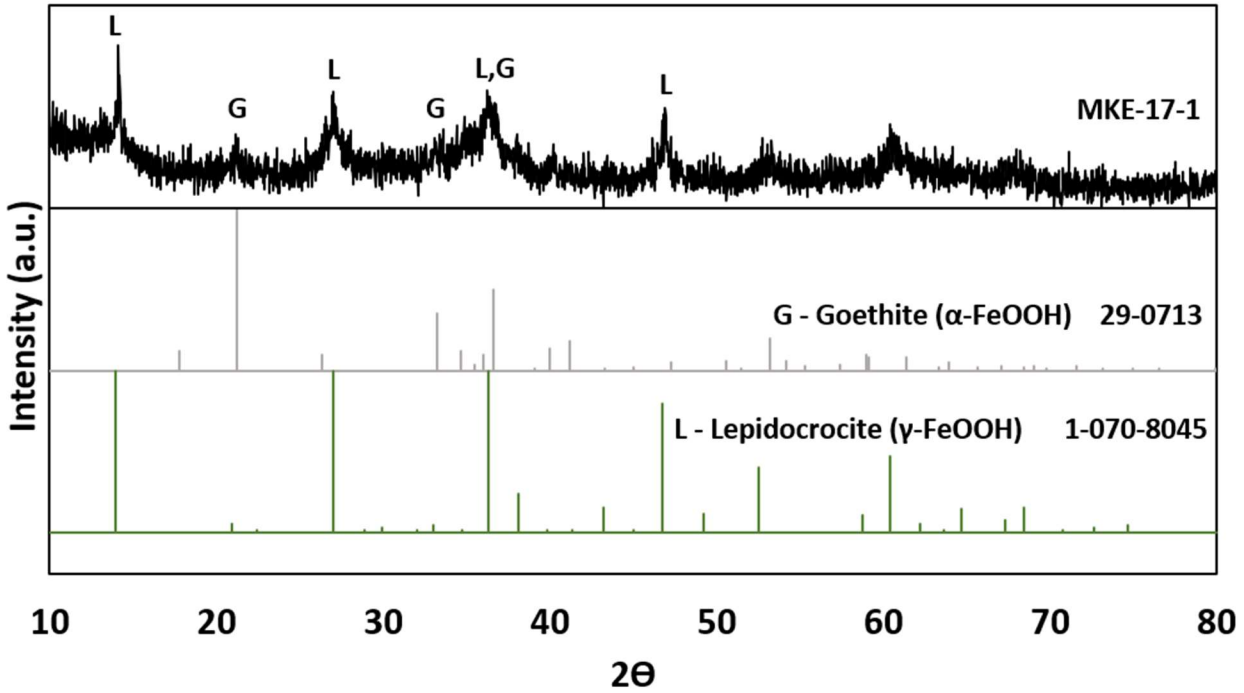

Figure A-38. XRD data for a cast iron main from Milwaukee. Dominant iron phases were iron oxide-hydroxide minerals goethite and lepidocrocite. Their reference patterns are shown beneath the sample instrument readings.

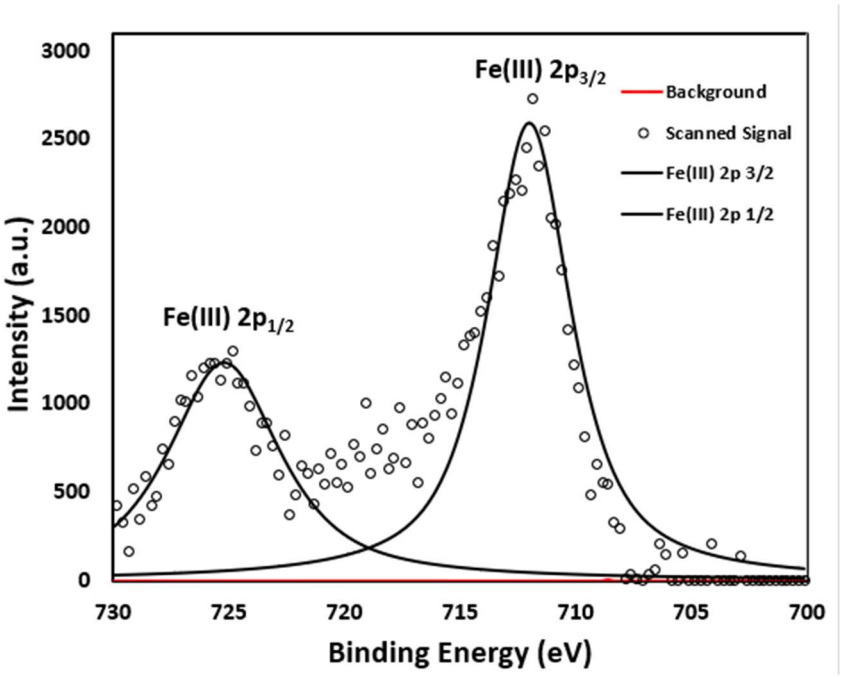

Figure A-39. XPS spectra for cast iron main MKE-17-1. XPSpeak41 software was used to fit the 2p orbital peaks and identify the Fe(III) chemical state.

OC-1 Copper Lateral (54 years old)

Figure A-40. Cross section of a copper lateral obtained from Oak Creek.

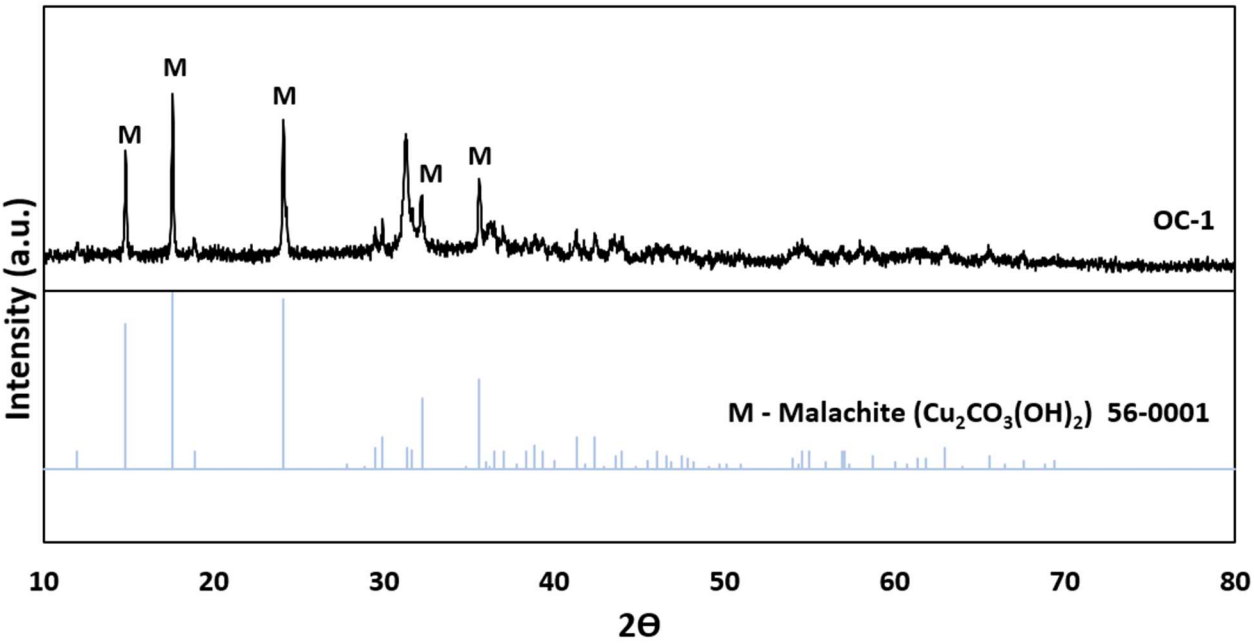

Figure A-41. XRD data for copper lateral OC-1. The primary mineral phase detected was malachite which is shown for reference (JCPDS 000-056-0001).

OC-2 Ductile Iron Main (38 years old)

Figure A-42. Inside of a large ductile iron main obtained from Oak Creek. Minimal corrosion was observed on the exposed brown pipe wall.

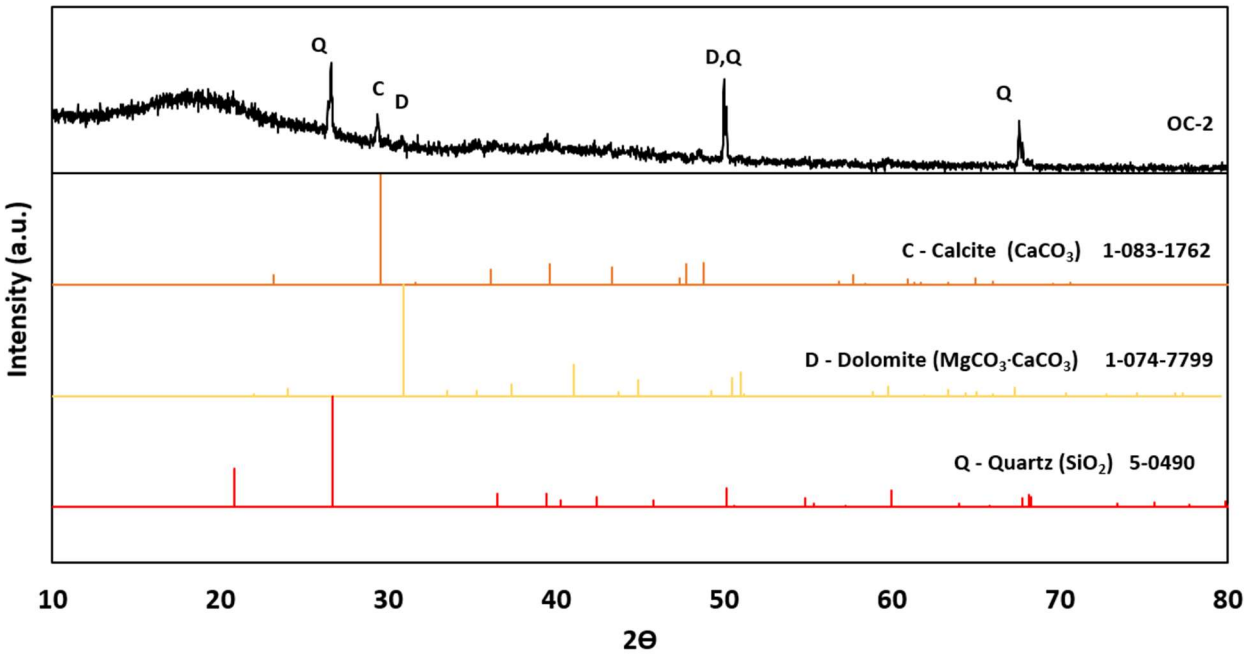

Figure A-43. XRD spectra obtained for Oak Creek ductile iron pipe OC-2. No iron mineral phases were detected. A possible amorphous iron phase could be hypothesized based on the concave shape prior to 20°. Associated minerals detected include calcite, dolomite, and quartz.

OC-4 Ductile Iron Main (33 years old)

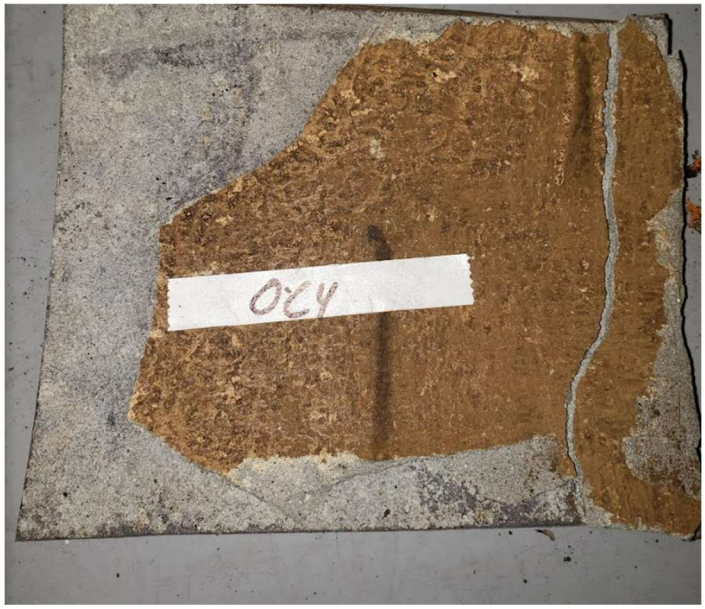

Figure A-44. Cross-section of ductile iron pipe OC-4 from Oak Creek. The brown region is the corrosive region sampled.

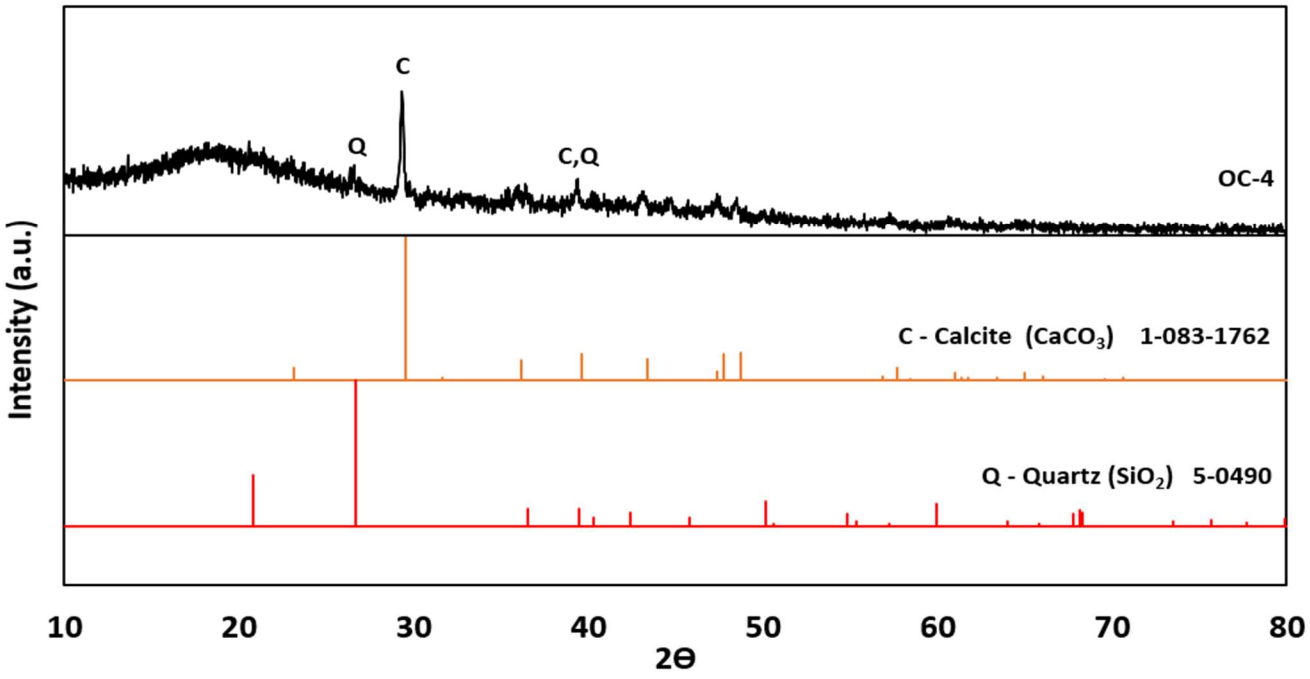

Figure A-45. XRD data from ductile iron main OC-4. Iron minerals were not detected within the sample, but an amorphous iron phase may be present indicated by the wide shape centered around 20°. Associated minerals found in this sample include calcite and quartz.

OC-5 Ductile Iron Main (38 years old)

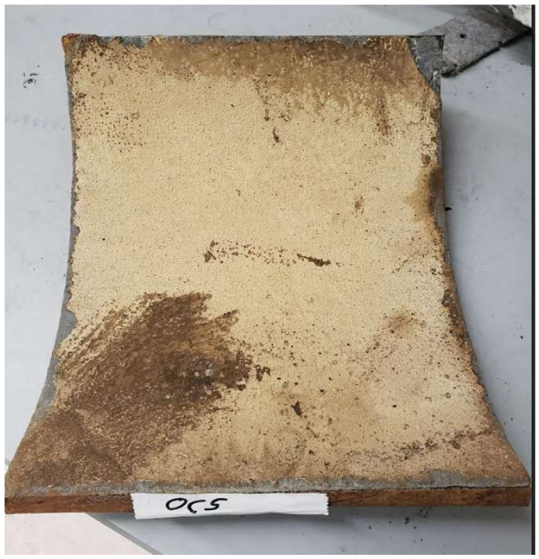

Figure A-46. Ductile iron pipe harvested from Oak Creek. The dark brown region represents the region sampled for analysis.

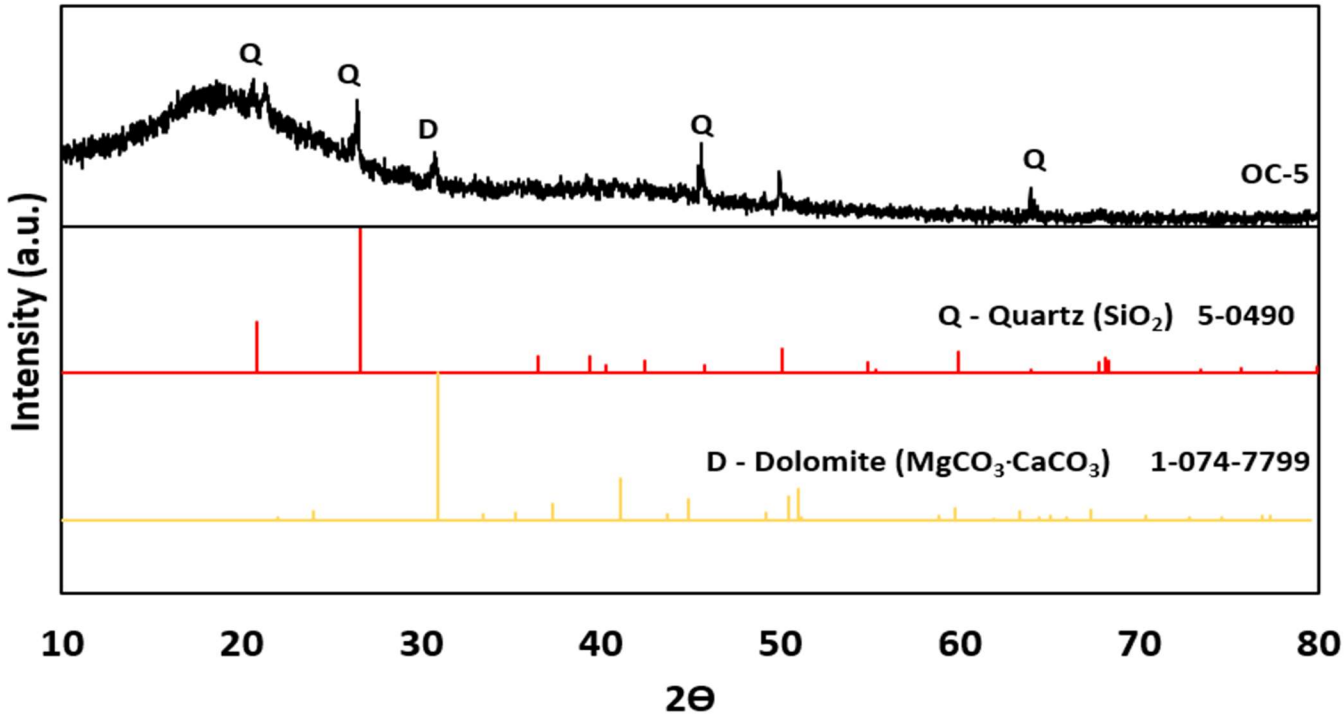

Figure A-47. XRD pattern for an Oak Creek ductile iron pipe. Iron minerals were not detected but could have an amorphous phase centered around 20°. Associated minerals detected were quartz and dolomite.

OC-6 Ductile Iron Main (38 years old)

Figure A-48. Ductile iron main obtained from Oak Creek. The brown region is the corrosive scale that was scraped and sampled.

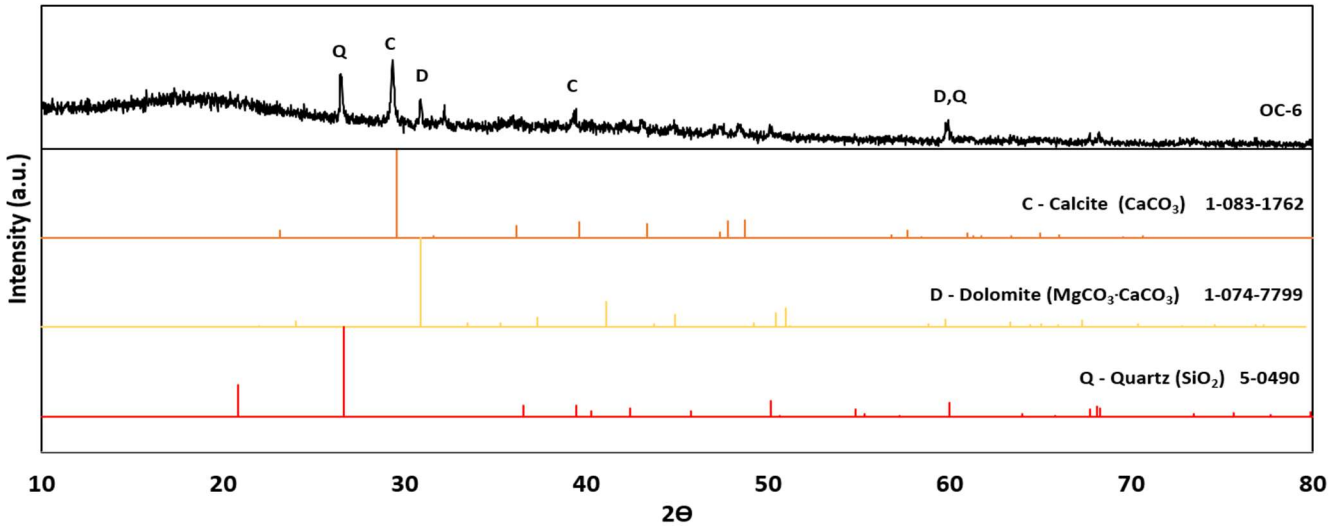

Figure A-49. XRD data for Oak Creek ductile iron main OC-6. Well defined crystalline iron phases were not found in this sample but could have been present as an amorphous phase identified by a broad peak prior to 20°. Associated minerals identified in this sample were calcite, dolomite, and quartz.

OC-7 Ductile Iron Main

Figure A-50. Cross-section of a ductile iron pipe cut longitudinally from Oak Creek.

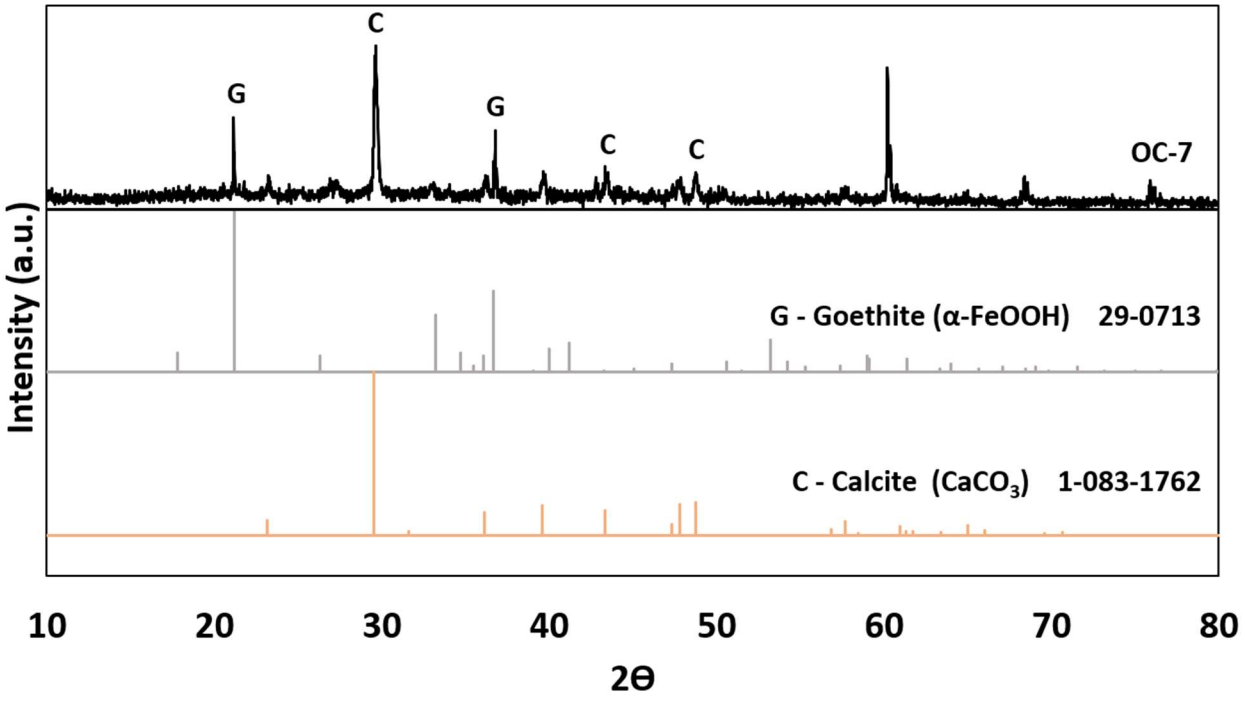

Figure A-51. XRD spectra from ductile iron pipe OC-7. Goethite was the primary iron phase detected. Associated mineral calcite was also observed and is shown for reference.

WK2-Pb Lead Lateral (105 years old)

Figure A-52. Cross-section of a lead-lateral obtained from Waukesha displaying corrosion discoloration.

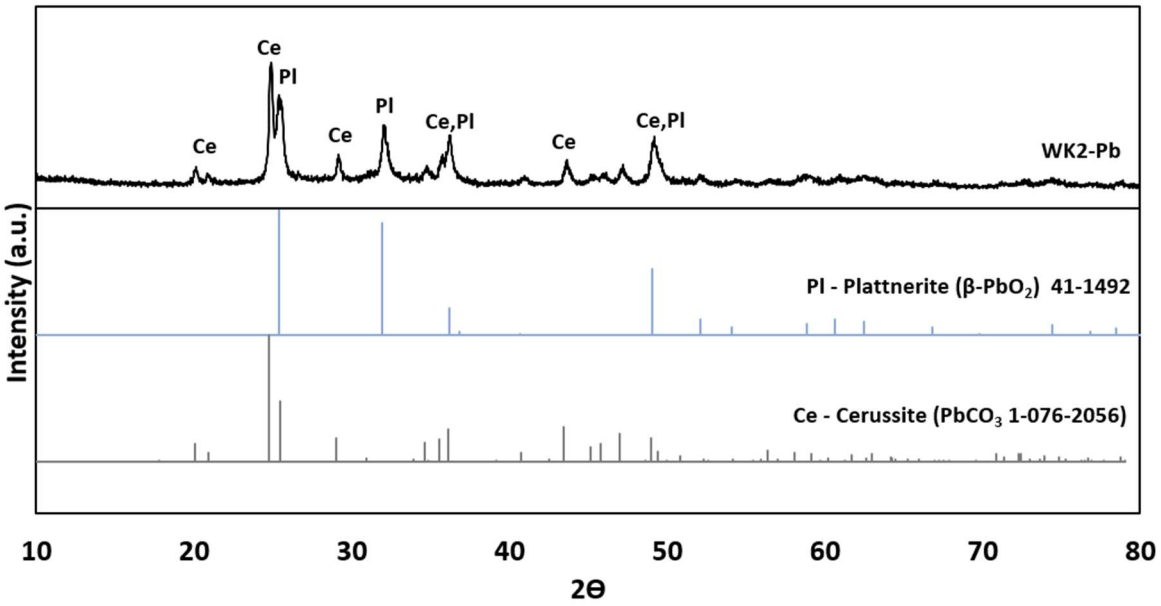

Figure A-53. XRD spectra of Waukesha lead service line WK2. Pb(II) and Pb(IV) minerals cerussite and plattnerite were detected (JCPDS 01-076-2056 and JCPDS 00-041-1492 respectively).

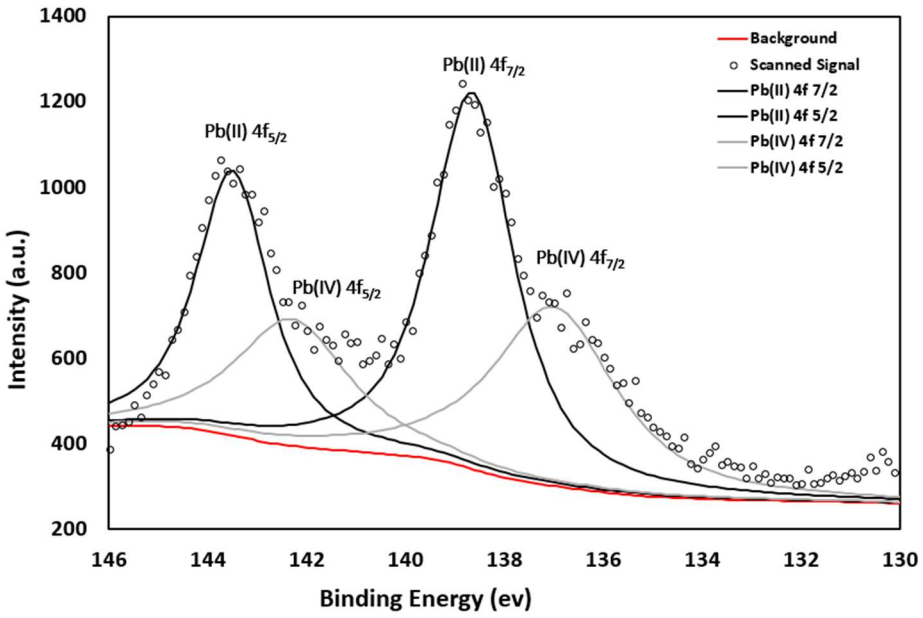

Figure A-54. XPS spectra of lead service line WK2 fit by XPSpeak41 software. The wide peak shoulders are explained by the dual-chemical state presence of Pb(II) and Pb(IV).

WK2-Fe Iron Lateral (105 years old)

Figure A-55. Cross-section of a cast iron lateral obtained from Waukesha. Rounded tubercles and significant corrosion accumulation are noted.

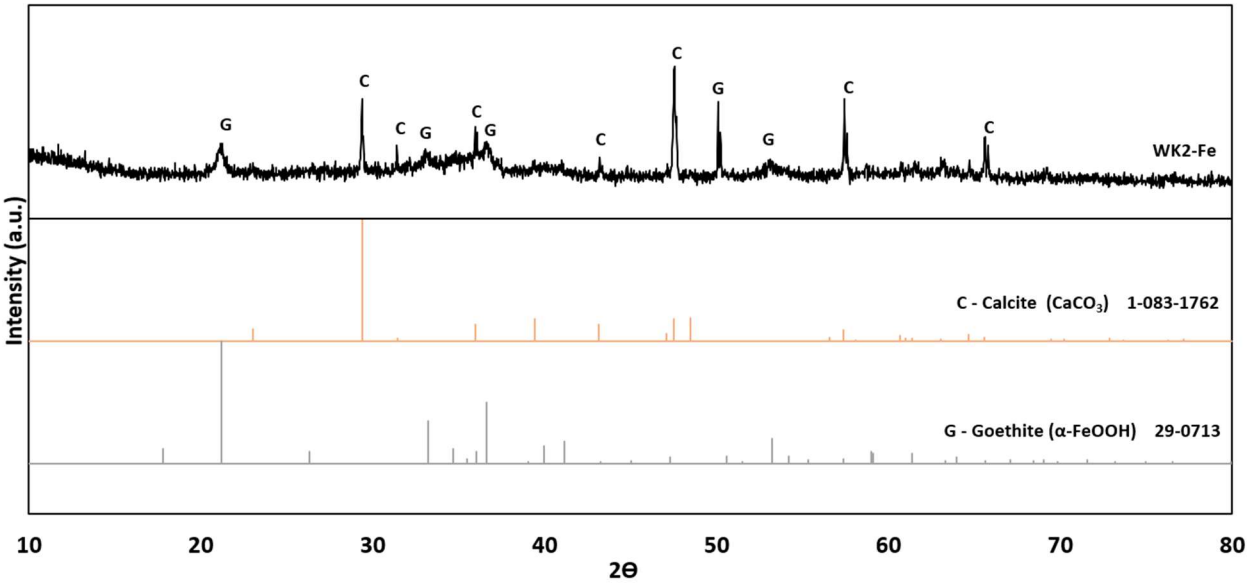

Figure A-56. XRD spectra for cast iron lateral WK-2. Goethite was the primary iron mineral detected. Associated mineral calcite was also observed.

WK3-Fe Iron Lateral (72 years old)

Figure A-57. Cross-section of an iron pipe section obtained from Waukesha.

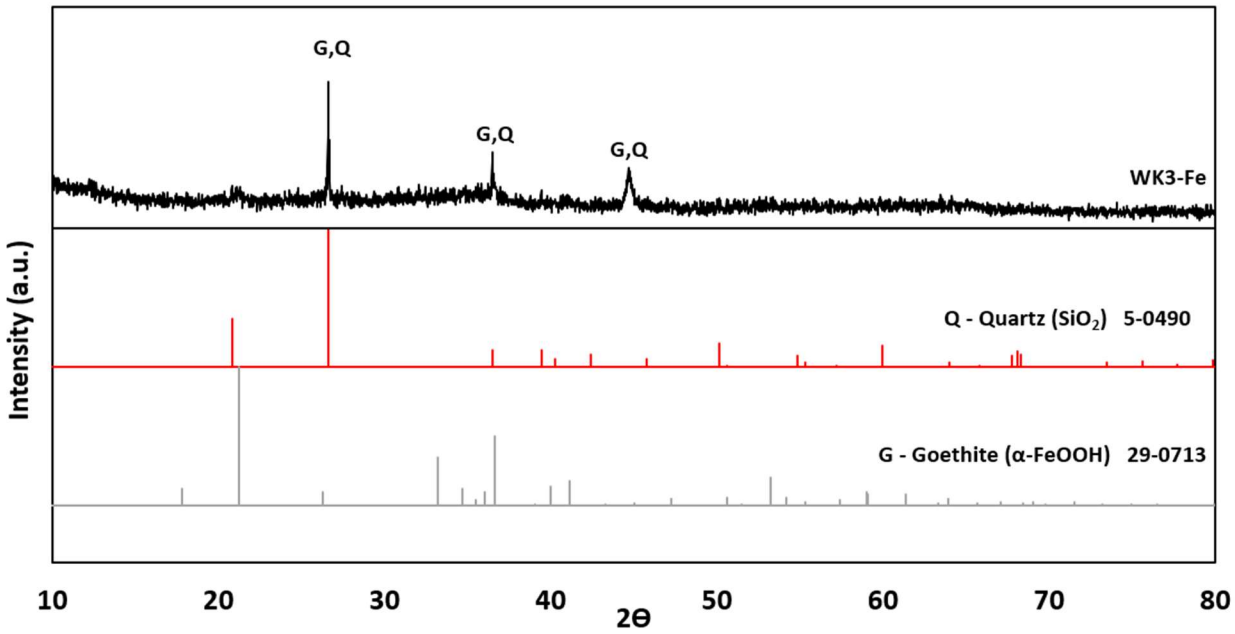

Figure A-58. XRD data obtained from sample WK3-Fe. Goethite was the primary iron mineral detected. Associated mineral quartz is shown for reference and also matches well with the sample peaks.

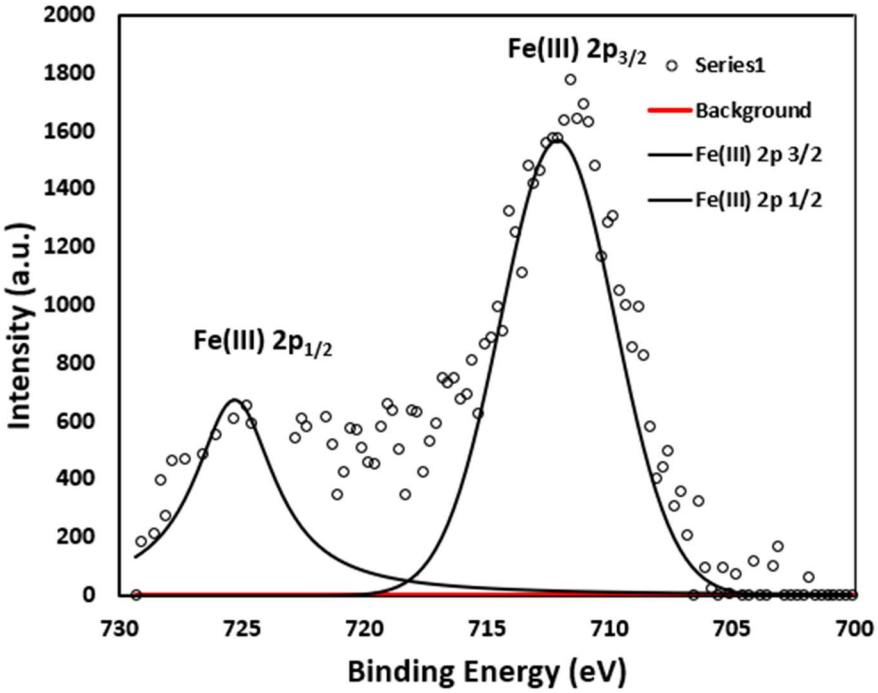

Figure A-59. XPS data for Waukesha cast iron pipe WK3-Fe. Peak fitting was done via XPSpeak41 software. Analysis concluded that the chemical state present in the sample was Fe(III).

WK-Cu Copper Lateral

Figure A-60. Inside of a copper lateral obtained from Waukesha.

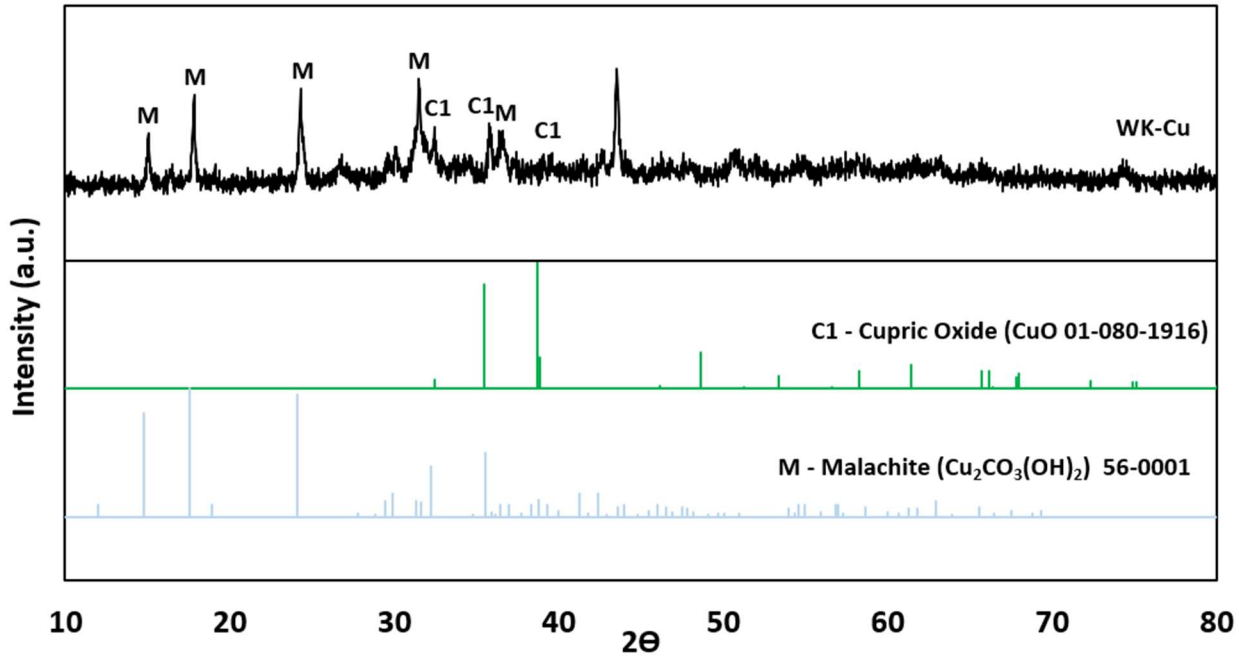

Figure A-61. XRD spectra obtained from Waukesha copper lateral WK-Cu. Cupric oxide and malachite were the main copper phases detected, and their reference patterns are shown (JCPDS 01-080-1916 and JCPDS 00-056-0001 respectively).

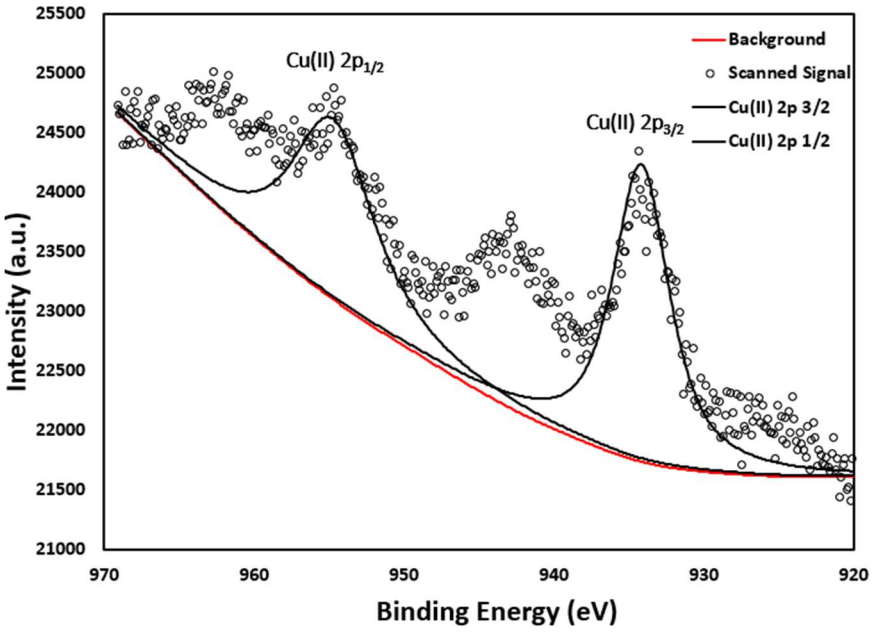

Figure A-62. XPS spectra for copper lateral WK-Cu. XRD observation of Cu(II) minerals was confirmed through peak fitting to chemical state Cu(II).